THE STUDY OF STORAGE-ENHANCED HEAT RECOVERY ROOM AIR-CONDITIONER (SEHRAC) FOR COMBINED SPACE COOLING AND WATER HEATING IN RESIDENTIAL BUILDINGS IN HONG KONG

JIA JIE

Ph.D

The Hong Kong Polytechnic University

2016

The Hong Kong Polytechnic University

Department of Building Services Engineering

The Study of Storage-Enhanced Heat Recovery Room Air-conditioner (SEHRAC) for Combined Space Cooling and Water Heating in Residential Buildings in Hong Kong

Jia Jie

A thesis submitted in partial fulfilment of the requirements for the degree of Doctor of Philosophy

December 2015

CERTIFICATE OF ORIGINALITY

I hereby declare that this thesis is my own work and that, to the best of my knowledge and belief, it reproduces no material previously published or written, nor material that has been accepted for the award of any other degree or diploma, except where due acknowledgement has been made in the text.

_____ (Signed)

_____Jia Jie_____ (Name of Student)

Department of Building Services Engineering

The Hong Kong Polytechnic University

Hong Kong, China

December 2015

ABSTRACT

Abstract of thesis entitled:	The Study of Storage-Enhanced Heat Recovery Room Air-conditioner (SEHRAC) for Combined Space Cooling and Water Heating in Residential Buildings in Hong Kong
Submitted by:	Jia Jie
For the degree of:	Doctor of Philosophy

At The Hong Kong Polytechnic University in December 2015

In subtropical climates such as Hong Kong's, air-conditioning and domestic water heating are two dominant energy end-uses in residential buildings. Local statistics show that out of the total energy consumption of the residential sector, 23% goes to air-conditioning and 19% goes to water heating. These figures clearly show that a technology that can simultaneously reduce energy use for space cooling and water heating is highly valuable.

Water heating utilizing condenser heat rejected from a refrigeration cycle is considered to be an energy efficient measure for domestic hot water production due to the associated heating efficiency is always higher than unity. On this basis, heat pump water heater is widely investigated for use in residential buildings. However, a majority of previous studies focused only on its heating capacity at the condenser.

The cooling performance at the evaporator under various operation conditions was seldom studied. This is because heat pump water heaters are often used as stand-alone water heating appliances with evaporator leaving air discharged to outdoors and thus the associated cooling effect is unexploited. Economic barrier also exists to limit its use in residential buildings, since a considerable investment must be made in the heat pump by the user. Therefore, a technology that allows a room air-conditioner to serve the combined purpose of space cooling and water heating is preferred, due to the fact that air-conditioners are commonly equipped in Hong Kong households to combat the hot and humid summer. However, considering the differences between a heat pump and a room air-conditioner, relevant research works are limited in public domain.

In view of this, a storage-enhanced heat recovery room air-conditioner (SEHRAC) was proposed. Besides space cooling, this installation can also provide water heating utilizing recovered condenser heat. In this study, the effectiveness, energy performance, operation characteristics, and performance improvement of SEHRAC when used for combined space cooling and water heating were investigated.

For the application of SEHRAC, a major concern is whether or not the amount of recoverable heat can meet the household water heating demand. The concern is particularly prominent in Hong Kong because most local residential units are small but the occupancy density is high (average living space is 12.9 m^2/person). The small space cooling load and thus the small amount of recoverable heat may not be sufficient to offset the high water heating demand. To address the concern, a typical residential estate in Hong Kong was chosen for a supply and demand analysis. The

analysis was based on hour-by-hour simulations using actual building characteristics and realistic equipment performance data. It was found that if a water tank was used for thermal energy storage, the daily cumulative recoverable heat far exceeded the daily household water heating demand, confirming the effective use of SEHRAC in Hong Kong. Further, for optimal design of the water tank of SEHRAC, its design requirements including the minimum required heat storage capacity and heat transfer effectiveness were also determined and discussed.

Room air-conditioners are often sized for satisfying peak cooling loads. At part load conditions, most air-conditioners operate intermittently to regulate their cooling outputs for maintaining the indoor set-point temperature. Intermittent operation of SEHRAC can lead to significant fluctuations in operating parameters on the refrigerant side. Adding that capillary tube is often used as the expansion device to magnify the fluctuations, whether SEHRAC can still operate satisfactorily in practice is of concern. Further, as operation of SEHRAC is affected by outdoor temperature and space cooling load, their influences on the energy performance of SEHRAC also need to be ascertained. In view of this, a prototype SEHRAC was designed and setup for laboratory experiments. The experimental results confirmed the satisfactory operation of SEHRAC. Its overall coefficient of performance (COP) was also found better than conventional room air-conditioner for a range of outdoor temperatures and space cooling load conditions. On this basis, a prediction model was developed for evaluating the sole use of SEHRAC for water heating in the entire air-conditioned season. The potential water heating energy saving on wider application of SEHRAC was estimated to be 9.1% of the overall energy consumption of the residential sector in Hong Kong.

Considering the significant refrigerant pressure fluctuations during the operation of SEHRAC, the selection of a suitable type of expansion device that can function properly despite the fluctuations is very important. In this study, the use of capillary tube (CT) and thermostatic expansion valve (TEV) in SEHRAC were side-by-side compared with the aim of optimizing the system configuration of SEHRAC. A prototype SEHRAC, which could be switched between the CT and TEV systems, was used for two identical sets of experiments. For each set of experiments, a series of tests under different outdoor temperatures were conducted. It was found that TEV could better regulate the refrigerant flow, maintain a stable evaporator superheat, and minimize the rise in refrigerant vapor content at the evaporator inlet during the operation of SEHRAC. The space cooling and water heating capacities for the TEV system were on average 16.3% to 19.4% and 18.5% to 23.4%, respectively, larger than the CT system. Its overall COP was also found 12.5% to 20.9% higher for the range of outdoor temperatures.

Accumulation of heat in the water tank of SEHRAC can result in an increase in tank water temperature, which will unavoidably affect the space cooling and water heating performances of SEHRAC. Measures to enhance the heat storage capacity of the water tank will thus be beneficial to the overall performance of SEHRAC. For achieving this objective, the use of phase change material (PCM) in the water tank was proposed in this study. To confirm and quantify the resultant performance improvement, laboratory experiments were conducted with and without the use of PCM (abbreviated as wPCM and woPCM scenarios). It was confirmed that the PCM could function as an internal heat sink to lower the rate of water temperature increase and to enhance the heat storage capacity of the water tank. As a result, the space

cooling and water heating capacities for the wPCM scenario, as compared to the woPCM scenario, were 5.4% and 16.1% larger, respectively. The overall COP was therefore found 6.9% to 9.8% higher. It was also revealed that the use of PCM could extend the heat retention time of the tank water by 21.1%.

From the above, the academic contributions of this thesis can be summarized into four aspects. First, the effectiveness of SEHRAC in satisfying the daily space cooling and water heating demands of Hong Kong households was confirmed. Second, the energy performance and operation characteristics of SEHRAC in comparison with conventional room air-conditioner under different outdoor temperatures and space cooling load conditions were examined. Third, the system configuration of SEHRAC was optimized by identifying a suitable type of expansion device. Last, the use of PCM to improve the overall performance of SEHRAC was proposed and confirmed.

PUBLICATIONS ARISING FROM THE THESIS

<u>Journal papers:</u>

Jia J, Lee WL, 2014. Applying storage-enhanced heat recovery room air-conditioner (SEHRAC) for domestic water heating in residential buildings in Hong Kong. Energy and Buildings, 78: 132-142.

Jia J, Lee WL, 2015. Experimental study of the application of intermittently operated SEHRAC (storage-enhanced heat recovery room air-conditioner) in residential buildings in Hong Kong. Energy, 83: 628-637.

Jia J, Lee WL, 2015. Experimental investigations on the use of capillary tube and thermostatic expansion valve in storage-enhanced heat recovery room air-conditioner. Energy and Buildings, 101: 76-83.

Jia J, Lee WL, 2015. Experimental investigations on using phase change material for performance improvement of storage-enhanced heat recovery room air-conditioner. Energy, 93: 1394-1403.

ACKNOWLEDGEMENTS

This thesis is the result of three years hard work. It would have never been completed without the help and support from many people.

I am grateful and honored to have the patient guidance of Dr. Lee Wai Ling, who is not only the best supervisor I have ever seen but also the best friend I have ever known in Hong Kong. Your calm, astute and flexible mentoring helped me find research that inspired, and your knowledge and advice helped it to fruition. Besides research, thanks also for your understanding and caring of my difficulties in life during these years. All of these enabled me to mature and evolve from a student to a researcher. Words cannot express my deepest and sincerest gratitude to you.

I am also thankful for the staffs and technicians of the Department of Building Services Engineering for the omnipresent help and convenience provided. The Hong Kong Research Grants Council and The Hong Kong Polytechnic University are also greatly acknowledged for the financial support of this program.

Thanks to all the friends, colleagues, and mentors who have helped and humored me along the way, especially Dr. Chau Chi Kwan, Fan Man, Li Han and Bao Ya Ni. Your help and accompany encouraged me to move forward, and your presence made these years more memorable. I wish you a bright future whatever may come, and whatever we create.

To Mom and Dad, who set the foundation and let me build, thanks for your emotional support that brings me balance and for your selfless love that always motivates me. Thank you for being there every step of the way.

My love and gratitude to Tian Jie, for keeping me sane and driving me crazy. This thesis is dedicated to you.

TABLE OF CONTENTS

LIST OF FIGURES

LIST OF TABLES

NOMENCLATURE

A	regression coefficient
ACL	annual cooling load (kWh)
AEC	annual energy consumption (kWh)
AREA	area (m^2)
c_p	specific heat capacity (kJ/kg K)
C	regression coefficient
COP	coefficient of performance
CR	compression ratio
h	specific mass enthalpy (kJ/kg)
H	amount of energy (kWh or MJ)
HR	hot water consumption duration (hour)
HS	household size (person)
k	number of air-conditioned hours in a day
K	number of air-conditioned hours in a year
m	mass flow rate (kg/s)
M	mass (kg)
N	number of air-conditioned rooms
OT	outdoor temperature (^{o}C)
P	pressure (Pa or MPa)

PLR	part load ratio
Q	heating/cooling rate (kW)
SMK	shading mask
T	temperature (^{o}C)
T*	absolute temperature (K)
UF	utilization factor
V	volume (m^3)
w	moisture content (kg/kg)
W	power consumption (kW)
x	refrigerant vapor content

Greek symbol

α	time spent for the entire experiment
ε	effectiveness
λ	latent heat of fusion (kJ/kg)
ρ	density (kg/m^3)
σ	latent heat of vaporization (kJ/kg)
τ	time (second, minute or hour)
φ	relative humidity

Subscript

a	air

b	atmosphere/beginning
cd	compressor discharge
cl	cooling load/capacity/output
cs	compressor suction
cum	cumulative
e	end
ei	evaporator inlet
er	evaporator return
es	evaporator supply
hd	heating demand
hi	heat exchanger inlet
ho	heat exchanger outlet
hw	hot water
id	indoor
m	average/mean
max	maximum
min	minimum
nor	normalized
oa	overall
od	outdoor
p	PCM
pa	paraffin

r	refrigerant
R	required
rated	rated
s	heat storage
sl	saturated liquid refrigerant
sw	saturated water vapor
t	total
ti	water tank inlet
to	water tank outlet
tw	tap water
us	un-shaded
w	water
wh	water heating/recoverable heat

CHAPTER 1

INTRODUCTION

1.1 Hong Kong Residences and Public Housing

Hong Kong is famous over the world for the modern culture, highly developed economy, as well as the crowded living space. As one of the most densely populated cities in the world, Hong Kong has an average population density of about 6300 persons per square kilometer (World Population Review, 2015), which is much higher than other cosmopolitan cities such as Singapore (about 6100 persons per square kilometer), Tokyo (about 5400 persons per square kilometer) and London (about 4500 persons per square kilometer).

The high and growing population density is a consequence of the influx of immigrants from the Mainland China. Adding to that is a continuous reduction in average household size from 3.4 persons in 1991 to 2.9 persons in 2015 (Housing Authority, 2015). As a result, the number of domestic households in the last 15 years has increased from 1.58 to over 2.37 million (Census and Statistics Department, 2015). This sharp increase has led to a sustained high demand of residential housing.

The Hong Kong SAR Government is according a high priority to providing adequate housing estates to its citizens. On this basis, the Government has adopted a housing supply target of 480,000 units for the ten-year period from 2015-16 to 2024-25

(Hong Kong Government, 2015). Public housing, which is offered by the Government for families of middle and low-class incomes, accounts for 60% of the total housing supply.

Public housing estates are located in different parts of Hong Kong. It was estimated by the Housing Authority (a statutory body responsible for implementing Hong Kong's public housing programs) that over 30% of the population in Hong Kong (about two million people) resides in public housing in 2015 (Housing Authority, 2015). As at the end of March 2015, the Housing Authority has a stock of 783,000 public housing units (Housing Authority, 2015). Of these units, 46% are located in Urban, 31% in Extended Urban, 22.7% in New Territories and 0.3% in Islands. In the future five years, 55% of the total to-be-built public housing units will be located in Urban district and 30% in Extended Urban district.

Attributed to the scarcity of residential land in Hong Kong, public housing units are typically built in small size. As at the end of March 2015, 46.1% of public housing units are of 30 to 39.9 square meters; 22.8% are of 20 to 29.9 square meters; 13.0% are of size less than 20 square meters; and 18.0% are of size bigger than 40 square meters (Housing Authority, 2015).

The small size of residential units has led to a dense living environment in Hong Kong. It was reported that the average living space in Hong Kong is currently 12.9 square meters per person (Housing Authority, 2015). Despite the average living space has seen a continuous increase in the last decade (it was 11.7 in 2005), it is still

much lower than Singapore, which has an average living space of 25 square meters per person (Yuen, 2010).

1.2   Hong Kong Residential Sector Energy Consumption

Due to the rapid economic development and urbanization in the past two decades, the energy consumption of residential sector in Hong Kong has risen sharply. According to the latest energy statistics (Electrical and Mechanical Services Department, 2015a), the total residential sector energy consumption has increased by 15.4% in the last decade (Figure 1.1).
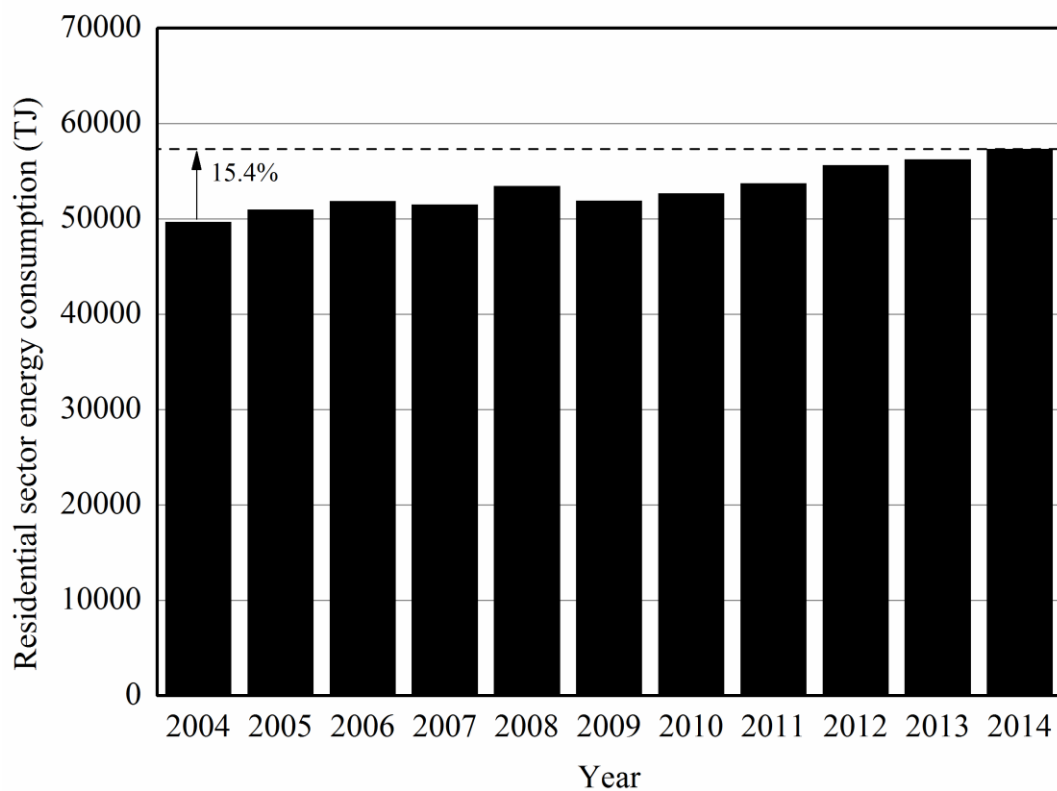
Figure 1.1   Residential sector energy consumption in Hong Kong

Among various energy end-uses, air-conditioning and domestic water heating are the two dominant uses, accounting for 23% and 19% (Electrical and Mechanical Services Department, 2015a), respectively, of the total energy consumption in residential buildings (Figure 1.2). These figures clearly show that a technology that can simultaneously reduce energy use for space cooling and water heating is highly valuable.
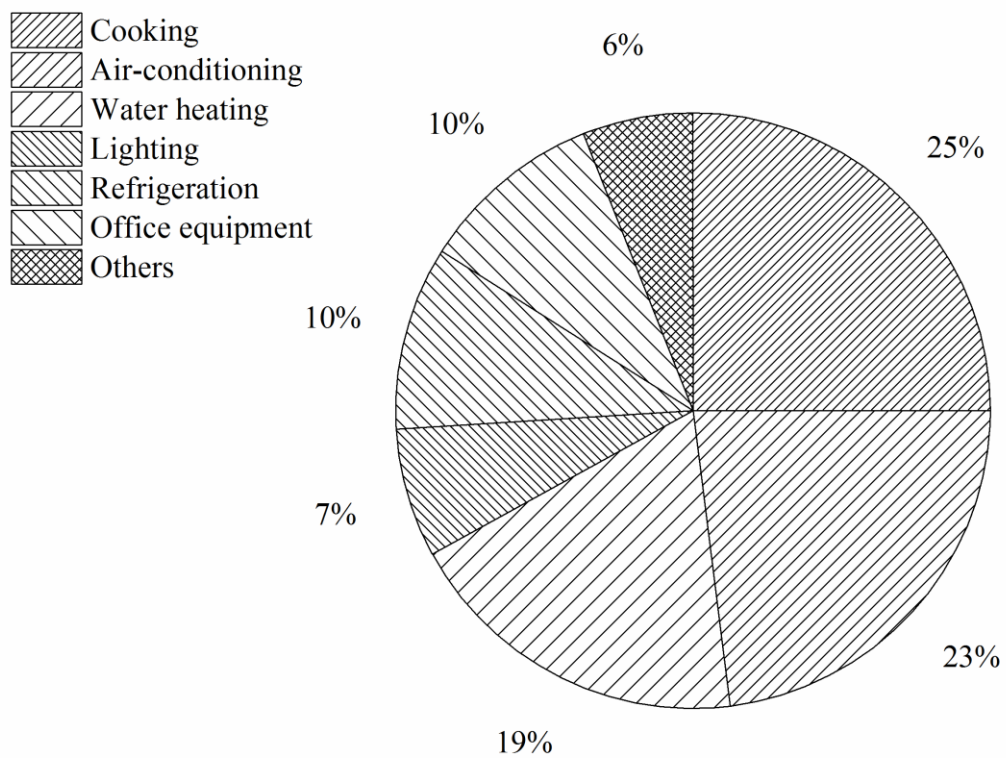
Figure 1.2   Energy consumption of various energy end-uses

1.3   Air-Conditioners and Water Heaters Used in Hong Kong

Air-cooled window- or split-type room air-conditioners are commonly equipped in Hong Kong households to combat the hot and humid summer. It was reported that

the penetration rate of air-conditioning in living/dining rooms of local residential units is 83%, and that in bedrooms is 78% (Chen and Lee, 2010).

Given that the energy use of an air-conditioner to output a given rate of cooling increases with the entering temperature of the medium for condenser cooling, the use of air-cooled units in Hong Kong is particularly inefficient, due to the high outdoor temperature of around 35 ^{o}C in summer. As a result, the achievable coefficient of performance of most air-cooled units is low, in the range of 2.2 to 2.4 (Lee et al., 2008). Another factor that upsets the efficiency of air-conditioners applied in Hong Kong is the common practice to locate their condensers in a recessed place. The recessed spaces are formed by individual flats extending outwards from the building's core in several directions, yielding more external walls and windows. These spaces can be used for multiple purposes. However, the most common but controversial use is to enable heat rejection of air-conditioners, since the hot air jet resulted from the heat rejection can lead to the development of a rising air plume to elevate the ambient temperature. The effect is particularly prominent at the upper levels of a residential building (Lee et al., 2008).

Electricity and town gas are the major fuels reported in use for domestic water heating in Hong Kong residential sector (Chen and Lee, 2010). The choice between using town gas and electricity is determined largely by the provisions already made when a residential building is built. It was estimated that the penetration rate of town gas water heater in Hong Kong households is 90%, while the remaining market share is dominated by electrical water heater (Chen and Lee, 2010). Domestic water heaters are generally categorized using energy efficiency ratings. A Mandatory

Energy Efficiency Labelling Scheme in Hong Kong is currently used as guidelines for manufacturing standards (Electrical and Mechanical Services Department, 2015b).

1.4   Objectives of This Study

Air-conditioners function to remove heat from indoor spaces and subsequently discharge this heat to the outside. The discharged waste heat, if recovered for water heating, can reduce energy use and greenhouse gas emissions. Along this line, a storage-enhanced heat recovery room air-conditioner (SEHRAC) is proposed in this study. SEHRAC is a conventional air-conditioner provided with an additional tank-immersed refrigerant-to-water heat exchanger between the compressor and the air-cooled condenser for recovery of condenser heat for water heating. This installation can serve the purpose of combined space cooling and water heating, and is particularly suitable for applications in tropical regions, where most residences are equipped with air-conditioners to combat the hot and humid summer.

The recoverable heat from condenser is affected by the simultaneous cooling load and power consumption of an air-conditioner. While the household water heating demand is determined by the domestic hot water consumption. Whether or not the heat supply can exceed the heating demand determines the effectiveness of SEHRAC when used for combined space cooling and water heating. In this study, a detailed supply and demand analysis will be carried out to evaluate the effectiveness of SEHRAC in a typical residential estate in Hong Kong.

Whether or not the proposed SEHRAC can achieve the energy saving objective depends on its energy performance under different outdoor temperatures and space cooling load conditions. In this study, the energy performance and operation characteristics of SEHRAC in comparison with conventional room air-conditioner will be examined through laboratory experiments.

In a SEHRAC, expansion device is one of the most important components. It functions to regulate the refrigerant flow to the evaporator and to maintain a pressure difference between the high and low pressure sides. Failure to function will be detrimental including refrigerant flooding to damage the compressor, refrigerant starving to lower the evaporator effectiveness, and hunting to cause large fluctuations in evaporator superheat. Therefore, an optimization of system configuration of SEHRAC by identifying a suitable type of expansion device is necessary. In this study, two types of expansion device that are most used in residential applications (i.e. capillary tube and thermostatic expansion valve) will be side-by-side compared for use in SEHRAC by experimental investigations.

Accumulation of heat in the water tank of SEHRAC can result in an increase in tank water temperature, which will unavoidably affect the space cooling and water heating performances of SEHRAC. For improving the overall performance of SEHRAC, the use of phase change material (PCM) in the water tank is proposed. In this study, the resultant performance improvement will be confirmed and quantified by experimental investigations.

To sum up, the specific objectives of this study are to:

1)   Examine the effectiveness of SEHRAC in satisfying the space cooling and water heating demands of Hong Kong households;

2)   Evaluate the energy performance and operation characteristics of SEHRAC under different outdoor temperatures and space cooling load conditions;

3)   Optimize the system configuration of SEHRAC by identifying a suitable type of expansion device; and

4)   Confirm and quantify the performance improvement of SEHRAC by the use of PCM.

1.5   Organization of This Thesis

This thesis comprises eight chapters, which include an introduction, a review of relevant research works, simulation and experimental studies on SEHRAC, as well as a summary of conclusions drawn from this study.

Chapter 1 introduces the backgrounds, motivations, and objectives of this study.

Chapter 2 provides a review of relevant research works and identifies the research gaps in previous studies.

Chapter 3 explains the research methodology adopted in this study.

Chapter 4 presents an effectiveness analysis on the use of SEHRAC in a typical residential estate in Hong Kong.

Chapter 5 investigates the energy performance and operation characteristics of SEHRAC under different outdoor temperatures and space cooling load conditions.

Chapter 6 presents a side-by-side comparison of capillary tube and thermostatic expansion valve for use in SEHRAC.

Chapter 7 examines the performance improvement of SEHRAC by the use of PCM.

Chapter 8 summarizes the conclusions draw from this study and provides several recommendations for future research.

CHAPTER 2

LITERATURE REVIEW

To identify the research gaps in previous studies, relevant research works are reviewed and key findings are summarized in this chapter.

2.1 Heat Pump Water Heaters

In Hong Kong or elsewhere in the world, domestic water heating is typically realized by using heat generating elements that consume fossil fuels (e.g. town gas) or electricity (Aguilar et al., 2005). Water heaters developed based on the principle are usually simple in configuration and installation, but less energy efficient. This is particularly true for an electrical water heater, for which fossil fuels need to be converted into electricity and then into thermal energy to provide heating effect, resulting in a very low overall energy efficiency (Kim et al., 2004).

An alternative to the conventional (electrical or gas) water heaters is a heat pump water heater (HPWH). It is an appliance that provides heating effect by using rejected condenser heat from a refrigeration cycle. Heat is then extracted from a heat source (typically ambient air) and transferred to the water being heated. It was reported that HPWH can deliver much more heat with the same amount of energy consumption as the conventional water heaters (Kim et al., 2004). The working cycle

of an air-source HPWH is shown in Figure 2.1. The heat pump is often used as a stand-alone water heating appliance as illustrated in Figure 2.2.
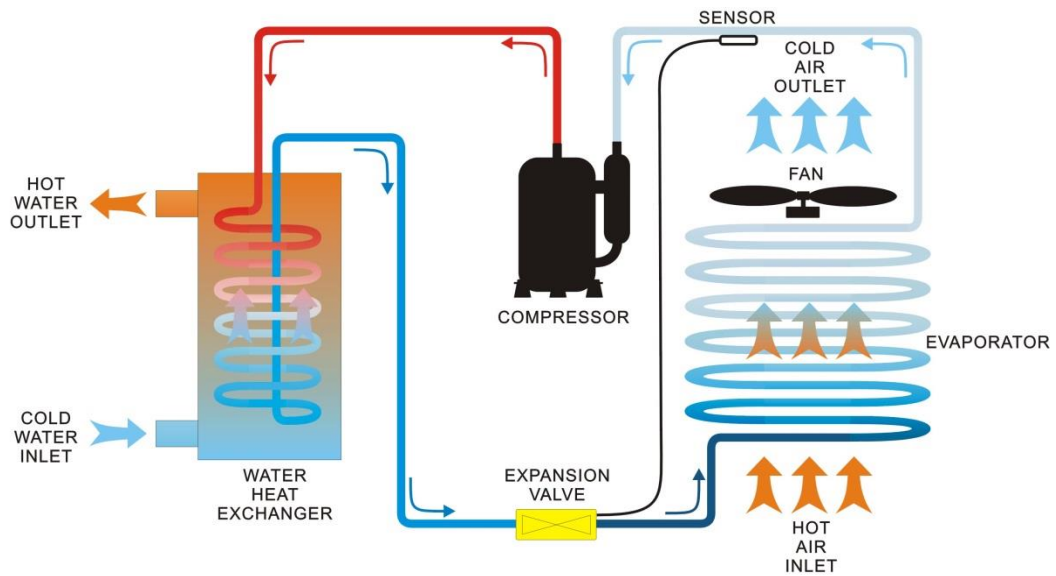
Figure 2.1   Working cycle of air-source HPWH (Paramount, 2013)
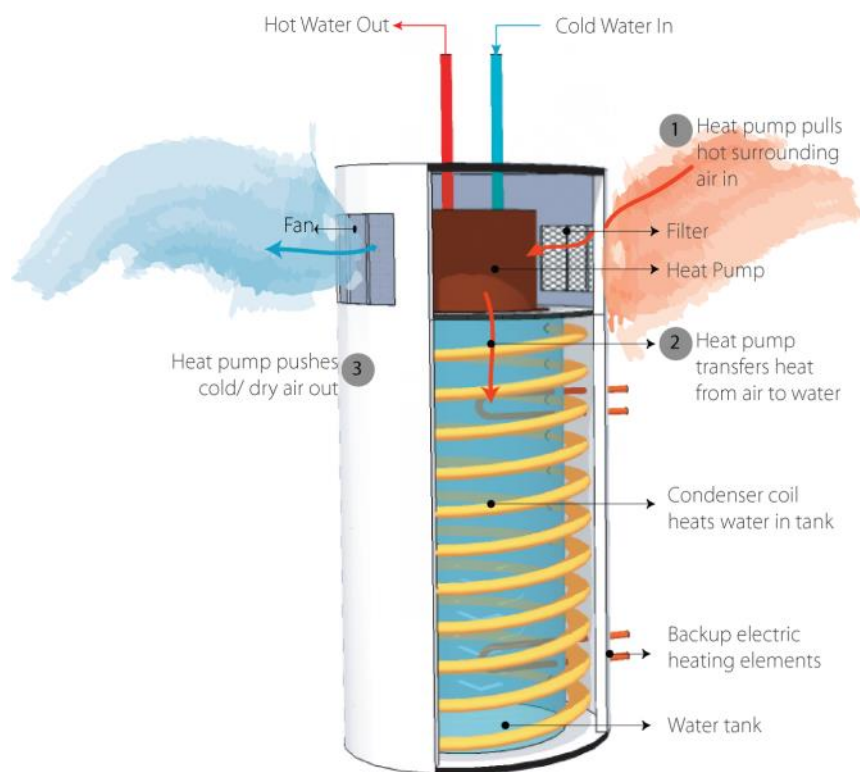
Figure 2.2   Schematic of air-source HPWH (Powertime, 2015)

Since the 1950s, HPWH is widely investigated as an energy efficient measure for water heating (Hepbasli and Kalinci, 2009). Previous studies mainly focused on its energy performance, operation characteristics, working fluids, and integration with renewable energy technologies.

On the energy performance, it was found that the efficiency of HPWH is affected by factors including the heat source temperature, the working fluid used, the temperature of water being heated, etc. Among the factors, its performance is most sensitive to the heat source temperature (Kara et al., 2008). For an air-source HPWH, it was found that it can readily generate hot water at around 60 ^{o}C when the ambient air temperature is 24 ^{o}C, but this may not be achieved if the air temperature drops to 1.7 ^{o}C. It was further concluded that there exists a threshold air temperature, below which HPWH can hardly provide any heating effect, thus other auxiliary heating elements should be activated to meet the water heating demand. Further, a lower air temperature can also increase the risk of frosting on the evaporator surface. To melt the frost formed, HPWH needs to be operated in defrost mode, which will further degrade the heat pump performance (Sakai et al., 1976).

Energy factor (EF) is usually used to quantify the efficiency of a water heater (Hoeschele and Springer, 2008). Air-source HPWH typically has an EF of between 2 and 3, while the EF for electrical water heater is approximately 0.9. This suggests a potential energy saving of 55% to 70% if electrical water heater is retrofitted by HPWH. However, due to the fluctuations in ambient air temperature and the requirement for defrosting, the actual energy saving will correspond to 40% to 60% (Hepbasli and Kalinci, 2009).

On the operation characteristics, Kim et al. (2004) constructed a mathematical model for HPWH with the aim to investigate its transient thermal behavior. In the study, finite volume method (FVM) was applied to describe the evaporator and condenser of HPWH, and a lumped parameter model was used to analyze the compressor. It was found that the transient behavior of HPWH is significantly affected by its system configuration. Yao et al. (2004) evaluated the operation characteristics of HPWH when evaporator frosting occurs. The evaluation was based on a distributed mathematical model for HPWH, in which the frost formed on evaporator surface is taken into account. Based on this model, the influence of frosting on the operation of HPWH was investigated. The criteria of evaporator design for mitigating the frost influence were also discussed. To enable a satisfactory operation of HPWH, the optimal set-point temperature for hot water supply was identified by Guo et al. (2011) through experimental investigations. It was found that the set-point is preferably higher than 46 ^{o}C in summer and 50 ^{o}C in other seasons.

On the working fluid, different pure refrigerants or refrigerant mixtures were investigated for used in HPWH. Pure refrigerant R22 was used in experimental prototypes constructed by Zhang et al. (2007) and Li et al. (2007). A HPWH based on zeotropic mixture R22/R142b was evaluated by Liebenberg and Meyer (1998) in terms of the viability of employing capacity control. It was found that the system efficiency is improved by using R22/R142b, which offers the possibility of continuous modulation of water heating capacity to match the demand. Zeotropic mixture R22/R600a was proposed by Feng et al. (2009) for use in HPWH. Through experimental investigations, an optimal content of R600a in the mixture was identified. However, R22 is currently being phased out for its high ozone depletion

potential (ODP) and global warming potential (GWP). In view of this, Vince et al. (2001) experimentally investigated the possibility of replacing R22 in the mixture with R407c in an existing HPWH. In the study, a HPWH originally designed for R22 was modified for R407c operation. Several tests, including baseline tests using R22 and comparison tests using R407c, were conducted. The results indicated that the R407c-based unit has a much higher water heating capacity than that of the R22-based unit. However, on energy efficiency, the R407c-based unit was found consuming more power at higher water temperature region. Similar study was also carried out by Karagoz et al. (2004) for evaluating the use of R134a as a substitute for R22 in HPWH.

Considering the environmental risk associated with (H)CFC, Neksa et al. (1998) proposed the use of CO_2 as the working fluid in HPWH. CO_2 is one of the few non-toxic and non-flammable working fluids that do not contribute to ozone depletion and global warming. Due to its relatively low critical temperature, CO_2 undergoes a transcritical cycle when used in HPWH. The temperature glide at heat rejection contributes favorably to water heating. For the CO_2-based prototype HPWH constructed by Neksa et al. (1998), a heating energy efficiency of 4.3 could be achieved. It was further found that hot water with temperatures up to 90 ^{o}C can be generated by the prototype without operation difficulties. Similar studies were also carried out by Saikawa et al. (2011), Laipradit et al. (2008), and Fernandez et al. (2010).

Among various renewable energy technologies for integration with HPWH, solar energy was most widely researched. The performance of HPWH with solar boosted

evaporator (i.e. solar-assisted HPWH (Figure 2.3) was investigated by Morrison (1994) under a range of climatic conditions. In the study, a simulation model was developed in TRNSYS environment to facilitate the investigations. Another mathematical model was constructed by Xu et al. (2006) based on fundamental principles of thermodynamics. Mohanraj et al. (2009) demonstrated that artificial neural network (ANN) was also suitable for modelling the performance of solar-assisted HPWH.
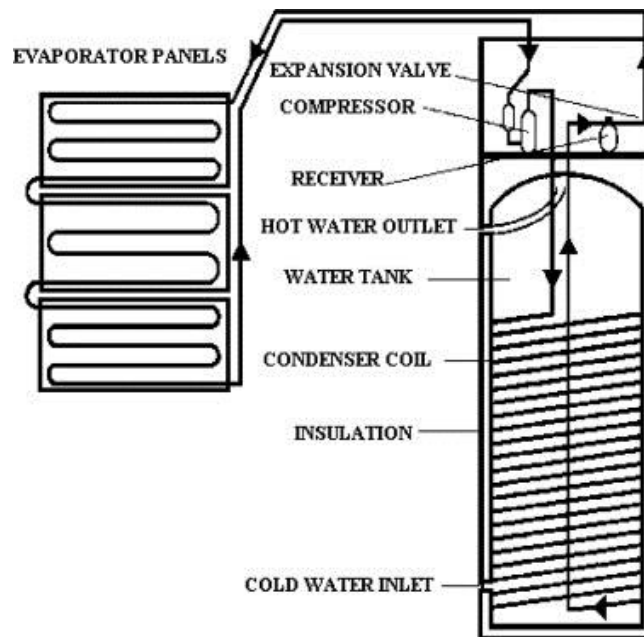
Figure 2.3   Schematic of solar-assisted HPWH (Anderson and Morrison, 2007)

Besides simulations, experimental studies on solar-assisted HPWH have also been done. Its long term performance was evaluated by Huang and Lee (2004) based on a prototype that had been running for over 20,000 hours. It was found that the prototype on average consumes 0.019 kWh of electricity for delivering one liter of hot water (at 57 ^{o}C). For its performance under full load and part load conditions, an experimental study was done by Anderson and Morrison (2007). A prototype was constructed for the experimental study. The constructed prototype utilized flat

unglazed aluminum solar evaporator panels to absorb solar and ambient energy. Its energy efficiency was found in the range of 5 to 7 under clear daytime conditions, and 3 to 5 under clear nighttime conditions. A variable capacity solar-assisted HPWH was proposed and constructed by Chaturvedi et al. (1998). The water heating capacity modulation was achieved by the use of a variable speed drive (VSD) to adjust the compressor speed to maintain a proper matching between the pumping capacity of the compressor and the evaporative capacity of the evaporator. Experimental results indicated that the energy efficiency of solar-assisted HPWH can be improved significantly by lowering the compressor speed as ambient temperature rises from winter to summer months.

2.2   Expansion Devices in Refrigeration Systems

Expansion device is one of the most important components in a refrigeration system. It functions to reduce the refrigerant condensing pressure (high pressure) to the evaporating pressure (low pressure) by a throttling operation and to regulate the refrigerant flow to the evaporator to match the equipment and load characteristics (Dincer and Kanoglu, 2011). In small capacity systems (such as room air-conditioners), capillary tube (CT) and thermostatic expansion valve (TEV) are most commonly used, due to fairly good reliability and low cost.

TEV (Figure 2.4) is essentially a pressure reducing valve installed between the high pressure and low pressure sides of a refrigeration system. It can automatically control the refrigerant flow to the evaporator at a rate that matches the system

capacity to the actual load (Dincer and Kanoglu, 2011). This is achieved by maintaining a nearly constant superheat at the evaporator outlet. As the evaporator superheat rises due to increase heat load on the evaporator, the TEV increases refrigerant flow until superheat returns to the valve's setting. Conversely, the TEV will decrease refrigerant flow when superheat is lowered as a result of a decreased heat load on the evaporator. The effect of this type of regulation allows the evaporator to remain as nearly fully active as possible under all load conditions (Sporlan, 2011).

TEV is a proportional controller, which responds to the difference between the pressure of the refrigerant at the position that the pressure-sensing connection is made and the pressure developed in the sensing bulb located at the outlet of the evaporator (Sporlan, 2011). A variable spring setting in the valve is provided to adjust the required superheat of the vapor leaving the evaporator (Figure 2.4).
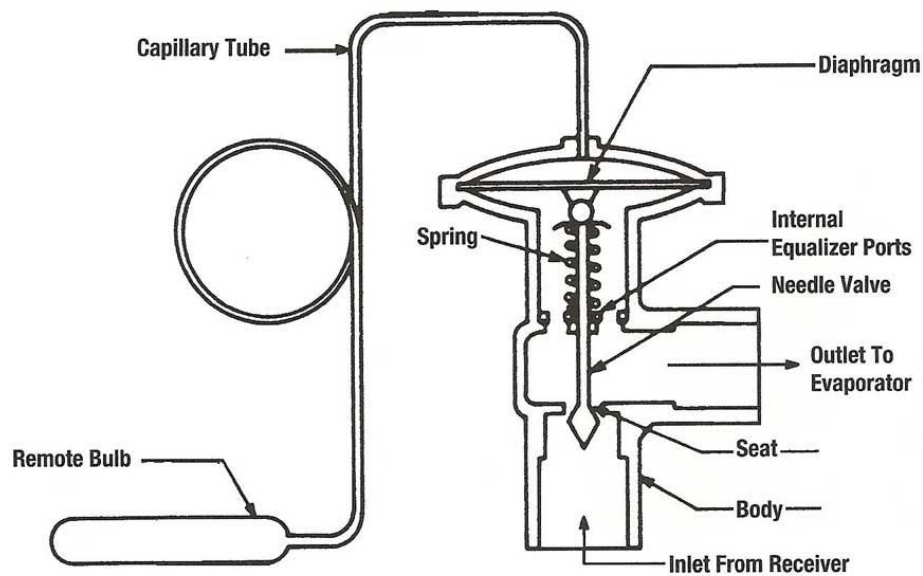
Figure 2.4   Schematic of TEV

CT is a length of small diameter tube (typically from 0.8 mm to 2 mm) and is a non-modulating expansion device. As liquid refrigerant flows through the tube, the pressure drops due to friction and acceleration of refrigerant, thus some of the liquid flashes into vapor (Hundy et al., 2008). The refrigerant mass flow rate through a CT is therefore strongly dependent on the upstream pressure and sub-cooling. Flow rate will also increase with lower outlet pressure down to a critical value, below which the flow rate does not change (Dincer and Kanoglu, 2011). The critical value occurs where sonic velocity is achieved at the exit, so that if CT is selected for a choked flow condition then the flow rate will actually be independent of the evaporating temperature.

CT is used almost exclusively in small capacity refrigeration systems and is self-regulating in a certain extent. Increasing ambient temperature results in increasing load on the conditioned space and the condensing pressure will rise, forcing more refrigerant flow (Hundy et al., 2008).

For a given refrigeration system, the expansion device needs to be properly chosen and sized to enable the satisfactory operation. Failure to function will be detrimental including refrigerant flooding to damage the compressor, refrigerant starving to lower the evaporator effectiveness, and hunting to cause large fluctuations in evaporator superheat (Dossat, 1997).

Previous relevant works on comparing the use of CT and TEV mainly focused on HPWHs and conventional room air-conditioners (CRACs). Choi and Kim (2002) investigated the influence of different expansion devices on the performance of a

HPWH under a range of operating conditions. The evaluations were based on an experimental setup illustrated in Figure 2.5. The experimental results concluded that the TEV system has an overall performance better than the CT system. Similar conclusion was also drawn by Kim and O'Neal (2005) and Zhang et al. (2007). However, Agrawal and Bhattacharyya (2008) came up with a different conclusion. They adopted a detailed steady state simulation model to evaluate the performance of a trans-critical CO_2 HPWH. It was found that with the use of a proper CT, the HPWH can operate efficiently under a wide range of condenser inlet water temperatures. It was also concluded that the performance of the CT system is on a par with the TEV system.
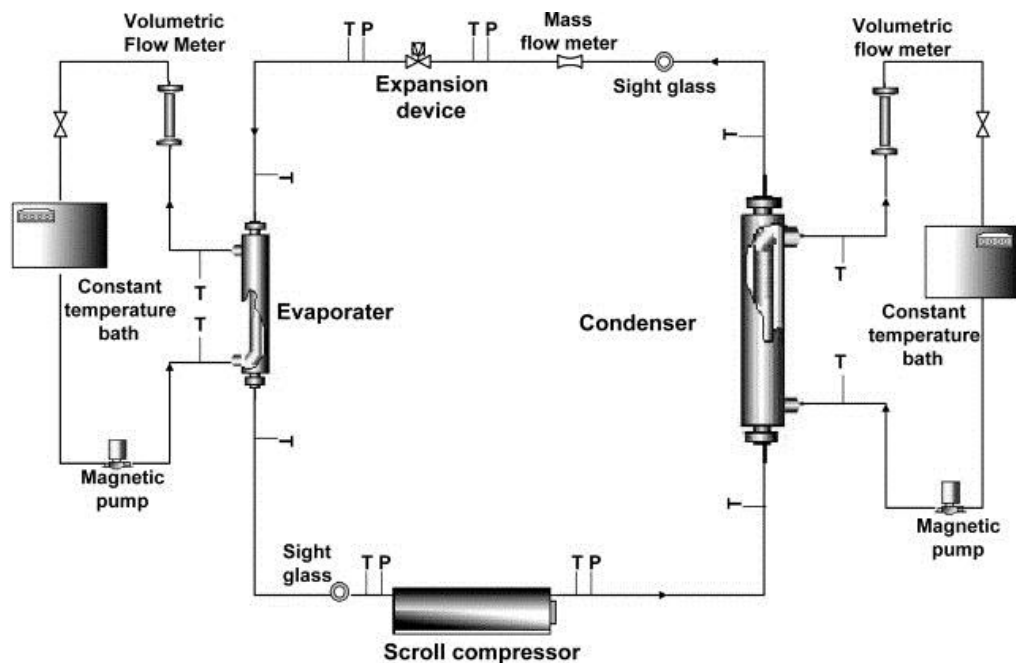
Figure 2.5   Experimental setup for comparing the use of CT and TEV in HPWH
(Choi and Kim, 2002)

For the use of CT and TEV in CRACs, Stoecker et al. (1981) found that by replacing the CT with a TEV, the overall energy efficiency of a CRAC can be improved by 2% to 3%. A similar study was conducted by Farzad and O'Neal (1993). It was found

that TEV can better regulate the refrigerant flow to meet the cooling demand at off-design conditions, but CT also performs fairly well in most conditions. It was also reported that the feasible use of TEV is restricted to some systems because of the valve instability problem. On this issue, Maidment et al. (1999) evaluated the use of CT and TEV in a CRAC serving a supermarket's display cabinet. It was found that CT is better than TEV in energy performance and in providing a more stable operating condition.
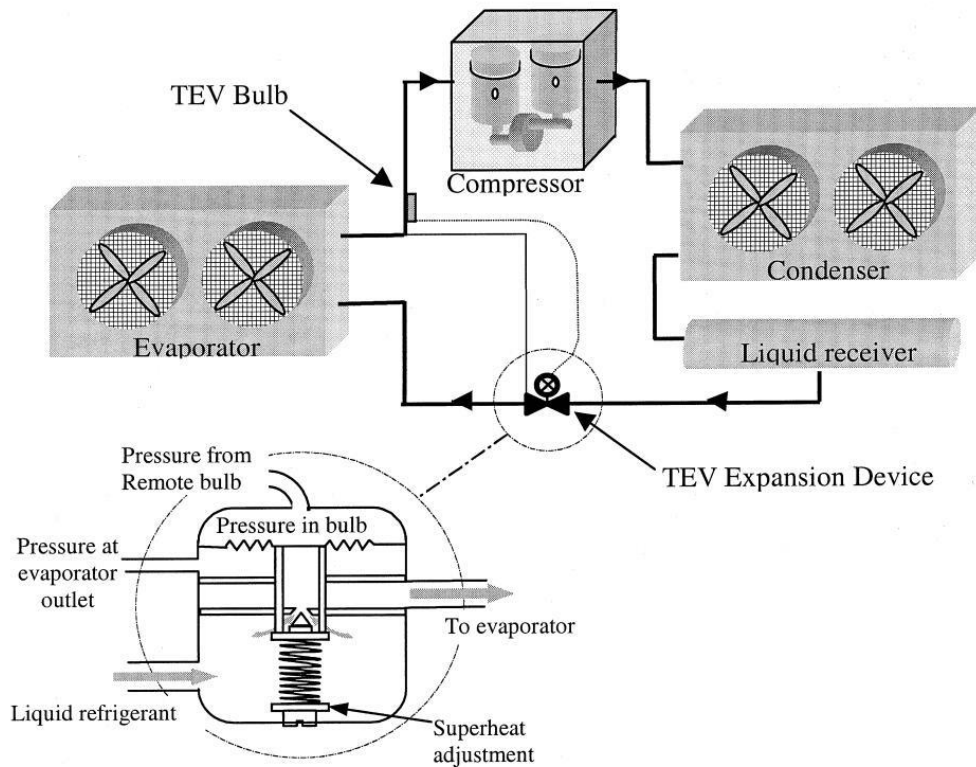
Figure 2.6   Experimental setup for comparing the use of CT and TEV in CRAC (Maidment et al., 1999)

2.3   Thermal Energy Storage

Thermal energy storage (TES) in the form of sensible and latent heat has become an important aspect of energy management in industry and buildings (Demirbas, 2006). It not only reduces the mismatch between supply and demand but also improves the performance and reliability of energy systems. When used for heat recovery, TES can lead to saving of primary fuels and makes the system more cost effective by reducing the wastage of energy and capital cost (Sharma et al., 2009).

TES deals with the storage of energy by cooling, heating, melting, solidifying, or vaporizing a material. The energy becomes available as heat when the process is reversed (Demirbas, 2006). Storage by causing a material to raise or lower its temperature is sensible heat storage (SHS). SHS system utilizes the heat capacity and the change in temperature of the material during the process of charging and discharging. The amount of heat stored depends on the specific heat of the medium, the temperature change and the amount of storage material. Water is a good SHS material because it is inexpensive and has a high specific heat. But above 100 ^{o}C, oils, molten salts and liquid metals are commonly used (Sharma et al., 2009).

Latent heat storage (LHS) is based on the heat absorption or release when a storage material undergoes a phase change from solid to liquid or vice versa. Compared to SHS, LHS offers higher energy storage density because energy is stored as latent heat of a material. As a result, LHS is characterized by a substantial reduction in required volume of storage material for the same amount of energy stored. It was reported that a LHS-based storage system is typically 5 to 10 times smaller than a system based on SHS (Zalba et al., 2003). Another advantage associated with LHS is

the isothermal nature of the heat storage and release processes, which can improve the stability of an energy system (Agyenim et al., 2010).

Due to the above mentioned advantages, LHS has been widely investigated for use in building envelops (Kuznik et al., 2008), refrigeration systems (Liu et al., 2012), renewable energy utilizations (Kenisarin and Mahkamov, 2007), equipment cooling (Baby and Balaji, 2012), thermal protection (Mesalhy et al., 2006), and waste heat recovery (Pandiyarajan et al., 2011).

2.4   Phase Change Materials

Storage materials used for LHS are phase change materials (PCMs). Thermal energy is stored or released when a PCM changes from solid to liquid or liquid to solid. Unlike SHS materials, PCMs absorb and release heat at a nearly constant temperature. Further, they can typically store 5 to 14 times more heat per unit volume than SHS materials such as water, masonry, or rock (Sharma et al., 2009).

A large volume of studies have been carried out on a wide range of materials for potential use as PCMs, which can be classified as organic, inorganic, and eutectic materials (Figure 2.7). However, for their employment in practice, these materials must exhibit certain desirable thermodynamic, kinetic and chemical properties (Zalba et al., 2003). Moreover, economic considerations and easy availability of these materials have also to be taken into account. Comprehensive reviews of PCMs that have been proposed or used, their characteristics, advantages and disadvantages,

as well as the various experimental techniques used to determine the thermal behaviors of these materials were presented by Abhat (1983), Lane (1983), and Dincer and Rosen (2002).
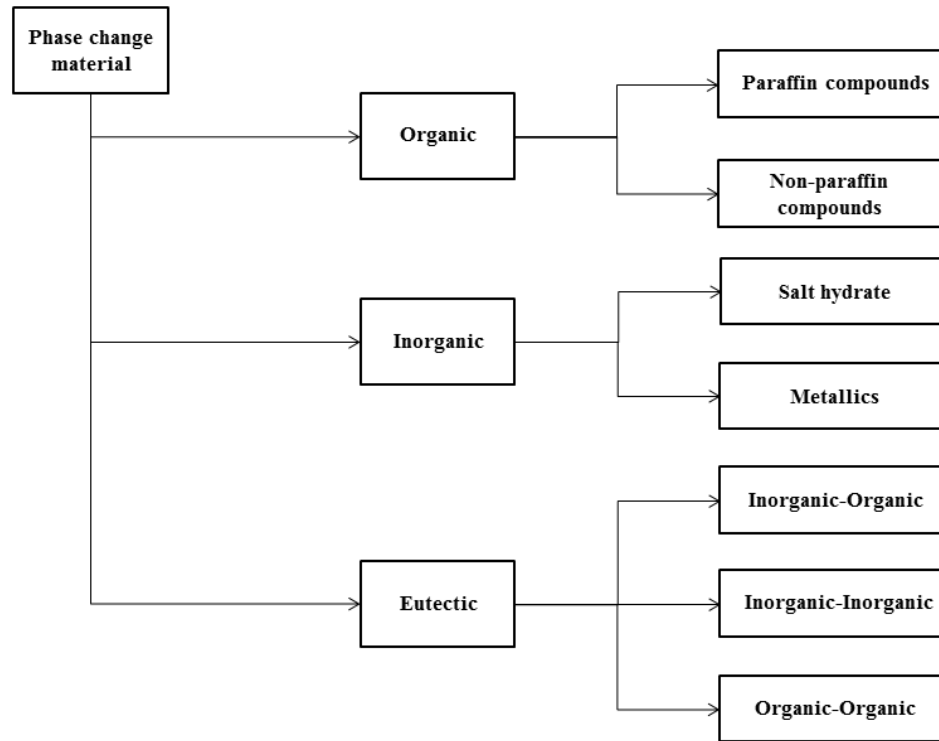
Figure 2.7   A classification of PCMs

PCMs to be used for LHS should have a large latent heat and a high thermal conductivity. The selection of an appropriate PCM for any application also requires the PCM to have phase change temperature within the practical range of application (Agyenim et al., 2010). Figure 2.8 shows an overview of commonly used PCMs according to their phase change temperatures and latent heats. Among the illustrated materials, PCMs with phase change temperatures in the range of from 0 ^{o}C to 65 ^{o}C are most widely investigated, as they are suitable for domestic water heating or cooling applications (Agyenim et al., 2010).

Most PCMs have unacceptably low thermal conductivities, leading to slow charging and discharging rates, hence heat transfer enhancement techniques are required for most LHS applications. The techniques commonly investigated in previous studies are summarized in Figure 2.9.
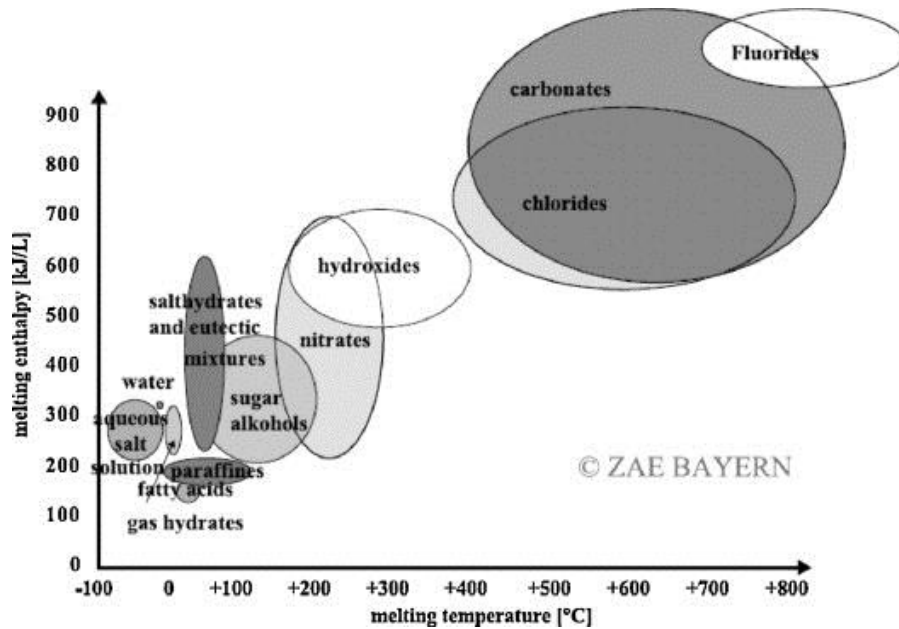
Figure 2.8   A thermodynamic classification of PCMs (Cabeza et al., 2011)

A majority of the heat enhancement techniques are based on the application of fins embedded in PCM. This is probably due to the simplicity, ease in fabrication and low cost of construction. This is followed by the impregnation of conductive matrix into PCM using high thermal conductivity materials such as graphite and carbon fiber (Agyenim et al., 2010).

Kalhori and Ramadhyani (1985) experimentally studied the melting and solidification characteristics of paraffin around a vertical tube. The results show that the existence of fins can mitigate the sub-cooling effect during the melting process of paraffin. Agyenim et al. (2009) found that, as compared to radial fins, LHS system

with axial fins has a better thermal performance in both melting and solidification processes. Choi and Kim (1992) found that the overall heat transfer coefficient of a LHS system can be enhanced by 3.5 times if axial fins are employed. Stritih (2004) numerically calculated the transient temperature field in a LHS system and found that the fin's geometry has a significant influence on the overall heat transfer performance. Inaba et al. (2003) studied the effect of fins on the heat transfer performance of a LHS system. It was concluded that the heat transfer rate increases with an increase in fin thickness and a decrease in fin pitch.
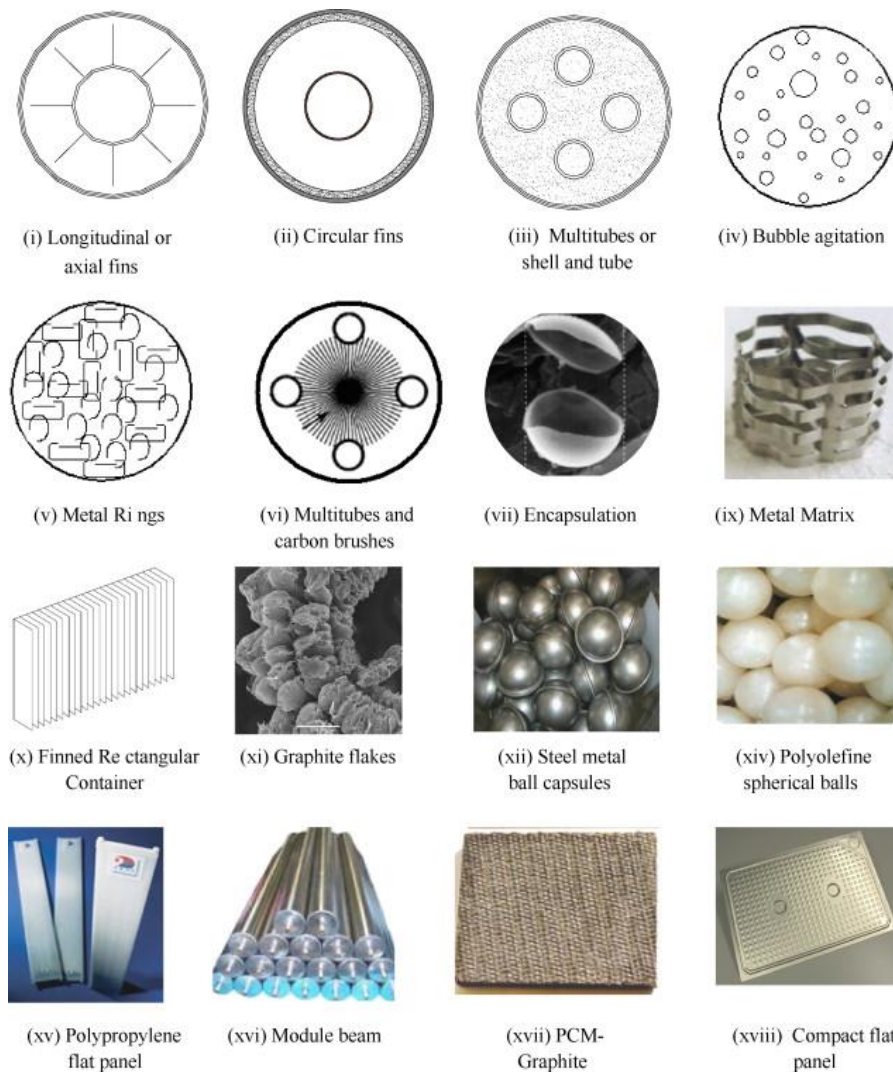
Figure 2.9　　　Summary of heat transfer enhancement techniques for LHS systems (Agyenim et al., 2010)

2.5   PCM Enhanced Water Tank

Among various applications, PCMs were also investigated for use in domestic hot water tank to enhance its thermal performance.

In relevant studies by Mehling et al. (2003), Cabeza et al. (2006), and Mazman et al. (2009), modules containing PCM were added at the top of a hot water tank with stratification (Figure 2.10).
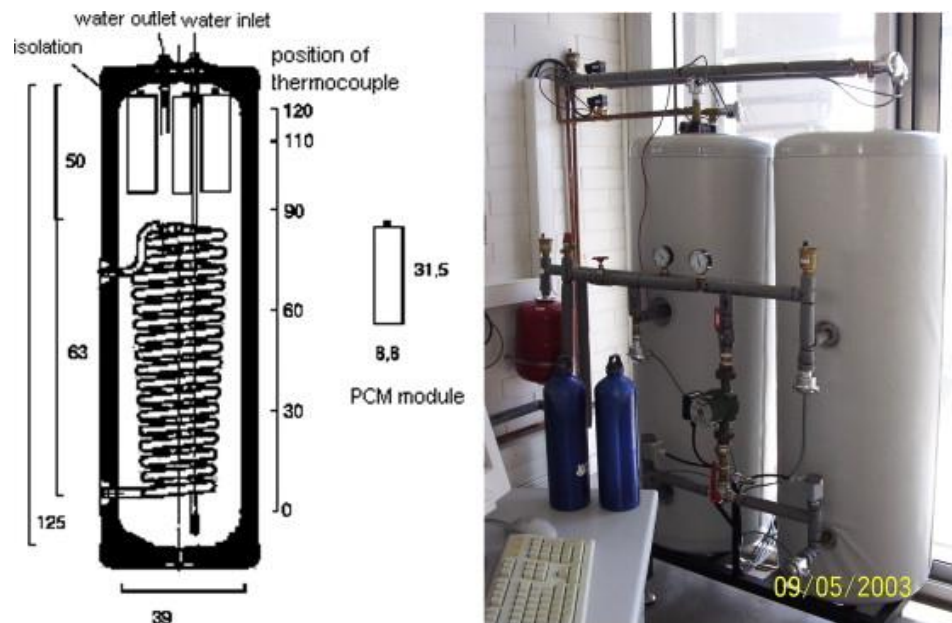
Figure 2.10   PCM modules at the top of the water tank (Mazman et al., 2009)

Through a series of experiments and simulations, Mehling et al. (2003) identified the advantages of adding PCM modules in a water tank, which are summarized as:

1)   The heat storage capacity of the water tank can be enhanced by adding PCM modules;

2)   The heat loss from the water tank can be compensated by the latent heat in the PCM modules; and

3)   The PCM modules can reheat the tank water after being partially unloaded.

Cabeza et al. (2006) conducted an experimental study to investigate the PCM's thermal behavior in a PCM enhanced water tank. It was found that the inclusion of PCM modules can allow hot water to stand for a longer period of time even without exterior energy supply, or to use smaller tanks for the same purpose. Mazman et al. (2009) compared the thermal performance of a PCM enhanced water tank when different organic PCMs were employed. It was found that a paraffin/stearic acid mixture gives the best results for thermal performance enhancement. It was also reported that the use of PCM can enhance the water tank's energy storage density and compensate the heat loss from the water tank.
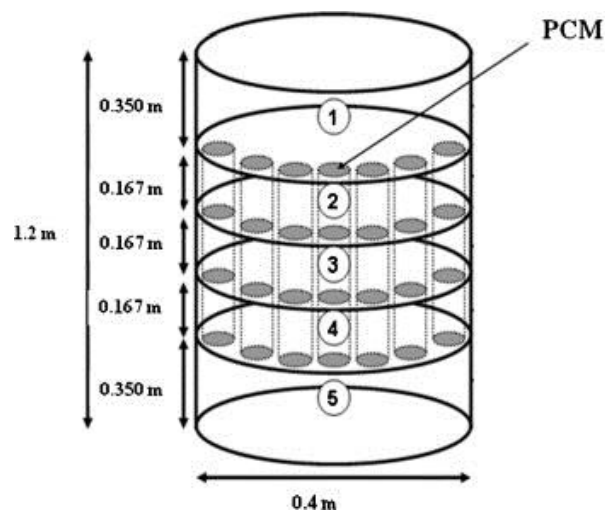
Figure 2.11   PCM modules at the middle of the water tank (Kousksou et al., 2011)

In other relevant studies, PCM modules were placed at the middle of a hot water tank (Figure 2.11). Kousksou et al. (2011) developed a detailed mathematical model for a solar heating system, in which a PCM enhanced water tank is used for storage of solar heating energy. It was found that the system's performance is highly sensitive to the first order design parameters (e.g. PCM's melting temperature). Therefore, a mathematical optimization is highly recommended in the early stage of the design process. Canbazoglu et al. (2005) carried out an experimental study on the thermal performance of a PCM enhanced water tank coupled with solar heating. It was reported that the overall system performance can be improved by the use of PCM. To understand the heat transfer between the PCM modules and water, Castell et al. (2008) developed a series of regression models to relate the natural heat transfer coefficient with PCM modules' geometry. It was found that the presence of fins on the external surface of a PCM module can significantly enhance the heat transfer. The temperature difference needed to achieve a certain natural heat transfer coefficient can also be reduced. A finite volume based numerical model describing the heat transfer during charging and discharging of a PCM enhanced water tank was developed by Gracia et al. (2011). Based on the model, a parametric study was carried out to optimize the PCM distribution inside the water tank.

2.6   Research Gaps

As discussed above, water heating utilizing rejected condenser heat from a refrigeration cycles is an energy efficient measure for domestic hot water production due to the associated EF is always higher than unity. On this basis, HPWH was

widely investigated for use in residential buildings. However, a majority of previous studies focused only on its heating capacity at the condenser. The cooling performance at the evaporator under various operation conditions was seldom studied. This is because HPWHs are often used as stand-alone water heating appliances with evaporator leaving air discharged to outdoors and thus the associated cooling effect is unexploited. Economic barrier also exists to limit its use in residential buildings, since a considerable investment must be made in the heat pump by the user. Therefore, a technology that allows a room air-conditioner to serve the combined purpose of space cooling and water heating is preferred, due to the fact that air-conditioners are commonly equipped in Hong Kong households to combat the hot and humid summer. However, considering the differences between a heat pump and a room air-conditioner, relevant research works are limited in public domain.

In view of this, a storage-enhanced heat recovery room air-conditioner (SEHRAC) is proposed in this study. This installation can serve the purpose of combined space cooling and water heating, and is particularly suitable for applications in subtropical regions.

In a SEHRAC, same as other refrigeration systems, expansion device is one of the most important components. As operation of SEHRAC can lead to significant refrigerant pressure fluctuations, the selection of a suitable type of expansion device that can function properly despite the fluctuations is very important.

Previous relevant works on comparing the use of CT and TEV mainly focused on heat pump water heaters (HPWHs) and conventional room air-conditioners (CRACs). It was revealed that whether CT or TEV is better depends largely on the associated operation characteristics of a refrigeration system. Therefore, previous studied results are not applicable to SEHRAC because its operation characteristics differ largely from HPHW and CRAC. In a HPHW, the water delivered to the condenser is usually tap water with very little variation in temperature throughout the year. Similar condition also applies to CRAC in the cooling months. While for SEHRAC, due to the heat recovery occurred in the water tank, the tank water temperature is highly fluctuating, varying between $25^{o}C$ and $55^{o}C$.

Further, despite many studies have been done on PCM enhanced water tank, a majority of them focused on its performance in isolation from other system components or performance when coupled with solar heating. There is virtually no study to date that enables an evaluation of its performance when integrated with a refrigeration system.

To fill the research gaps, the effectiveness, energy performance, operation characteristics, and performance improvement (by the use of PCM) of SEHRAC when used for combined space cooling and water heating will be investigated in this study based on both simulation and experimental evaluations.

CHAPTER 3

METHODOLOGY

This chapter presents the research methodology adopted in this study for investigating the effectiveness, energy performance, operation characteristics, and performance improvement of SEHRAC when used for combined space cooling and water heating. The investigations, as explained below, are based on both simulation and experimental studies.

3.1   Building Energy Simulations

For evaluating the amount of recoverable heat and thus the effectiveness of using SEHRAC for water heating, a series of simulations were performed to ascertain the space cooling loads and air-conditioner energy use of carefully selected units in a typical residential estate in Hong Kong. The space cooling loads were predicted by using HTB2 (Alexander, 1996), while the air-conditioner energy use for offsetting the loads was obtained from BECRES (Yik, 2000). The simulation package (HTB2 and BECRES) was adopted due to its popularity in Hong Kong since the introduction of HK-BEAM in 1996 (Centre of Environmental Technology, 1999). Previous evaluations indicated that it is in compliance with ASHRAE Standard 140 (ASHRAE, 2011) and is considered to be equivalent to DOE-2 (Winkelmann et al., 1993). Further, considering the high building density in Hong Kong, the inter-

shadowing effect among building blocks was taken into account in the simulations by using ECOTECT (Marsh, 2010). Brief descriptions of the computer programs are given below. A flowchart illustrating their integration in this simulation study is shown in Figure 3.1.
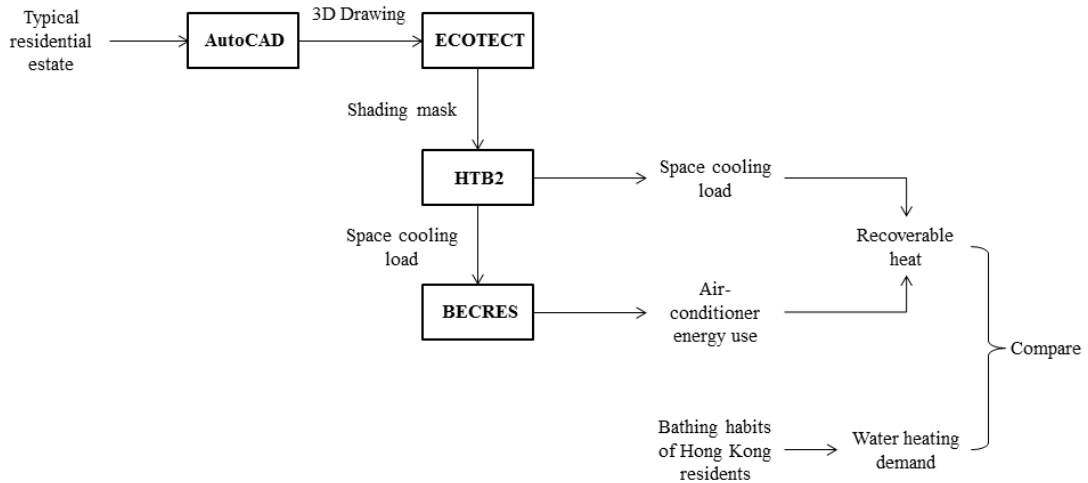
Figure 3.1 Flowchart of the simulation study

3.1.1 ECOTECT Simulation

To account for the inter-shadowing effect among building blocks, the shading mask (a mechanism that records which parts of the sky are obstructed from a particular point in a building) concept was adopted (Alexander et al., 1997). The building design simulation software ECOTECT was used to calculate the shading mask in this study.

For a given set of obstacles, the shading mask of a position is the fraction of un-shaded area of the sky vault at that position which can be represented as follows:

$$SMK_i = \frac{Area_{us}}{Area_t} \qquad\qquad (3.1)$$

where SMK_i is the shading mask of the target surface for sky vault position i; $Area_{us}$ is the un-shaded area of the target surface for the sky vault position (m^2); $Area_t$ is the total area of the target surface (m^2).

In preparation for the ECOTECT simulation, a scaled 3D model of the studied residential estate was drawn by using AutoCAD (Autodesk, 2004). On exporting the AutoCAD file to ECOTECT, a shading mask table was generated for each window surface. Based on the obtained shading mask tables, HTB2 could take into account the inter-shadowing effect in cooling load predictions.

3.1.2 HTB2 Simulation

HTB2 is a detailed dynamic building heat transfer simulation program, in which a building is modeled as a series of spaces linked to each other and to the outside by building elements (walls, windows, etc.). The simulation is driven by outdoor conditions, by heating/cooling systems and by a network of incidental heat sources. The approach adopted in HTB2 to represent the complex set of interactions, which constitute the thermal behavior of a building, is to divide time into discrete intervals and to assume that, within a time interval or time-step, each heat transport mechanisms remain constant and independent of each other (Wan, 2003). At the end of each time-step, a new set of conditions is calculated based on the accumulative effects of these heat transports. These new values are in turn held constant for the

duration of the next time-step and the cycle repeated for the duration of the simulation run.

This simplified idea underlying HTB2 may be regarded as an extension of the assumptions on which the explicit finite difference approximation of fabric heat flow is based, to cover the full range of thermal processes in a building. The length of the time-step used, however, must be small, which is effectively dictated by the stability criteria for the fabric transport modelling procedure and would normally be less than one minute (Wan, 2003). The structure of HTB2 has been developed to take advantage of this short time-step so that, for instance, heat sources may be altered or data can be output at this time scale.

A special Hong Kong Version of HTB2 is available, which is capable of modelling 100 spaces and allow the space cooling loads and the outdoor conditions to be grouped and written to files designated by the user, in a format that can be used directly as input files for BECRES. The subroutines or modules of HTB2 are organized into three levels to facilitate program management.

The top level module is the main program responsible for managing the data input, the simulation itself, and the output modules. The input contains information necessary for the management of the simulation run, such as the length of time-step, type of output data and format, and whether to enable individual subroutines in a simulation run.

The second level subroutines are divided into two groups. The first group reads the input data files, sets initial values, maintains the clock and updates the database at the end of each time-step. The second group covers the processes such as fabric transport, internal radiative exchange, outdoor conditions, insolation, ventilation, incidental gains, scheduling event, space sensible and latent heat balance. The input contains general data on each of the main subsystems.

The third level subroutines consist of specific algorithms for the calculation parts of the operation for which the calling subroutine is responsible. The input contains definition data required for a simulation run such as the physical parameter properties of building elements.

3.1.3 BECRES Simulation

BECRES is a computer simulation program functions to predict the air-conditioner energy use in residential buildings (Yik, 2000). BECRES, however, does not include a simulation routine for the prediction of the space cooling loads of various air-conditioned rooms, but relies on HTB2 to provide such predictions, and the two are to be used as a simulation package.

BECRES includes a Windows front-end program to facilitate data input and program execution. The input data can be saved in the form of text files, which can be retrieved later, modified if required, for further simulation runs.

The performance model incorporated in BECRES for predicting the air-conditioner energy use is shown in the following equations (Yik, 2000):

$$Q_{cl,nor} = \frac{Q_{cl}}{Q_{cl,rated}} = A_1 + A_2 T_{od} + A_3 T_{id} \tag{3.2}$$

$$W_{nor} = \frac{W}{W_{rated}} = A_4 + A_5 T_{od} + A_6 T_{id} \tag{3.3}$$

where $Q_{cl,nor}$ and W_{nor} are the normalized cooling output and compressor power (kW); Q_{cl} and W are the actual cooling output and compressor power (kW); T_{od} and T_{id} are the simultaneous outdoor and indoor temperatures (^{o}C); $Q_{cl,rated}$ and W_{rated} are the rated cooling capacity and compressor power (kW); A_1 to A_6 are regression coefficients that can be found in Chapter 4.

3.2   Laboratory Experiments

For assessing the performance characteristics of SEHRAC, a prototype was setup and tested in a test facility located at The Hong Kong Polytechnic University. Experimental conditions were carefully determined to simulate the conditions that SEHRAC may encounter in practical situations. In the experiments, the operating parameters on the refrigerant, air and water sides of the prototype were closely monitored. Descriptions of the test facility, prototype design, and measuring instruments used are presented below.

3.2.1 Test Facility

The test facility comprised two completely insulated and separated environmental chambers resembling indoor and outdoor conditions. Each chamber measured 3.9 m in length, 3.8 m in width and 2.2 m in height, which was constructed in conformity with ASHRAE Standard 16 (ASHRAE, 1983) for rating of room air-conditioners.

The outdoor chamber was conditioned by a built-in air-conditioning system (BIACS) and was provided with a set of sensible and latent load generation units (LGUs). The indoor chamber was provided with another set of LGUs.
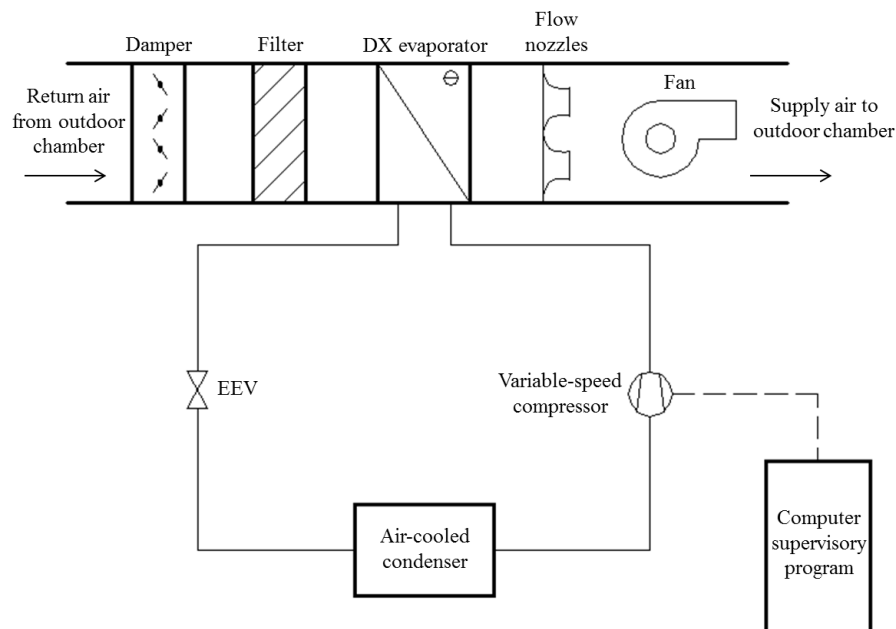
Figure 3.2   Schematic of the BIACS

The BIACS mainly consisted of a direct expansion (DX) chiller, an air supply fan, a well-insulated air-duct, and other relevant fittings. Its schematic is shown in Figure 3.2. The DX chiller had a variable-speed compressor, of which the specifications are indicated in Table 3.1. An electric expansion valve (EEV) was used to maintain a

desirable refrigerant superheat at the evaporator outlet. Other relevant devices, such as oil separator, refrigerant receiver, and overloading protections, were also provided (but not shown in Figure 3.2) to ensure robustness of the DX chiller. The chiller had a nominal cooling capacity of 9.9 kW, while its actual cooling output could be varied in the range of from 15% to 110% of the nominal capacity by varying the compressor speed.

The nominal generation rates of sensible and latent heat of the LGUs were 12 kW and 4.8 kW, respectively. While the actual outputs were adjustable by using solid state relay (SSR) to vary the power input to the LGUs.

A computer supervisory program developed based on LabVIEW was adopted to regulate the outputs of the BIACS and the LGUs. The program was capable of reading air temperatures and humidities on a real-time basis from sensors located in the chambers and generating control signals for output adjustments to maintain the air conditions at pre-set values.

Table 3.1　　　Specifications of the variable-speed chiller

Model	HITACHI THS20MC6-Y
Type	Rotary
Frequency range	15 to 110 Hz
Rated capacity	9900 W at 90 Hz
Displacement	3.04 ml/rev

3.2.2　Prototype Design

To accomplish the objectives of this study, a prototype SEHRAC was designed and setup for laboratory experiments. A schematic representation and a photograph of the prototype are shown in Figures 3.3 and 3.4, respectively. It mainly comprised a split-type air-cooled air-conditioner, a heat recovery water tank, and a refrigerant-to-water heat exchanger immersed in the water tank. Table 3.2 summarizes the specifications of these key components.
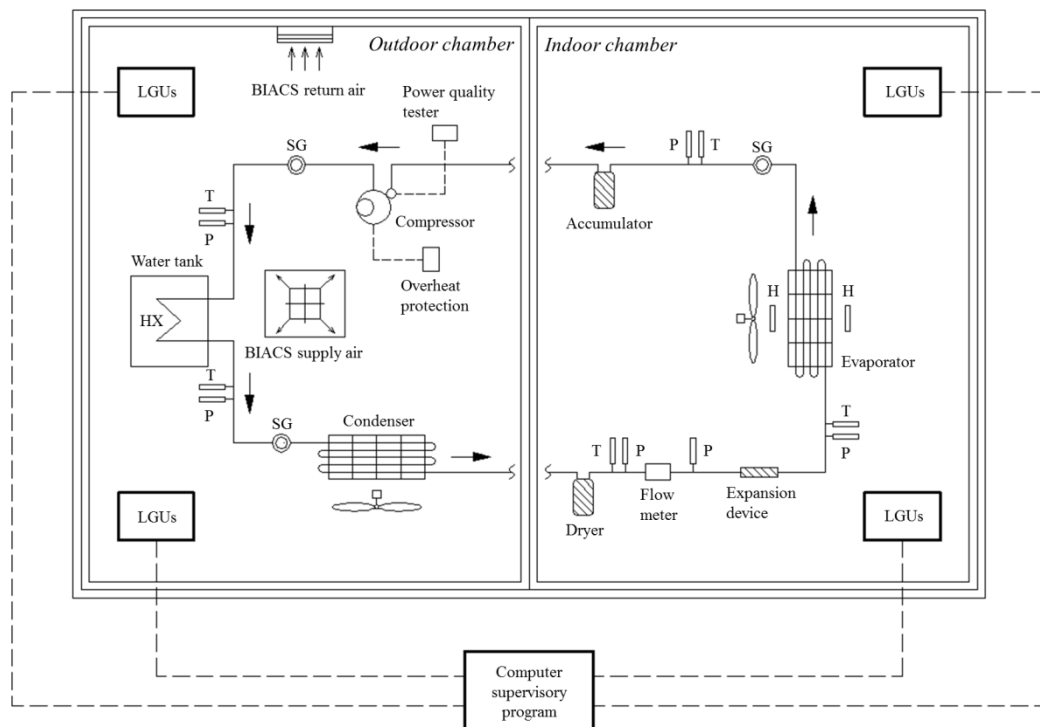
Figure 3.3   Schematic of the prototype SEHRAC

(T: Thermocouple; P: Pressure transmitter; H: Hygrometer; HX: Heat exchanger)

The split-type air-cooled air-conditioner had a nominal cooling capacity of 2.5 kW. The indoor unit was basically a DX evaporator with copper tubes and aluminum fins. The outdoor unit consisted of an air-cooled condenser and a rotary type compressor. There was no capacity control provided for the compressor. The cooling output was adjusted by intermittent operation of the compressor in accordance with the indoor

set-point temperature. A capillary tube was used as the expansion device. Non-hydroscopic insulation material was used to insulate the connecting pipings. The amount of refrigerant charged into the system was determined according to the actual piping length and the manufacturer's recommendations.

The heat recovery water tank was cylindrical in shape and contained 130 L of water. It was insulated with rock wool wrapped with a layer of aluminum foil with a total thickness of 50 mm. The maximum heat loss during the experiments was estimated to be 21 W.

The refrigerant-to-water heat exchanger was a helical coil made of copper. It was installed between the compressor and the air-cooled condenser and was immersed vertically in the water tank with top inlet to cater for the density change of vapor-liquid refrigerant.

In the prototype, the evaporator functions to absorb heat from the indoor chamber into the evaporating refrigerant. An accumulator is provided at the evaporator outlet to ensure that pure vapor refrigerant is supplied to the compressor. Subsequently, the pressure and temperature of the vapor are raised by compression, and the high pressure, high temperature vapor is discharged from the compressor into the heat exchanger for water heating. The refrigerant leaving the heat exchanger is further cooled in the condenser located in the outdoor chamber and then dried in a drier before it flows through the expansion device, where its pressure and temperature are reduced to enable the cooling of the indoor chamber.
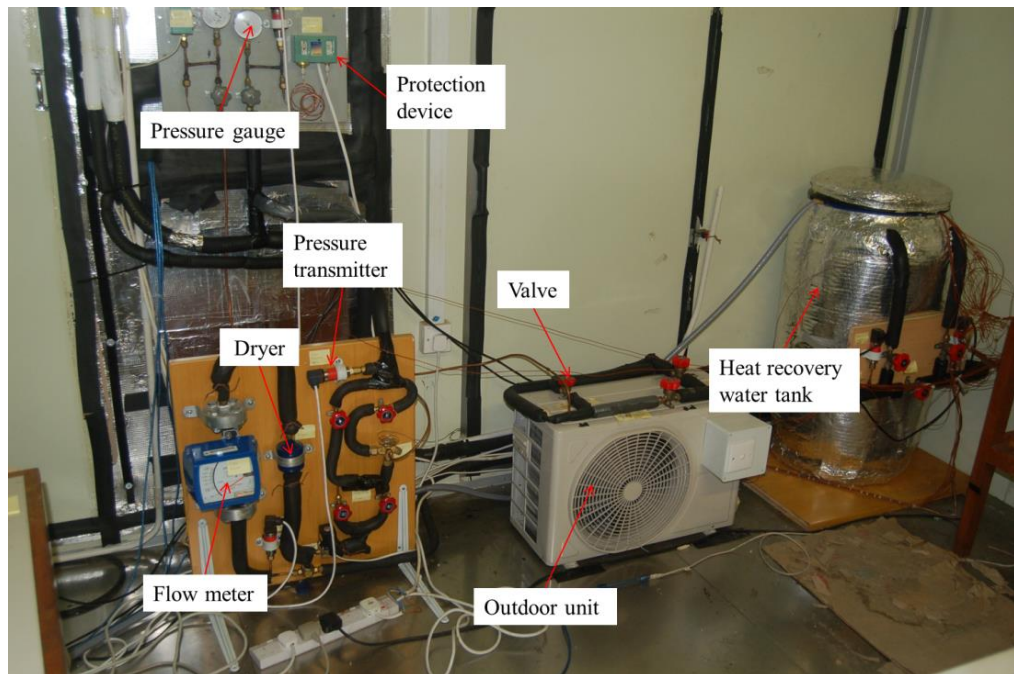
Figure 3.4   Photograph of the prototype SEHRAC

Table 3.2   Specifications of the prototype SEHRAC

Air-conditioner	
Model	Mitsubishi SRK09CMP
Nominal cooling capacity	2.5 kW
Nominal power consumption	0.925 kW
Compressor	Hermetic and rotary type
Evaporator and condenser	Copper tubes and aluminum fins
Expansion device	Capillary tube
Working fluid	R22
Heat exchanger	
Material	Copper
Tube diameter	10 mm
Total length	15.6 m
Heat recovery water tank	
Material	High-density polyethylene (HDPE)
Insulation layer	Rock wool and aluminum foil (Thermal conductivity=0.038W/m K)

Due to the incorporation of the heat exchanger into the air-conditioner, the refrigerant pipe work became exceptionally long, requiring a very large amount of refrigerant. As such, to avoid over-loading of the compressor, additional safety and control devices were installed. Enormous efforts were therefore made in adjusting the sensitivities of these devices to ensure robustness of the prototype and continuity of the experimental study during the lengthy study period.

To enable an optimization of system configuration of SEHRAC, a thermostatic expansion valve was also installed on the prototype. The capillary tube and the expansion valve were parallel-connected on a manifold feeding the evaporator. They could be alternatively activated by the gate valves provided, thus enabling the direct comparison of their performances under the same experimental conditions. Detailed specifications of the expansion valve used are given in Chapter 6.

Further, for improving the performance of SEHRAC, a container filled with phase change material (PCM) was immersed in the water tank to enhance the tank's heat storage capacity. Detailed specifications of the PCM used and dimensions of the PCM container are given in Chapter 7.

3.2.3   Measuring Instruments

In the experiments, the operating parameters on the refrigerant, air and water sides of the prototype were closely monitored. The measuring instruments used in this study and their corresponding accuracies are summarized in Table 3.3. The refrigerant

temperatures were measured by calibrated thermocouples (K type). The refrigerant high and low side pressures were measured by pressure transmitters of appropriate ranges for minimizing the measurement error. The refrigerant flow rate was measured by a variable area flow meter installed between the air-cooled condenser and the expansion device. The pressure drop across the flow meter was measured (= 2.1 kPa). It was much lower than the ASHRAE's recommended limit of 82.7 kPa to confirm fulfilling the accuracy requirement (ASHRAE, 2010). The evaporator return and supply air conditions were measured by hygrometers. The supply air flow rate was measured by thermal anemometers. The hygrometers and the thermal anemometers were positioned according to the distribution method recommended by British Standard 5141 (BSI, 1975). The water temperatures at various radial and axial positions in the water tank were measured by Pt100 RTDs. The power consumption of the prototype was measured by a power quality tester.

Table 3.3   Summary of the measuring instruments

Instrument	Model	Measurement range	Accuracy
Hygrometer	ROTRONIC HygroFlex	-40 ^{o}C to 85 ^{o}C 0 to 100% RH	±0.1 ^{o}C ±1% RH
Thermal anemometer	E+E 70-VT62B5	0 to 5 m/s	±2% F.S.
Pt100 RTD	Omega 1/10 DIN	-100 ^{o}C to 400 ^{o}C	±0.05 ^{o}C
Thermocouple	Omega TT-K-24	0 ^{o}C to 1250 ^{o}C	±0.1 ^{o}C
Pressure transmitter	Danfoss AKS	-0.1 MPa to 1.2 MPa -0.1 MPa to 3.4 MPa	±0.3% F.S.
Variable area flow meter	KROHNE H250/RR/M9	0 to 3.2 L/min	±1.6% F.S.
Power quality tester	ISO-TECH IPM-3005	0.01 kW to 9.999 kW	±20 W

All the instruments used were connected to two data loggers (Agilent 34970A), which allowed all measured data to be real-time monitored, recorded and processed. In the experiments, the measurements were taken at a short time interval of 5-second to better capture the dynamic variations in operating parameters of the prototype.

CHAPTER 4

ANALYSIS OF EFFECTIVENESS OF USING SEHRAC

IN RESIDENTIAL BUILDINGS IN HONG KONG

For the application of SEHRAC, a major concern is whether or not the amount of recoverable heat can meet the household water heating demand. Another barrier is the need to use a water tank for thermal energy storage, due to the fact that space is always a concern in Hong Kong. To address the concerns, this chapter presents a detailed supply and demand analysis on the use of SEHRAC in a typical residential estate in Hong Kong. Further, for optimal design of the water tank, its design requirements including the minimum required heat storage capacity and heat transfer effectiveness were also determined and discussed.

4.1   Introduction

For the application of SEHRAC, whether or not the amount of recoverable heat can meet the household water heating demand to achieve the water heating objective is a major concern. The concern is particularly prominent in Hong Kong because most local residential units are small but the occupancy density is high. The small space cooling load and thus the small amount of recoverable heat may not be sufficient to offset the high water heating demand. Further, the need to use a water tank for

thermal energy storage is also a barrier to the wide adoption of SEHRAC, considering that space is always a concern in Hong Kong. To address the concerns, an accurate and precise prediction of recoverable heat and water heating demand, together with the water tank design requirements for achieving its optimal design, are necessary.

In this study, for providing such information, a typical residential estate in Hong Kong was chosen for a detailed supply and demand analysis. In the analysis, the space cooling loads and air-conditioner energy use of selected residential units were carefully determined by building energy simulations taking into account the inter-shadowing effect among building blocks, the realistic building characteristics, as well as the daily patterns of occupant activity, internal load and air-conditioner utilization. On this basis, the recoverable heat of each studied residential unit was determined and then compared against the water heating demand. Further, for optimal design of the water tank of SEHRAC, its design requirements were also determined and discussed.

4.2   Simulation Study

4.2.1   Case Study Estate

A public housing estate of Harmony One design (at Tseung Kwan O, Hong Kong) consisting of 16 blocks was chosen as the case study estate (Figure 4.1). It was chosen because over 30% of the population in Hong Kong resides in this type of

housing blocks, and it is a standard design adopted by most newly developed public housing estates (Housing Authority, 2015). Each housing block in the estate is of 40-floor and has 20 units per floor. Among the 16 blocks, Building A is surrounded by other building blocks from almost all directions to increase the inter-shadowing effect and thus lowering the space cooling load. Accordingly, Building A is considered the worst scenario for having the lowest recoverable heat and was chosen as the case study building block.
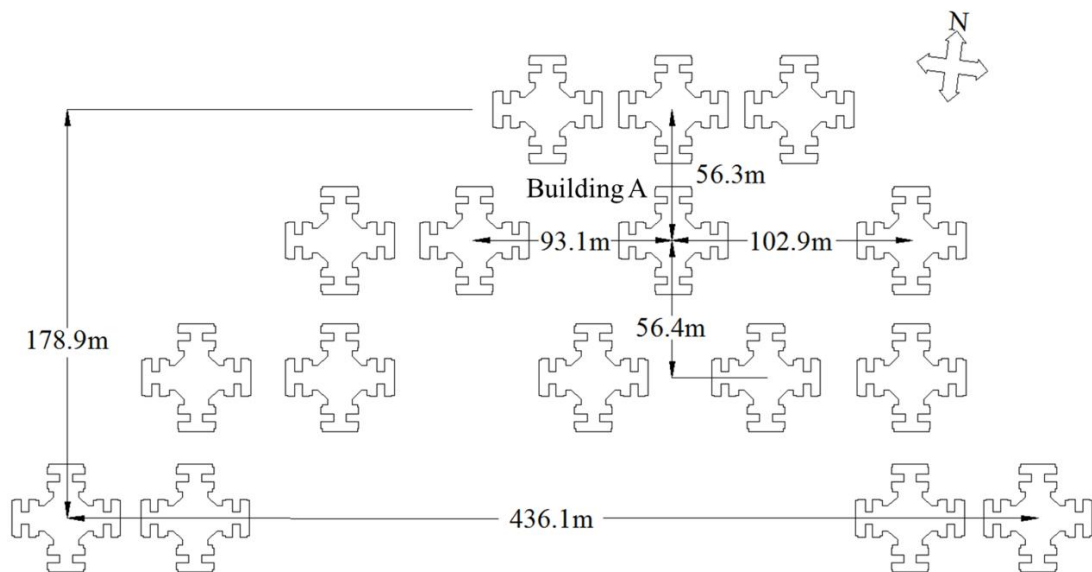
Figure 4.1   Schematic of the case study estate

The typical floor layout of Building A is shown in Figure 4.2, illustrating that there are four wings on each floor (denoted as A-D), and each wing comprises five units (denoted as 1-5). The units can be grouped into three types: studio unit (denoted as 1P), one-bedroom unit (denoted as 1B), and two-bedroom unit (denoted as 2B). Each unit is provided with one bathroom and one kitchen. Each habitable room (i.e. living/dining room and bedroom) of a unit has one external window, except for units A1, A3, C1 and C3, of which the living/dining room has two external windows.

According to the allocation standard for public housing (Housing Authority, 2015), the studio unit is for one person, the one-bedroom unit is for a family of two, and the two-bedroom unit is for a family of four. This corresponds to an average living space of 15.6, 16.8 and 10.4 m^2/person, respectively, with the two-bedroom unit having the densest living condition.
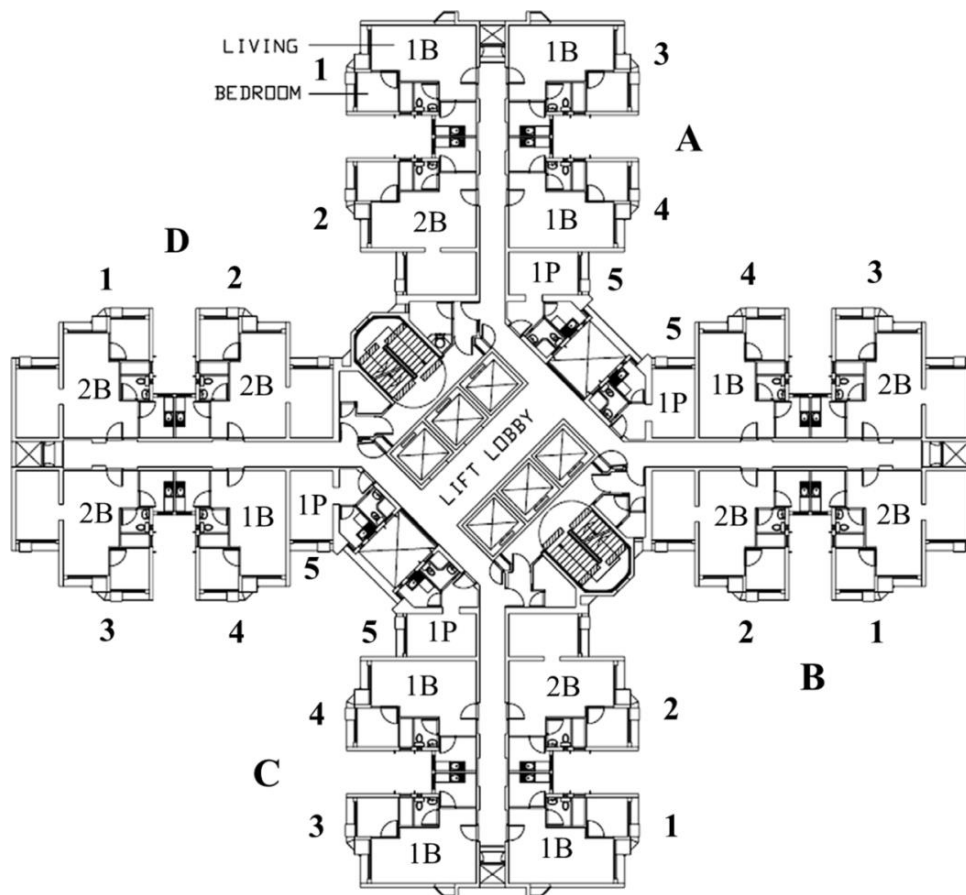
Figure 4.2   Typical floor layout of Building A

To account for the thermal inertia of building envelope in response to intermittent operation of air-conditioners and highly variable outdoor conditions, the actual building construction details, which are typical for public housing estates in Hong Kong (Housing Authority, 2015), were used in this simulation study.

4.2.2   Energy End-Use Characteristics

To enable an accurate and precise space cooling load prediction, references were made to residential energy end-use characteristics reported in various sources (Lam, 1993; Wan and Yik, 2004; BEAM Society, 2010). These include installed powers and utilization patterns of various lightings and small power appliances (e.g. TV). Among them, only heat generating ones in air-conditioned space were considered. The obtained end-use characteristics are appended in Tables A.1 and A.2. In the tables, the utilization patterns of lightings and small power appliances are in fraction of their respective installed powers. The occupancy patterns, represented by a fraction of the total number of occupants of a unit, are also summarized in Tables A.1 and A.2. To enable formulating the water heating demand, the bathing habits of Hong Kong residents, including the hot water supply temperature, as well as the consumption rate and duration, are summarized in Table 4.1 (Chen and Lee, 2010).

Table 4.1   Bathing habits of Hong Kong residents

Item	Range	Average
Hot water supply temperature (^{o}C)	32 to 50	40.4
Hot water consumption rate (kg/s)	0.096 to 0.168	0.133
Hot water consumption duration (minutes)	6 to 10	8

For air-conditioning, it was assumed that all habitable rooms of a unit are provided with independent air-conditioners sized for satisfying the peak cooling loads of corresponding rooms. The air-conditioned season was assumed to be from April 1 to October 31, during which the air-conditioners are utilized according to the patterns

indicated in Tables A.1 and A.2, while outside the air-conditioned season, they were assumed to be left idle.

4.2.3 Space Cooling Load and Air-Conditioner Energy Use Predictions

The hourly space cooling loads of residential units were predicted by using HTB2 (Alexander, 1996). HTB2 has been subjected to third party validations to confirm its predictions are within an acceptable error band (Lomas et al., 1997). The energy use of air-conditioners for offsetting the space cooling loads was determined by using BECRES (Yik, 2000). BECRES functions as a post-processor for HTB2 and is used specifically for application to residential buildings that utilize room air-conditioners for space cooling. Detailed descriptions of HTB2 and BECRES can be found in Sections 3.1.2 and 3.1.3. An empirical model, as shown in Equations (3.2) and (3.3), is used by BECRES for describing the energy performance of air-conditioners. The coefficients in the model were determined from regression analysis of experimental data and are summarized in Table 4.2 (Wan, 2003). The accuracy of BECRES simulations has been confirmed by Chen et al. (2008).

Table 4.2   Summary of regression coefficients in Equations (3.2) and (3.3)

A_1	0.7651
A_2	-0.0086
A_3	0.0199
A_4	0.0320
A_5	0.0191
A_6	0.0102

4.2.4   Inter-Shadowing Effect Analysis

To account for the inter-shadowing effect introduced by other blocks on Building A, the shading mask (a mechanism that records which parts of the sky are obstructed from a particular point in a building) concept was adopted in this study (Alexander et al., 1997). For a given set of obstacles, the shading mask of a position is the fraction of un-shaded area of the sky vault at that position (Equation (3.1)) (Chapter 3).

In this study, ECOTECT was adopted to evaluate the shading mask at windows of each residential unit on every 20th floor of Building A. Accordingly, there were three floors (i.e. 1st, 20th and 40th floors) and 44 air-conditioned rooms per floor, making a total of 144 windows for shading mask calculations. In preparation for the ECOTECT simulation, a 3D model of the case study estate was drawn by using AutoCAD. On exporting the AutoCAD file to ECOTECT, a shading mask table was generated for each window surface. Based on the obtained shading mask tables, HTB2 can take into account the inter-shadowing effect in cooling load predictions.

4.3   Results and Discussion

4.3.1   Inter-Shadowing Effect

In this study, the inter-shadowing effect introduced by other blocks on Building A was evaluated by using the shading mask concept. In quantifying the shading mask value for a solar position, the sky vault is divided into small segments with a solid

angle of approximately 10 degrees which corresponds to 324 equal area segments (i.e. 0° to 360° from azimuth, and 0° to 90° horizon to zenith). The shading mask table generated by ECOTECT therefore comprises 36 rows and 9 columns, making a total of 324 figures. Of the 324 figures, 50% can be ignored because they correspond to sky vault positions at the back of the window surface. Further, the figures are independent and of equal importance, as they are from equal sky segments.

Figure 4.3   Inter-shadowing effect comparisons

It is therefore acceptable to use arithmetic mean of the figures to represent the average shading mask (SMK_m) of a window surface:

$$SMK_m = \frac{\sum_{i=1}^{162} SMK_i}{162} \tag{4.1}$$

The wing averaged SMK_m on the three studied floors (i.e. 1st, 20th and 40th floors) of Building A were then calculated to enable a comparison of inter-shadowing effect among different wings and floors. Results are summarized in Figure 4.3. It can be seen that the wing averaged SMK_m decreases with a decrease in floor levels, indicating a more remarkable inter-shadowing effect for lower floors. Further, among the four wings on the same floor, Wing D is most shadowed as reflected by a smaller wing averaged SMK_m as compared to other wings.

4.3.2   Space Cooling Load and Air-Conditioner Energy Use

Based on the actual construction details of Building A and the obtained shading mask tables, the annual and peak cooling loads of residential units on the three studied floors were determined from the hourly outputs of HTB2. The weather conditions used in the simulations were referred to the hourly outdoor conditions of Hong Kong in 1989, which is the typical meteorological year (TMY) for use in building energy simulations for compliance with the performance-based building energy code in Hong Kong (Electrical and Mechanical Services Department, 2007).

The annual cooling load (ACL) of a residential unit can be determined by:

$$ACL = \sum_{j=1}^{N} \sum_{i=1}^{K} \left(Q_{cl,i,j} \times 1\text{hour} \right) \qquad (4.2)$$

where $Q_{cl,i,j}$ is the space cooling load of room j on the ith hour in the air-conditioned season (kW); N is the number of air-conditioned rooms of the residential unit (=1 for

53

1P; =2 for 1B; =3 for 2B); K is the number of air-conditioned hours from April 1 to October 31.

Figure 4.4 shows the ACL of residential units on the three studied floors of Building A. It can be seen that there is a marginal increase in ACL for the 20th floor as compared to the 1st floor. This is reasonable because the inter-shadowing effect, which can reduce the solar heat gain, is more significant for the 1st floor (Figure 4.3). However, due to the additional roof area exposed to the outside environment, a remarkable increase in ACL is observed for the 40th floor. Furthermore, as can be seen, for the same type of unit on a floor, ACL varies with orientation.
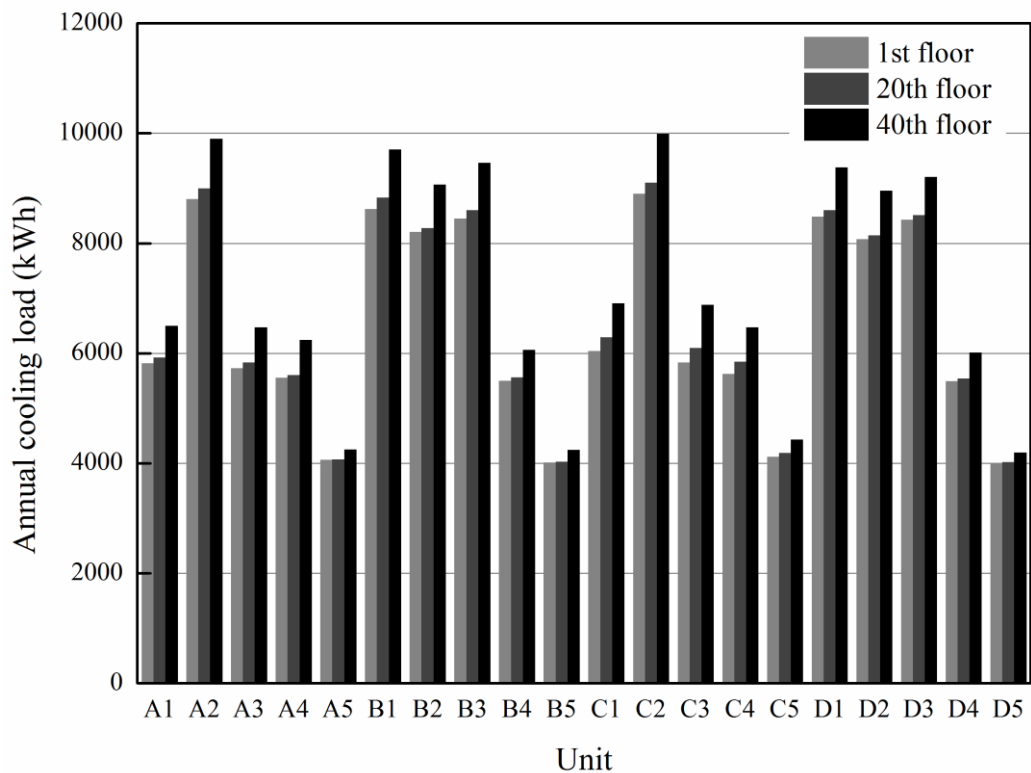
Figure 4.4 ACL of residential units on the three studied floors

BECRES was then used to determine the energy use of air-conditioners based on the obtained cooling load predictions. On this basis, the annual (total) energy

consumption (*AEC*) of all air-conditioners in a residential unit was calculated. Results are shown in Figure 4.5. It is reasonable to observe that units with higher *ACL* have greater *AEC*. It can also be seen from Figures 4.4 and 4.5 that units D2, D4 and D5 have the lowest *ACL* and *AEC* among their respective unit types (2B, 1B and 1P). This is because these units are located at recessed space of the wing, and Wing D is most influenced by the inter-shadowing effect as revealed in Figure 4.3.
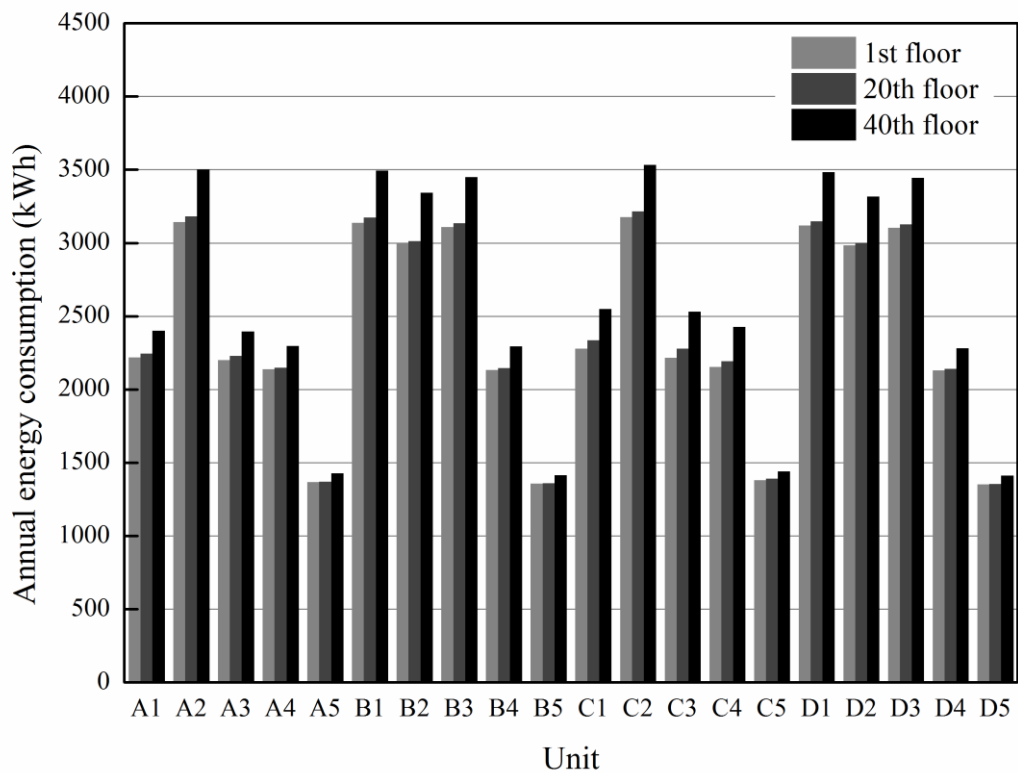
Figure 4.5   *AEC* of residential units on the three studied floors

Table 4.3   Simulation results for the three representative residential units

Characteristic	Unit					
	D2			D4		D5
	BED1	BED2	LDRM	BED	LDRM	BED
ACL (kWh)	2562.3	2824.6	2753.8	2579.6	2959.6	4020.5
AEC (kWh)	985.0	1056.0	958.2	989.5	1150.7	1353.9
Peak load (kW)	0.99	1.14	2.37	0.99	2.60	3.13

Therefore, as far as condenser heat recovery is concerned, units D2, D4 and D5 on the ground floor (i.e. 1st floor), which have the smallest space cooling load among their respective unit types, were considered as the worst scenario and thus chosen as the representative residential units for subsequent analysis. Their space cooling load and air-conditioner energy use characteristics are summarized in Table 4.3.

4.3.3   Recoverable Heat and Water Heating Demand

Two possible designs for condenser heat recovery from room air-conditioners were identified and evaluated in this study. The first is SEHRAC, of which the schematic is shown in Figure 3.3. The second is a tank-less SEHRAC (referred to as HRAC). Due to the absence of water tank, HRAC relies on a tube-in-tube heat exchanger to enable heat transfer between compressor discharged refrigerant and water. Therefore, HRAC can only provide space cooling and water heating on a simultaneous basis.

For assessing the effectiveness of using HRAC, the instantaneous water heating demand and recoverable heat need to be determined. The instantaneous water heating demand ($Q_{hd}(\tau)$) can be quantified by:

$$Q_{hd}\left(\tau\right) = m_{hw}c_{p,w}\left[T_{hw} - T_{tw}\left(\tau\right)\right] \tag{4.3}$$

where m_{hw} is the hot water consumption rate (kg/s); $c_{p,w}$ is the water specific heat capacity (kJ/kg K); T_{hw} is the required hot water supply temperature ($^{\circ}$C); $T_{tw}(\tau)$ is the tap water temperature at time τ ($^{\circ}$C).

To determine the tap water temperature, the following equation relating $T_{tw}(\tau)$ with outdoor temperature ($T_{od}(\tau)$) can be used (Chen and Lee, 2010):

$$T_{tw}(\tau) = -0.0156T_{od}^2(\tau) + 1.2683T_{od}(\tau) + 4.6356 \qquad (4.4)$$

Based on Equations (4.3) and (4.4), $Q_{hd}(\tau)$ of the three representative units (i.e. D2, D4 and D5 on the ground floor) can be determined. Unit D2, being a two-bedroom unit with the densest living condition, has the highest $Q_{hd}(\tau)$, ranging between 6.115 kW and 9.739 kW in the air-conditioned season.

The maximum recoverable heat from condenser ($Q_{wh}(\tau)$) can be determined based on the first law of thermodynamics, which is the sum of simultaneous cooling output ($Q_{cl}(\tau)$) and compressor power ($W(\tau)$):

$$Q_{wh}(\tau) = Q_{cl}(\tau) + W(\tau) \qquad (4.5)$$

where $Q_{cl}(\tau)$ and $W(\tau)$ can be obtained from HTB2 and BECRES simulations.

In accordance, $Q_{wh}(\tau)$ of the three representative units can also be determined. Figure 4.6 shows the profiles for $Q_{wh}(\tau)$ of unit D2 on the minimum (April 10) and peak (July 17) cooling days. In the figure, $Q_{wh}(\tau)$ of bedroom air-conditioner (Bedroom 2 for having a higher $Q_{wh}(\tau)$) and living/dining room air-conditioner are separately illustrated.

It is evident from Figure 4.6 that the amount of recoverable heat ($Q_{wh}(\tau)$) is constantly lower than the simultaneous water heating demand ($Q_{hd}(\tau)$) on both minimum and peak cooling days, indicating that the use of a HRAC to provide simultaneous space cooling and water heating is not feasible in Hong Kong households.
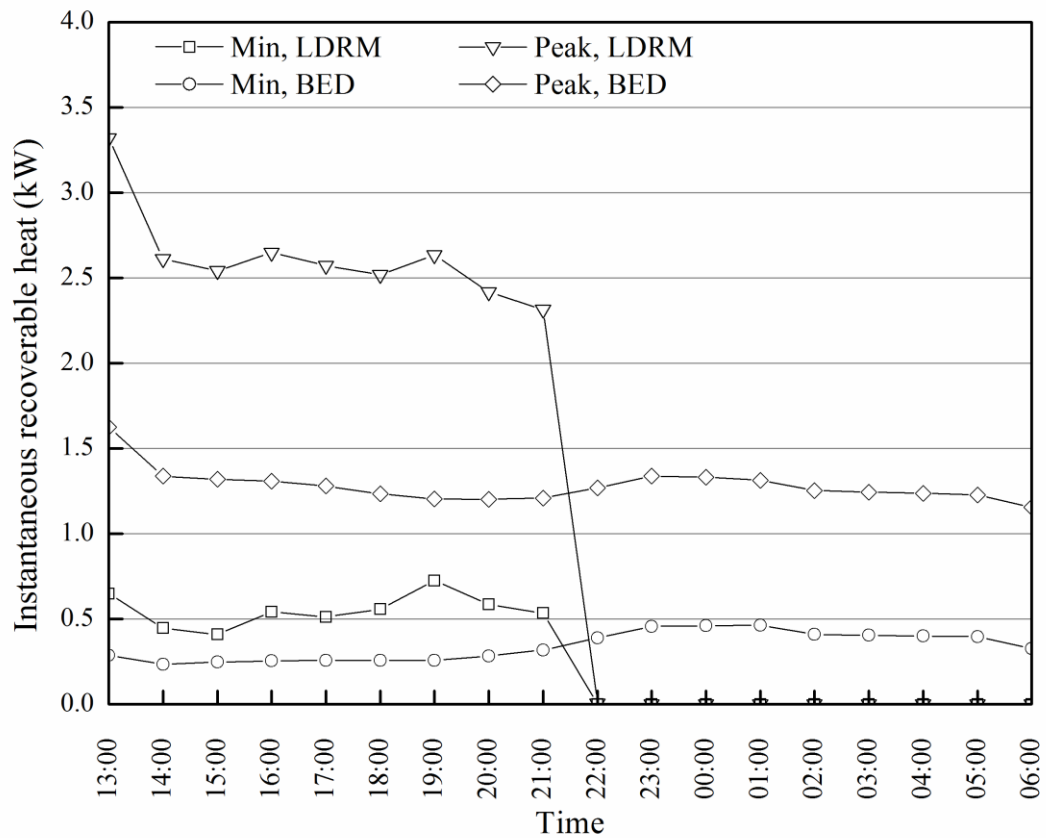
Figure 4.6   Instantaneous recoverable heat of unit D2

(Min: Minimum cooling day; Peak: Peak cooling day)

For assessing the effectiveness of using SEHRAC in achieving the water heating objective, the cumulative recoverable heat on daily basis ($H_{wh,cum}$) was determined by Equation (4.6) for comparison against the daily maximum household water heating demand ($H_{hd,max}$).

58

$$H_{wh,cum} = \sum_{\tau=1}^{k} Q_{wh}(\tau) \times 1\text{hour} \tag{4.6}$$

where k is the number of air-conditioned hours in a day.

The household water heating demand on hourly basis ($H_{hd}(\tau)$) can be determined by Equation (4.7), if each household member takes one bath a day (Chen and Lee, 2010).

$$H_{hd}(\tau) = Q_{hd}(\tau) \times HR \times HS \times UF(\tau) \tag{4.7}$$

where HR is the hot water consumption duration in hour; HS is the household size (=1 for 1P; =2 for 1B; =4 for 2B); $UF(\tau)$ is the hourly hot water utilization factor defined as a fraction of the daily hot water consumption (=$HR \times HS$).

Accordingly, $H_{hd,max}$ occurs at the hour when the corresponding outdoor temperature is the daily minimum and all household members take shower consecutively within that hour (i.e. $UF(\tau)=1$):

$$H_{hd,max} = \max_{\tau=1\sim24}\left[H_{hd}(\tau)\right] = \max_{\tau=1\sim24}\left[Q_{hd}(\tau)\right] \times HR \times HS \tag{4.8}$$

Figure 4.7 compares the profiles for $H_{wh,cum}$ and $H_{hd,max}$ of unit D2. In calculating $H_{wh,cum}$, only rejected heat from bedroom air-conditioner (Bedroom 2 for unit D2) was considered due to its longer and more stable daily operation characteristics. As can be seen, if a water tank is used to store the daily rejected condenser heat, $H_{wh,cum}$

is always sufficient to offset $H_{hd,max}$ in the entire air-conditioned season to confirm the effective use of SEHRAC in Hong Kong households. Further, due to a higher space cooling load and a smaller water heating demand, a huge surplus in heat supply (>300%) can be seen in summer months (e.g. July).
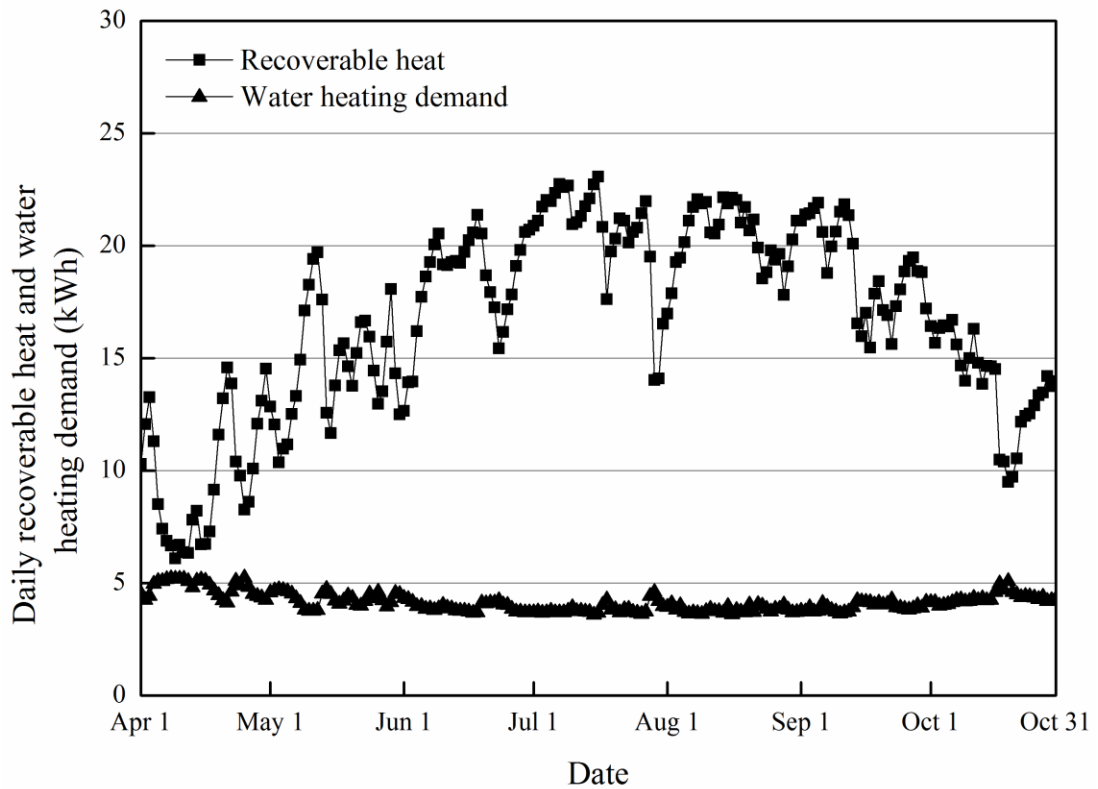
Figure 4.7   Daily recoverable heat and water heating demand of unit D2

4.3.4   Water Tank Design Requirements

For the use of SEHRAC, if completely free water heating is to be achieved in the entire air-conditioned season, the day with the minimum heat supply and the maximum heating demand was considered as the worst scenario. Therefore, to avoid under-sizing the water tank, $H_{hd,max}$ on the minimum cooling day should be taken as

its required heat storage capacity. Results are summarized in Table 4.4. As can be seen in the table, unit D5 has the highest $H_{wh,cum}$ and the lowest $H_{hd,max}$. This is reasonable because unit D5 has the highest bedroom cooling load (Table 4.3) and the lowest occupancy density (one person household).

Table 4.4   Summary of the minimum required heat storage capacities

Description		Unit		
		D2	D4	D5
Minimum cooling day	$H_{wh,cum}$ (kWh)	6.11	5.16	8.84
	$H_{hd,max}$ (kWh)	5.19	2.60	1.30
Peak cooling day	$H_{wh,cum}$ (kWh)	23.08	21.37	30.43
	$H_{hd,max}$ (kWh)	3.68	1.84	0.92
Minimum required heat storage capacity (kWh)		5.19	2.60	1.30

It should be noted that the above discussions assumed a theoretical maximum recoverable heat (the sum of cooling output and compressor power), which may not be achievable in practice. To ensure a successful use of SEHRAC, the minimum required heat transfer effectiveness between compressor discharge refrigerant and tank water needs to be evaluated. The effectiveness (ε) is defined as a ratio of actual amount of heat transfer over the maximum possible amount that can be transferred.

In this study, the actual and maximum amount of heat transfer were taken as $H_{hd,max}$ and $H_{wh,cum}$, respectively, on the minimum cooling day for determining the minimum required effectiveness (ε_{min}). It is reasonable to expect that if the water tank is designed to satisfy the minimum effectiveness requirement, the water heating objective can be achieved by the use of SEHRAC in the entire air-conditioned season.

On this basis, ε_{min} for the three representative units (D2, D4 and D5) were estimated to be 0.85, 0.50 and 0.15, respectively. It was found that ε_{min} for unit D2 is much higher, indicating special attention should be given to enhance the heat transfer performance of the corresponding water tank.

4.4   Summary

The space cooling loads and air-conditioner energy use of residential units in a typical estate in Hong Kong were carefully simulated based on the actual building construction details. On the basis of the simulation results, the recoverable heat and water heating demand profiles were formulated for three representative residential units. A comparison of the profiles indicated that in the entire air-conditioned season, the water heating objective could be achieved by the use of SEHRAC. For optimal design of the water tank to satisfy the daily household water heating demand, its design requirements including the minimum required heat storage capacity and heat transfer effectiveness were determined. The results clearly showed that SEHRAC is worthy of application even in dense living environment like Hong Kong. The space cooling load, recoverable heat and water heating demand profiles established in this study will also be useful for future studies on energy performance of SEHRAC.

CHAPTER 5

ENERGY PERFORMANCE AND OPERATION

CHARACTERISTICS OF SEHRAC: AN

EXPERIMENTAL STUDY

The effectiveness of using SEHRAC for domestic water heating in residential buildings in Hong Kong was confirmed in Chapter 4. However, given the simulation study assumed a theoretical maximum recoverable heat, whether its use is still energy effective in practice, in particular under intermittent operation, is of concern. Intermittent operation of SEHRAC can lead to significant fluctuations in operating parameters on the refrigerant side. Adding that capillary tube is often used as the expansion device to magnify the fluctuations, whether SEHRAC can still operate satisfactorily is another concern. To address the concerns, an experimental study is presented in this chapter for evaluating the energy performance and operation characteristics of SEHRAC when used for combined space cooling and water heating.

5.1   Introduction

In Chapter 4, a supply and demand analysis on the use of SEHRAC in a typical residential estate in Hong Kong was presented based on hour-by-hour simulations. It

was confirmed that the water heating objective can be achieved by the use of SEHRAC. However, considering that the simulation study assumed a theoretical maximum recoverable heat (the sum of cooling output and compressor power), which may not be achievable in practice, it is still not clear whether the use of SEHRAC is energy effective in practical situations.

Room air-conditioners are often sized for satisfying peak cooling loads. At part load conditions, most air-conditioners operate intermittently to regulate their cooling outputs for offsetting the actual space cooling load. Intermittent operation of SEHRAC will lead to reduced amount of recoverable heat, since condenser heat is only available during the compressor on-cycle. Further, as the heat rejection performance of SEHRAC is influenced by outdoor temperature, the amount of recoverable heat is also affected. Therefore, for evaluating the energy performance of SEHRAC, the influences of outdoor temperature and space cooling load need to be ascertained.

For the application of SEHRAC, another concern is the use of capillary tube as the expansion device. Despite capillary tube is widely used in small capacity room air-conditioners for economic and simplicity considerations, its feasibility when used in SEHRAC is in doubt, considering the highly fluctuating refrigerant pressures during the operation of SEHRAC. Therefore, whether SEHRAC using capillary tube can actually operate satisfactorily, in particular under intermittent operation, is subject to experimental investigations.

To facilitate the said investigations, a prototype SEHRAC was designed and setup for an experimental study. Two identical sets of experiments with and without water heating under a range of outdoor temperatures (*OT*s) and space cooling load conditions (represented by part load ratios (*PLR*s)) were conducted. In the experiments, different operating parameters on the water, refrigerant and air sides of the prototype were measured and recorded. Based on the experimental results, the space cooling, water heating and overall energy performances of the prototype, as well as its dynamic operation characteristics were evaluated. On this basis, the potential water heating energy saving on wider application of SEHRAC in Hong Kong was also assessed.

5.2   Experimental Study

5.2.1   Test Facility

The experiments were conducted in a test facility located at the Hong Kong Polytechnic University. The test facility comprised two completely insulated and separated environmental chambers resembling indoor and outdoor conditions. Detailed descriptions of the test facility can be found in Section 3.2.1.

In this study, the desired temperature in the outdoor chamber (referred to as outdoor temperature) was achieved and maintained by the BIACS and the LGUs. While the LGUs located in the indoor chamber were used to simulate various space cooling loads.

5.2.2 Prototype Design

To accomplish the objectives of this study, a prototype SEHRAC was designed and setup for laboratory experiments. Its schematic is shown in Figure 5.1. The prototype mainly consisted of a split-type air-cooled air-conditioner, a refrigerant-to-water heat exchanger and a cylindrical water tank. The indoor unit of the air-conditioner was basically a DX evaporator with copper tubes and aluminum fins. The outdoor unit consisted of an air-cooled condenser and a rotary type compressor. Detailed specifications of the prototype can be found in Section 3.2.2.
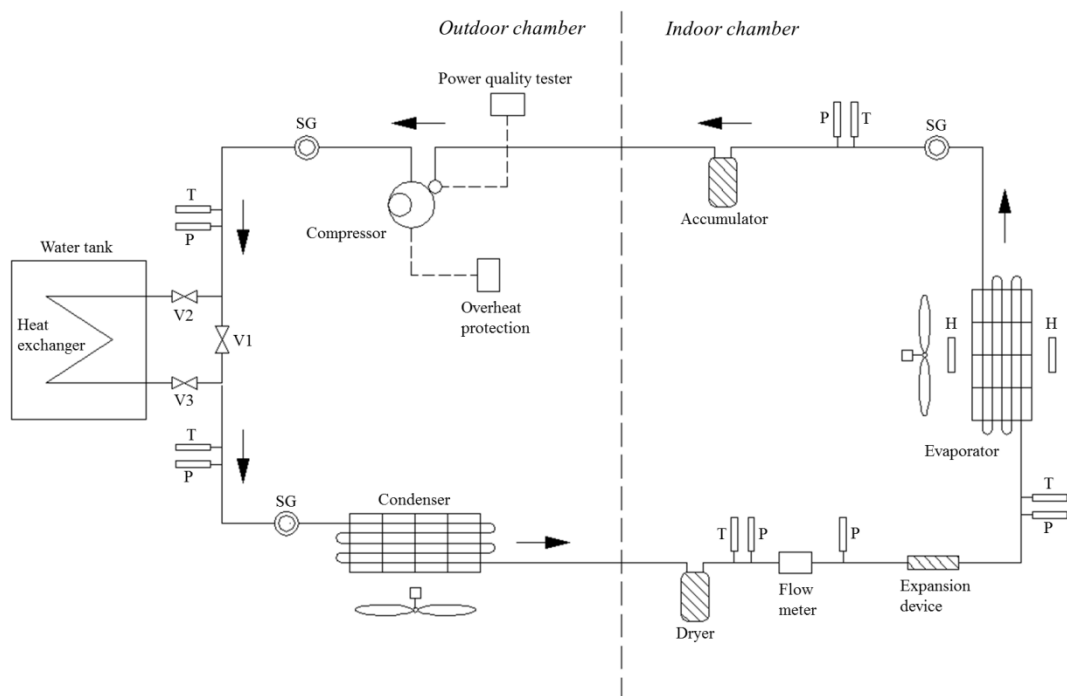
Figure 5.1   Schematic of the prototype for performance evaluation of SEHRAC
(T: Thermocouple; P: Pressure transmitter; H: Hygrometer; SG: Sight glass)

There was no capacity control provided for the compressor. The cooling output was adjusted by intermittent operation of the compressor in accordance with the indoor

set-point temperature. The original capillary tube supplied with the air-conditioner was used as the expansion device.

Between the compressor and the condenser, a by-pass line for the water tank was provided to enable switching between the combined cooling and heating (CH) mode and the conventional cooling (CC) mode. For the CH mode, valves V2 and V3 were opened while valve V1 was closed. For switching to the CC mode, V2 and V3 were closed while V1 was opened to by-pass the water tank.

5.2.3   Measurements

In the experiments, different operating parameters on the water, refrigerant and air sides of the prototype were measured and recorded. The measuring instruments used are summarized in Section 3.2.3.

5.2.4   Experimental Conditions

The experimental conditions adopted in this study were carefully determined to simulate the conditions that SEHRAC may encounter in practical situations, which were mainly based on the simulation results obtained in Chapter 4.

As SEHRAC is intended for use in bedrooms to recover the nighttime condenser heat, the cooling load characteristics, including the peak cooling load, the range of

*PLR*s, and the sensible heat ratio of the representative bedroom identified in Chapter 4 (Bedroom 2 of unit D2 in Building A, Figure 4.2), were set as the indoor chamber conditions (Table 5.1).

Table 5.1　　　Summary of the experimental conditions

Conditions		Controlled Range
Outdoor chamber	Outdoor temperature (*OT*)	25 $^{\circ}$C to 35 $^{\circ}$C (with 5 $^{\circ}$C intervals)
	Relative humidity	50%
Indoor chamber	Peak cooling load	0.99 kW
	Part load ratio (*PLR*)	0.4 to 1 (with 0.2 intervals)
	Sensible heat ratio	0.8
Tank water	Initial temperature	25 $^{\circ}$C
	Total volume	130 L

The outdoor chamber conditions are also summarized in Table 5.1. The range of *OT*s was the outdoor temperature range in Hong Kong during the season when air-conditioning is used (BEAM Society, 2010). The maximum (=35 $^{\circ}$C) followed the maximum dry-bulb temperature in 1989. The initial tank water temperature was taken as 25 $^{\circ}$C, which is Hong Kong's annual average tap water temperature (Chen and Lee, 2010). The total volume of the tank water was 130 L, which corresponds to two persons' daily hot water consumption (Chen and Lee, 2010).

5.2.5　Experimental Procedures

Two identical sets of experiments with the prototype operated in the CH mode and the CC mode were conducted. At the beginning of each experiment, the outdoor

chamber was first conditioned to the pre-determined temperature and humidity (Table 5.1) by the use of the BIACS and the LGUs. The tank water was heated to 25 ^{o}C. Upon achieving the desired conditions, the prototype, the LGUs in the indoor chamber and all the measuring instruments were powered on to maintain the indoor chamber at 22 ^{o}C (indoor set-point temperature recommended by BEAM Society (2010)). The prototype was then operated intermittently to offset the pre-determined space cooling load generated by the LGUs, while the outdoor chamber condition was maintained unchanged throughout each experiment.

For the CC mode, the experiments were stopped when the operating parameters of the prototype reached a steady state. While for the CH mode, the experiments were continued until the average tank water temperature reached 50 ^{o}C (maximum required hot water temperature for Hong Kong residents (Chen and Lee, 2010)).

5.3   Results and Discussion

This section discusses the energy performance and operation characteristics of the prototype operated in the CH mode as compared to the CC mode.

5.3.1   Water Side Performance

SEHRAC uses the rejected condenser heat for water heating. Whether the heat recovered is sufficient to achieve the water heating objective needs to be evaluated.
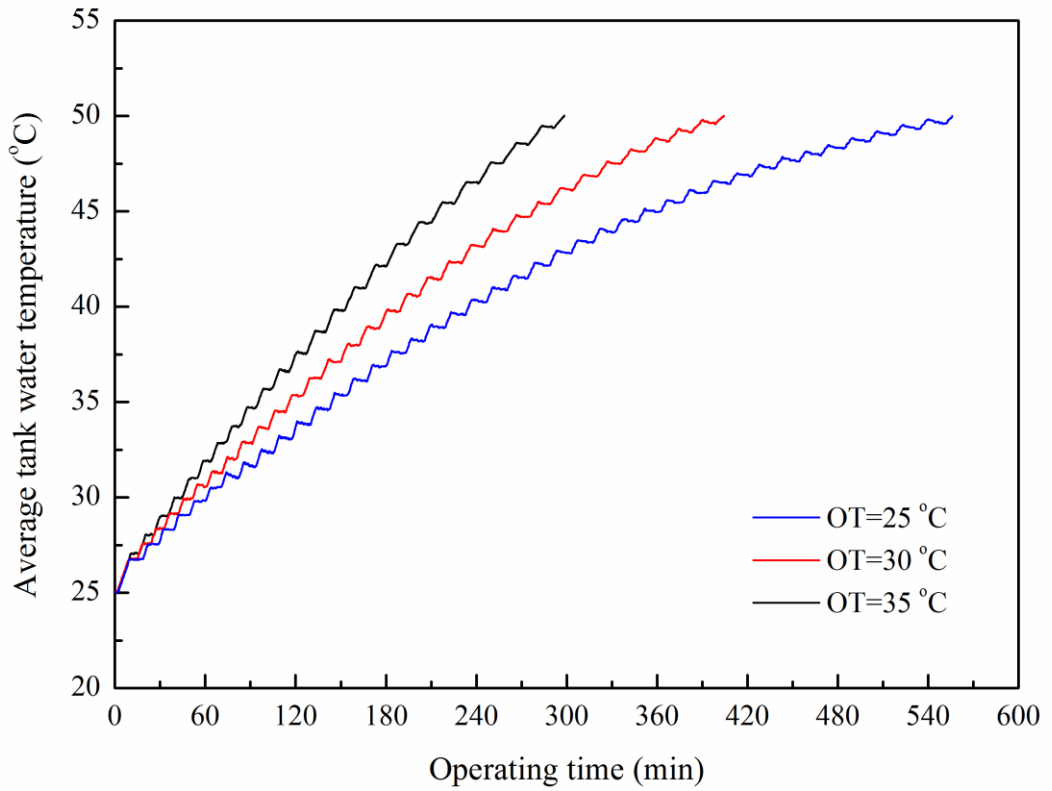
Figure 5.2   Variations of T_w with τ for different OTs (PLR=0.8)
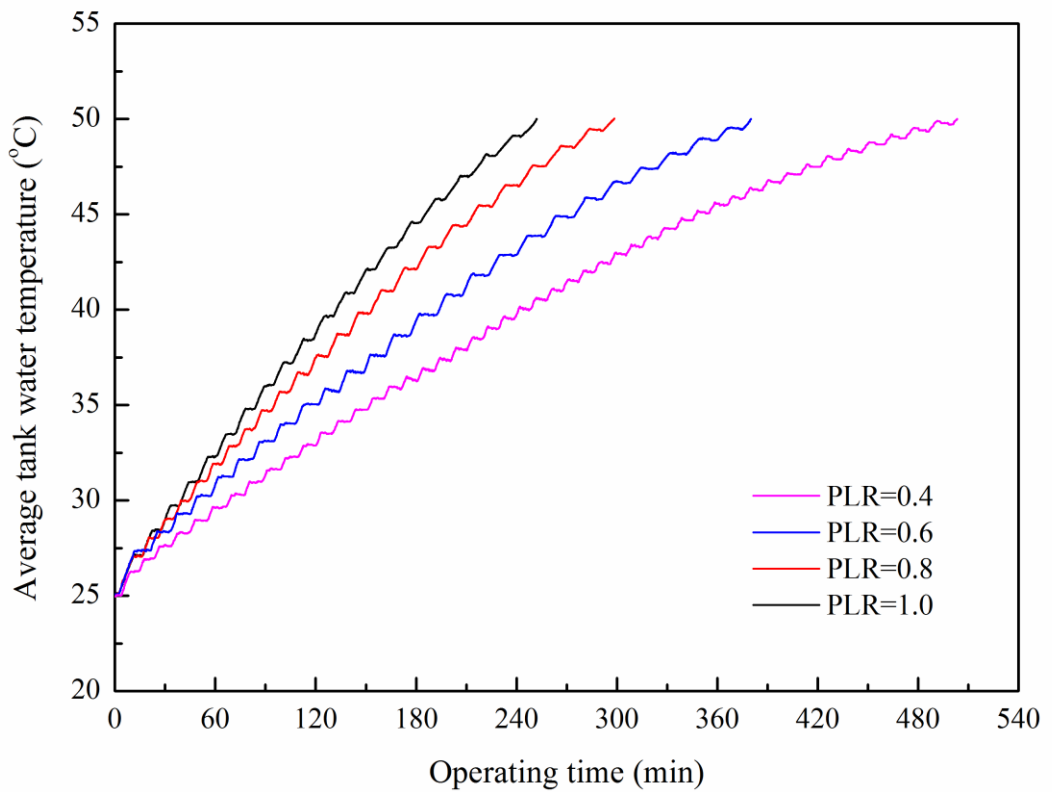
Figure 5.3   Variations of T_w with τ for different PLRs (OT=35 ^{o}C)

Figures 5.2 and 5.3 depict the average tank water temperature (T_w) against operating time (τ) for different OTs and PLRs, respectively. T_w is taken as the arithmetic mean of the water temperatures measured at 12 different locations in the water tank:

$$T_w = \sum_{i=1}^{12} T_{w,i} \bigg/ 12 \qquad\qquad (5.1)$$

where $T_{w,i}$ is the tank water temperature measured at the i-th location.

It is obvious that T_w exhibits a stepwise increase with operating time due to intermittent operation of the compressor. It can also be seen that the rate of temperature increase is higher initially and decreases gradually. This can be explained by the fact that as T_w increases, the heat transfer performance of the heat exchanger drops so that the amount of superheated refrigerant condensed in the heat exchanger is reduced to lower the heat rejection in the water tank. Figures 5.2 and 5.3 also indicate that due to the lower heat rejection rate when OT or PLR decreases, longer time is needed to heat the water to 50 ^{o}C.

Figure 5.4 shows the vertical water temperature variations for different operating times in a typical experimental condition (OT=30 ^{o}C and PLR=0.8). This condition is shown because it occurs most frequently in the air-conditioned season. It can be seen that water temperatures in the upper part of the water tank are much higher initially and then the isothermal layer gradually expands to the lower part. This is due to the top inlet design of the heat exchanger, as explained in Section 3.2.2. Hot refrigerant from the compressor therefore flows from top to bottom of the water tank. As can be

seen, T_w reaches 48.9 ^{o}C in 360 minutes with a maximum temperature of 50.5 ^{o}C and two-third of water above 50 ^{o}C.
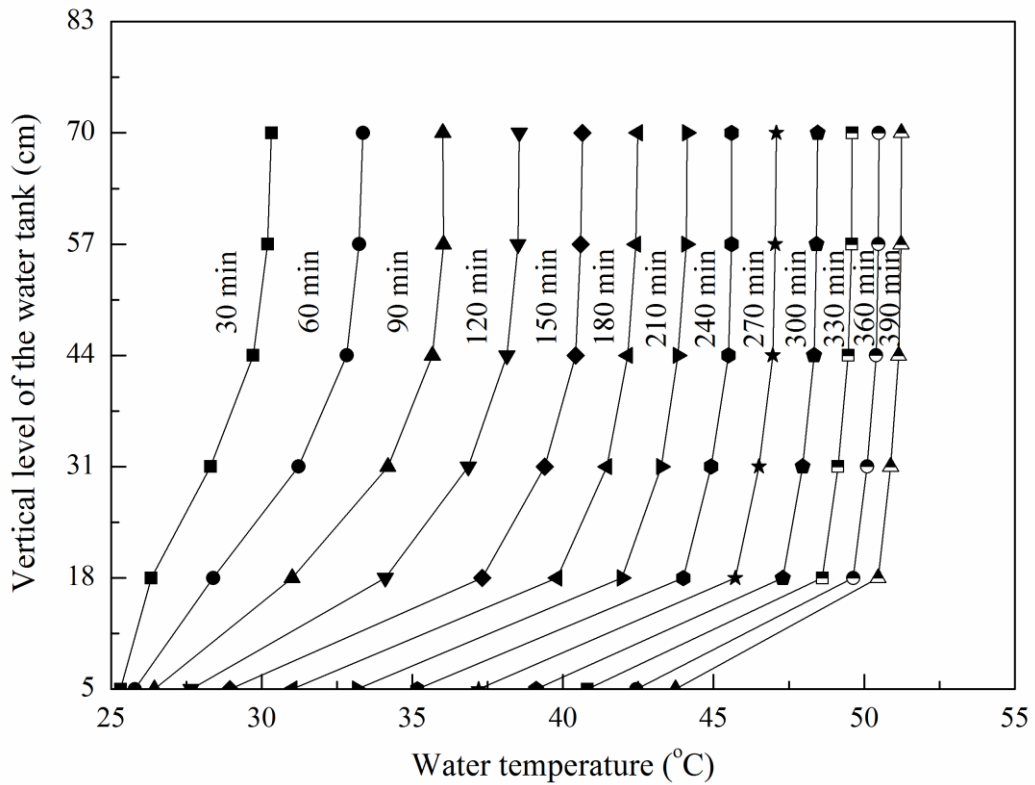
Figure 5.4   Vertical water temperature variations for different operating times

The total time required (τ_R) for each experiment to heat T_w from 25 to 50 ^{o}C is summarized in Table 5.2. To check if the daily operation duration of a bedroom air-conditioner will exceed τ_R, references were made to previous studies on utilization patterns of air-conditioners in Hong Kong (BEAM Society, 2010; Chen and Lee, 2010) which indicate that bedroom air-conditioners normally run 10 to 18 hours overnight. It can therefore be seen that for all experimental conditions, τ_R is less than 18 hours. Among them, τ_R is more than 10 hours only under three specific conditions (OT=25 ^{o}C and PLR=0.4 or 0.6; OT=30 ^{o}C and PLR=0.4). The results confirm the

feasible use of intermittently operated SEHRAC as the bedroom air-conditioner to reduce the water heating energy use in residential buildings in Hong Kong.

Table 5.2   Required water heating time (τ_R) for different experimental conditions

OT (°C)	Required water heating time (minutes)			
	PLR=0.4	PLR=0.6	PLR=0.8	PLR=1.0
25	971	724	556	390
30	733	550	405	309
35	503	380	298	252

5.3.2 Refrigerant Side Performance

As T_w increases, the heat rejection performance of SEHRAC drops continuously, leading to significant fluctuations in operating pressures and temperatures on the refrigerant side. To illustrate, selected operating parameters from the typical experimental condition, except otherwise stated, are chosen for a detailed discussion in Figures 5.5 and 5.6. The parameters were selected because they fluctuate most in response to an increase in T_w.

Figure 5.5 shows the variations of compressor discharge ($P_{cd,r}$) and suction ($P_{cs,r}$) pressures with operating time. It can be seen that both $P_{cd,r}$ and $P_{cs,r}$ fluctuate on cutting in of the compressor. Upon continuous operation of the compressor, the pressures become stable but display a rising trend with operating time. On cutting out of the compressor, the pressures become equalized due to the refrigerant migration from the condenser to the evaporator.
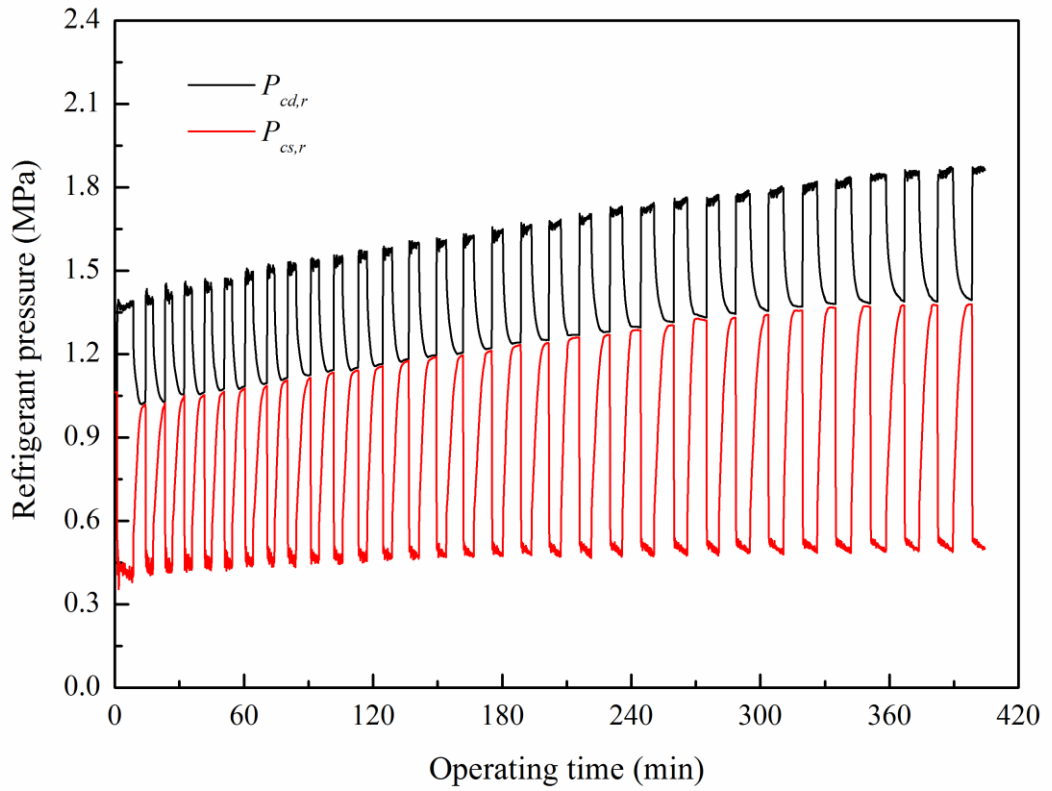
Figure 5.5　　　Variations of $P_{cd,r}$ and $P_{cs,r}$ with τ
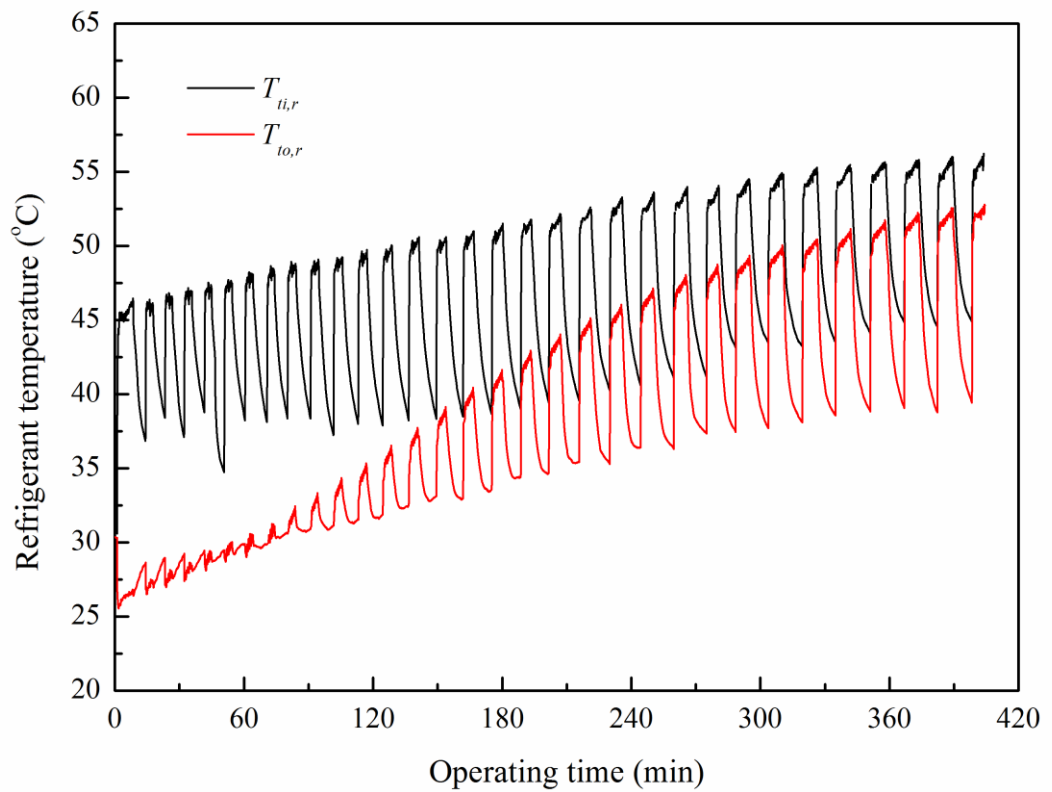
Figure 5.6　　　Variations of $T_{ti,r}$ and $T_{to,r}$ with τ

Pressure variations during compressor cutting in and out are considered normal. The steady increase in $P_{cd,r}$ and $P_{cs,r}$ with operating time is attributed to the increase in T_w. As T_w increases, the condensing pressure needs to be elevated to enable heat rejection. Therefore, $P_{cd,r}$ is increased to reduce the refrigeration effect and thus increase the evaporator outlet pressure (i.e. $P_{cs,r}$). Moreover, as revealed in Figure 5.5, $P_{cs,r}$ is less influenced by the condenser heat recovery because it increases at a much lower rate than $P_{cd,r}$.

Figure 5.6 shows the variations of refrigerant temperatures at water tank inlet ($T_{ti,r}$) and outlet ($T_{to,r}$) with operating time. It can be seen that both $T_{ti,r}$ and $T_{to,r}$ experience a significant increase but their difference decreases with operating time. The increase in $T_{ti,r}$ can be explained by the increase in $P_{cd,r}$, while the decrease in the temperature difference is caused by the drop in heat transfer performance of the heat exchanger.

To check if the extents of pressure fluctuations are within acceptable ranges to confirm the satisfactory operation of SEHRAC using capillary tube, the compression ratio (*CR*), defined as the ratio of the absolute discharge pressure to the absolute suction pressure, is used as an indicator. However, in view of the vast amount of experimental data collected, the average $P_{cd,r}$ and $P_{cs,r}$ of a compressor on-cycle were calculated to give $P_{cd,r,m}$ and $P_{cs,r,m}$. Therefore, the average compression ratio (CR_m) is given by:

$$CR_m = \frac{P_{cd,r,m} + P_b}{P_{cs,r,m} + P_b} \tag{5.2}$$

where P_b is the barometric pressure.

Figure 5.7 shows the variations of CR_m for different OTs (PLR=0.8). To enable pairwise comparison of the results, the corresponding average operating times (τ_m) were calculated to form the X-axis. The results of other PLRs have not been shown because they display the same order of variations with OTs, and differ only in the rate of increase in CR_m.

As revealed in Figure 5.7, CR_m increases with operating time and ranges between 2.74 and 3.23. The increase is attributed to the higher rate of increase in $P_{cd,r}$ than $P_{cs,r}$ (Figure 5.5). The range of CR_m (2.74 to 3.23) is judged to be acceptable because it is within the allowable limit of 10 as recommended by most compressor manufacturers (Copeland, 1982). It can also be seen that at any given time, higher OT gives higher CR_m. This is because higher OT means higher heat rejection rate, resulting in a higher T_w at a given time, and thus higher $P_{cd,r,m}$ and CR_m.

According to the lubrication oil's properties (Whitman et al., 2005), for an air-conditioner to operate properly, the compressor discharge temperature should never exceed 105 °C. Figure 5.8 shows the variations of average compressor discharge temperature (i.e. $T_{ti,r,m}$) for different OTs (PLR=0.8). It can be seen that despite $T_{ti,r,m}$ has increased significantly with operating time (44 °C to 56.5 °C); it is still far lower than the allowable limit of 105 °C.
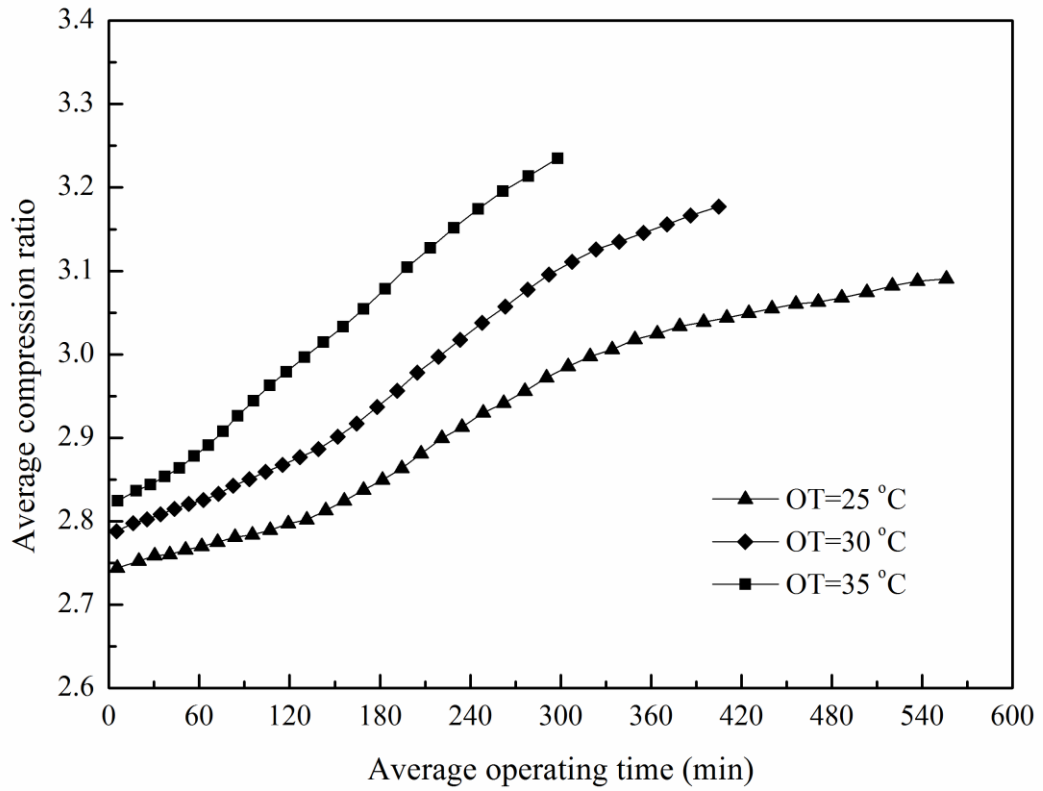
Figure 5.7   Variations of CR_m with τ_m for different OTs (PLR=0.8)
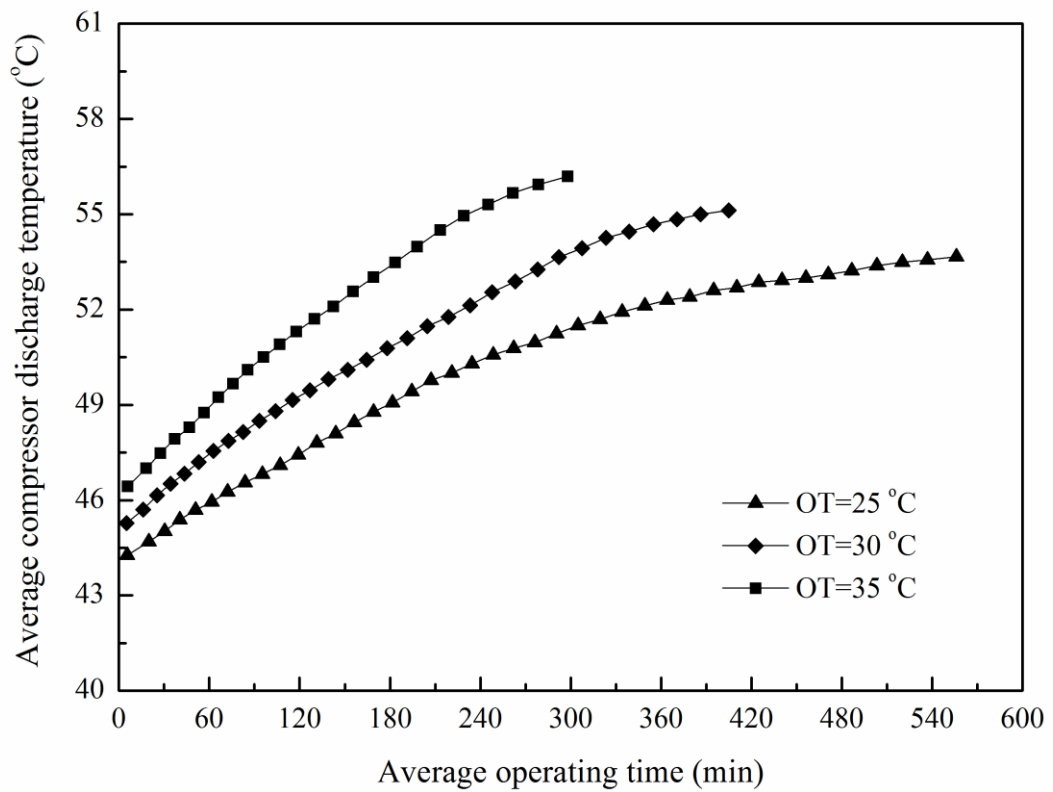
Figure 5.8   Variations of $T_{ti,r,m}$ with τ_m for different OTs (PLR=0.8)

It is evident from the above discussions that the fluctuations in operating pressures and temperatures on the refrigerant side can be well-explained and are within acceptable ranges to confirm the satisfactory operation of SEHRAC using capillary tube as the expansion device.

5.3.3 Energy Performance

5.3.3.1 CH Mode

The energy performance of the prototype operated in the CH mode is analyzed based on the average space cooling output, water heating capacity, power consumption and overall coefficient of performance of each compressor on-cycle. The average values are used because of the intermittent operation characteristics of the prototype.

The average space cooling output ($Q_{cl,m}$) is determined by:

$$Q_{cl,m} = m_a \left(h_{er,a,m} - h_{es,a,m} \right) \tag{5.3}$$

where m_a is the evaporator supply air flow rate (kg/s); $h_{er,a,m}$ and $h_{es,a,m}$ are the average return and supply air enthalpies (kJ/kg), respectively, of the evaporator within a compressor on-cycle.

The following equations are used to determine the air enthalpy (ASHRAE, 2009):

$$h_a = 1.006T_a + w\left(2501 + 1.86T_a\right) \tag{5.4}$$

$$w = 0.622\frac{\varphi P_{sw}}{P_b - \varphi P_{sw}} \tag{5.5}$$

$$\ln P_{sw} = C_1/T_a^* + C_2 + C_3 T_a^* + C_4 T_a^{*2} + C_5 T_a^{*3} + C_6 \ln T_a^* \tag{5.6}$$

where T_a is the air temperature (^{o}C); w is the moisture content (kg/kg); φ is the relative humidity; P_{sw} is the saturation vapor pressure over liquid water (Pa); C_1 to C_6 are the regression coefficients summarized in Table 5.3 (ASHRAE, 2009); T_a^* is the absolute air temperature.

Table 5.3   Summary of the regression coefficients in Equation (5.6)

C_1	-5.800E+03
C_2	1.391E+00
C_3	-4.864E-02
C_4	4.176E-05
C_5	-1.445E-08
C_6	6.546E+00

The average water heating capacity ($Q_{wh,m}$) is given by:

$$Q_{wh,m} = c_{p,w}M_w\left(T_{w,e} - T_{w,b}\right)\big/\Delta\tau \tag{5.7}$$

where $c_{p,w}$ is the specific heat capacity of water (kJ/kg ^{o}C); M_w is the total mass of the tank water (kg); $T_{w,e}$ and $T_{w,b}$ are the average water temperatures at the end and

the beginning, respectively, of a compressor on-cycle (^{o}C); $\Delta\tau$ is the time duration of the compressor on-cycle in second.

The average overall coefficient of performance ($COP_{oa,m}$), which takes into account $Q_{cl,m}$, $Q_{wh,m}$ and average power consumption (W_m), is mathematically expressed as:

$$COP_{oa,m} = \frac{Q_{cl,m} + Q_{wh,m}}{W_m} \tag{5.8}$$

The calculated $Q_{cl,m}$, $Q_{wh,m}$, W_m and $COP_{oa,m}$ for all experimental conditions are summarized in Figures 5.9 to 5.12, respectively. For direct comparison of results for different experimental conditions, $T_{w,m}$, derived from further averaging T_w (Equation (5.1)) over a compressor on-cycle, is taken as the X-axis.

It can be seen in Figures 5.9 and 5.10 that both $Q_{cl,m}$ and $Q_{wh,m}$ decrease with an increase in $T_{w,m}$. They have dropped correspondingly by 26% and 55% over the entire range of $T_{w,m}$ for OT at 35 ^{o}C. The drop in $Q_{cl,m}$ can again be explained by the increase in the condensing pressure to lower the refrigeration effect, while the decrease in $Q_{wh,m}$ is due to the drop in temperature difference between the refrigerant discharged from the compressor and the water. For the same reason, it can be seen that $Q_{wh,m}$ drops at a much lower rate in the first 30 minutes due to a higher temperature difference initially. It can also be seen that for a given $T_{w,m}$, higher OT results in smaller $Q_{cl,m}$ but larger $Q_{wh,m}$. In other words, OT introduces a cancellation effect between $Q_{cl,m}$ and $Q_{wh,m}$.
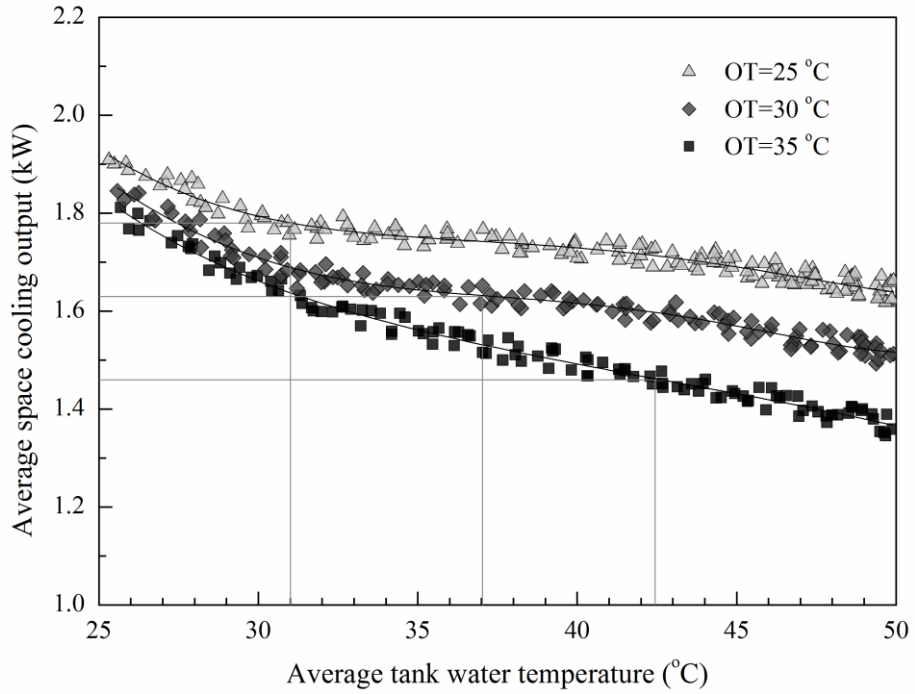
Figure 5.9   Variations of $Q_{cl,m}$ with $T_{w,m}$ for all experimental conditions
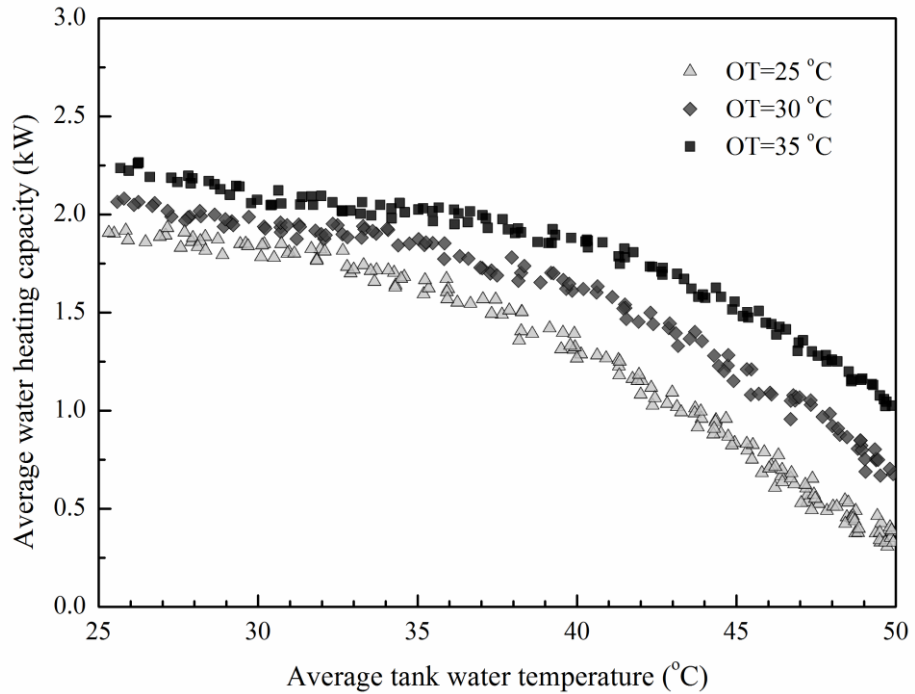
Figure 5.10   Variations of $Q_{wh,m}$ with $T_{w,m}$ for all experimental conditions

Figure 5.11 shows that when $T_{w,m}$ increases from 25 $^{\circ}$C to 50 $^{\circ}$C, W_m increases approximately by 17%. This is due to the increase in CR_m as explained in Section

5.3.2 (Figure 5.7). Moreover, for a given $T_{w,m}$, W_m is larger for conditions with higher OT.
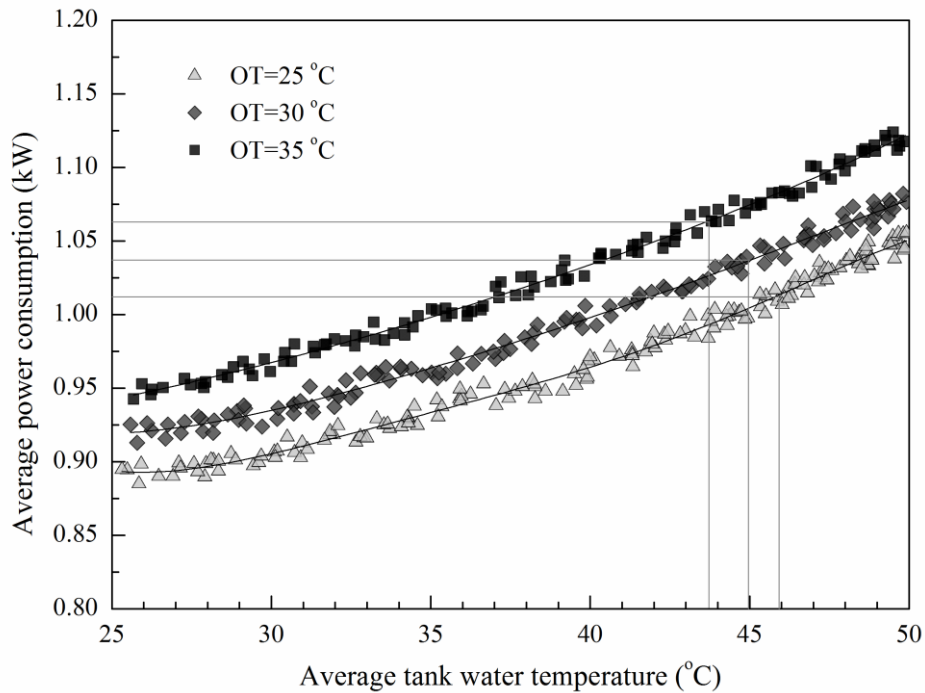
Figure 5.11   Variations of W_m with $T_{w,m}$ for all experimental conditions

For the overall energy performance, it can be seen in Figure 5.12 that $COP_{oa,m}$ decreases with an increase in $T_{w,m}$. This is due to the corresponding increase in W_m, as well as the decrease in $Q_{cl,m}$ and $Q_{wh,m}$ as explained earlier. Considering the dominant influence of water temperature as well as the cancellation effect between $Q_{cl,m}$ and $Q_{wh,m}$, it is reasonable to see that OT has only a small influence on $COP_{oa,m}$ for a given $T_{w,m}$. A closer examination of the results shows that the $COP_{oa,m}$ profiles for different OTs intersect when $T_{w,m}$ is at approximately 38 °C, implying that lower OT gives slightly higher $COP_{oa,m}$ when $T_{w,m}$ is below 38 °C. Figure 5.13 shows the average coefficient of performance for space cooling only ($COP_{cl,m}$). As can be seen, similar to $COP_{oa,m}$, $COP_{cl,m}$ also decreases with an increase in $T_{w,m}$. This is attributed to the continuous decrease in $Q_{cl,m}$ and increase in W_m with $T_{w,m}$.
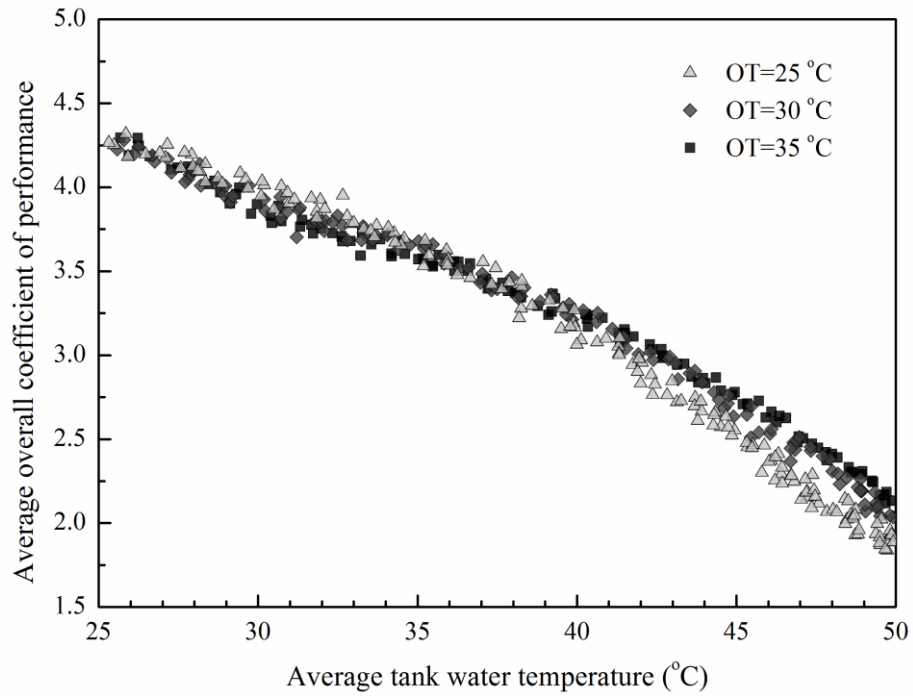
Figure 5.12   Variations of $COP_{oa,m}$ with $T_{w,m}$ for all experimental conditions
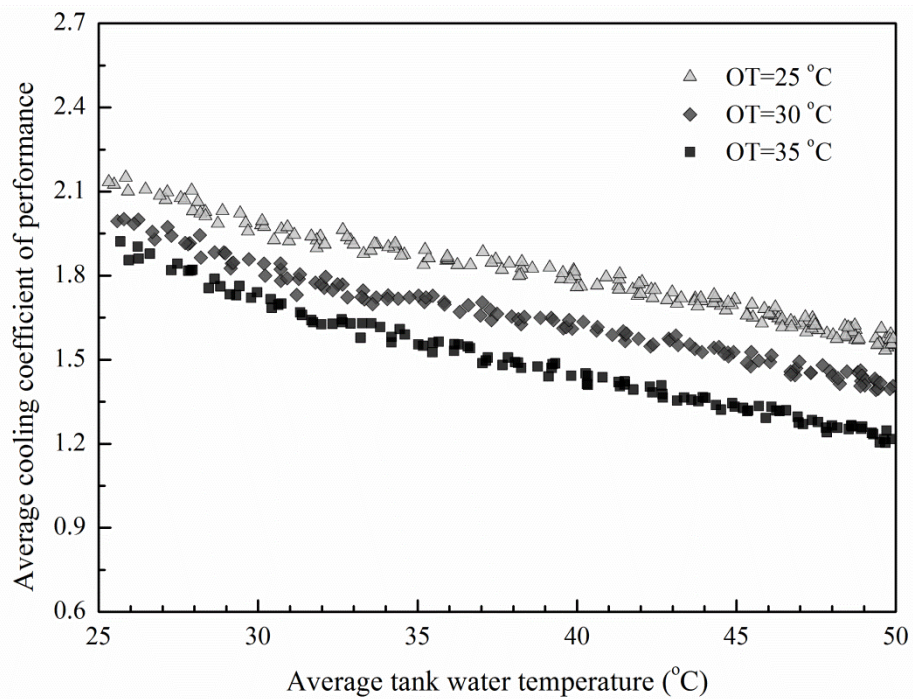
Figure 5.13   Variations of $COP_{cl,m}$ with $T_{w,m}$ for all experimental conditions

5.3.3.2 CC Mode

For the CC mode, $Q_{cl,m}$ is also determined by Equations (5.3) to (5.6). Given that $Q_{wh,m}$ in Equation (5.8) equals 0, the average coefficient of performance (COP_m) can therefore be calculated by:

$$COP_m = \frac{Q_{cl,m}}{W_m} \tag{5.9}$$

$Q_{cl,m}$, W_m and COP_m were calculated for different OTs and PLRs. However, it was noted that PLR introduces very little influence on their values, and thus Table 5.4 summarizes only the calculated $Q_{cl,m}$, W_m and COP_m for different OTs. The results are also shown in Figures 5.9 and 5.11 to enable direct comparison with the CH mode.

Table 5.4   Energy performance of the prototype operated in the CC mode

OT (^{o}C)	Energy performance		
	$Q_{cl,m}$ (kW)	W_m (kW)	COP_m
25	1.78	1.01	1.76
30	1.63	1.04	1.57
35	1.46	1.06	1.38

As can be seen in Figure 5.9, at OT of 25 ^{o}C, 30 ^{o}C and 35 ^{o}C, $Q_{cl,m}$ of the CH mode falls below the CC mode when $T_{w,m}$ exceeds an intersection temperature of 31 ^{o}C, 37 ^{o}C and 42 ^{o}C, respectively. But the difference is less than 10% even when $T_{w,m}$ reaches 50 ^{o}C. The existence of the intersection temperatures can be explained by the interactive influence of refrigeration effect and refrigerant flow rate on $Q_{cl,m}$.

For the CH mode, the condensing pressure is low to give a higher refrigeration effect at lower $T_{w,m}$, resulting in a larger $Q_{cl,m}$. But when $T_{w,m}$ exceeds the intersection temperature, despite the condensing pressure being still lower than that in the CC mode, the reduction in refrigerant flow rate due to lower pressure difference between the condenser and evaporator outweighs to give a smaller $Q_{cl,m}$.

To explain the above observations, Figure 5.11 compares the calculated W_m for the two modes. It can be seen that W_m of the CH mode is lower than the CC mode before $T_{w,m}$ reaches 44 ^{o}C, 45 ^{o}C and 46 ^{o}C, respectively, mainly due to the lower condensing pressure.

For the overall energy performance, due to the additional $Q_{wh,m}$, $COP_{oa,m}$ of the CH mode, as compared to COP_m of the CC mode, is higher for the entire $T_{w,m}$ range. Therefore, as far as energy performance is concerned, within the studied $T_{w,m}$ range, SEHRAC is always more efficient than conventional room air-conditioner as long as water heating is needed.

5.4   Potential Water Heating Energy Saving

The discussions in Section 5.3.1 indicated that the water heating objective can be achieved by the use of SEHRAC for the given experimental conditions. To further evaluate the sole use of SEHRAC for water heating in the entire air-conditioned season, and to enable prediction of the potential water heating energy saving, a prediction model relating τ_R with OT and PLR needs to be developed.

In this study, τ_R for different combinations of OT and PLR (Table 5.2) were used for developing the prediction model. The resultant model (r^2=0.9), developed based on polynomial regression analysis, is shown in Equation (5.10):

$$\tau_R = A_1 + A_2 OT + A_3 PLR + A_4 OT^2 + A_5 OT \times PLR + A_6 PLR^2 \qquad (5.10)$$

where τ_R is the required water heating time in minute; A_1 to A_6 are regression coefficients summarized in Table 5.5.

Table 5.5   Summary of the regression coefficients in Equation (5.10)

A_1	3605
A_2	-91.9
A_3	-3022
A_4	0.4
A_5	53.8
A_6	510.4

For the use of Equation (5.10) to predict τ_R, the coincident OT and PLR need to be determined. However, considering that the space cooling load of the representative bedroom, as revealed from the simulation results presented in Chapter 4, does not deviate much during the hours when air-conditioning is used, the simulated daily average OT and PLR were therefore used for prediction of the daily τ_R. The predicted values are summarized in Table 5.6.

Based on the obtained daily τ_R, it is estimated that if the daily operation duration of bedroom air-conditioner is taken as 18 hours (=1080 minutes), within the air-conditioned season, the water heating demand (hot water daily consumption: 130 L;

T_w: from 25 $^{\circ}$C to 50 $^{\circ}$C) can be fulfilled for 179 days. On this basis, if both bedrooms of unit D2 in Building A (Figure 4.2) is equipped with SEHRAC, the annual water heating demand and thus energy saving will be 49.0% (= 179/365). The energy saving is estimated based on the demand saving and thus is a fuel-neutral estimation.

Furthermore, according to the latest energy statistics (Electrical and Mechanical Services Department, 2015a), the water heating energy consumption of the residential sector in Hong Kong was 2.95 TWh. Therefore, based on the above water heating demand and energy saving potential, it is estimated that if all residential buildings are designed to use SEHRAC, the total water heating energy saving will be 1.45 TWh per annum (=2.95$\times$49.0%), or 9.1% of the overall energy consumption of the residential sector(=15.93 TWh).

Table 5.6　　　Prediction of the energy saving potential

Application	Description	Value(s)
Unit D2 in Building A	Daily τ_R predicted by Equation (5.10)[a]	400.8 min to 1666.9 min
	Daily air-conditioned hours	18 hours (=1080 min)
	Number of days when $\tau_R < 1080$ minutes	179 days
	% water heating energy saving	179/365$\times$100%=49.0%
The residential sector	Water heating energy consumption	2.95 TWh[b]
	Annual water heating energy saving	2.95$\times$49.0%=1.45 TWh
	Overall energy consumption	15.93 TWh[c]
	% saving of the residential sector	1.45/15.93$\times$100%=9.1%

[a] Within the air-conditioned season.

[b] Water heating energy consumption of the residential sector in Hong Kong.

[c] Overall energy consumption of the residential sector in Hong Kong.

5.5   Uncertainty Analysis

For a result Y which needs to be determined from a number of independent variables (v_i) (Equation (5.11)), if the uncertainties in the measured values of these variables (δv_i) can be ascertained, the uncertainty in the result (δY) can be estimated by using Kline and McClintock's method (Doebelin, 1983; Holman, 1989):

$$Y = f\left(v_1, v_2, ..., v_n\right) \tag{5.11}$$

$$\delta Y = \sqrt{\sum_{i=1}^{n}\left(\frac{\partial Y}{\partial v_i}\delta v_i\right)^2} \tag{5.12}$$

Therefore, Equations (5.13) to (5.15), derived on the basis of Equations (5.3), (5.7) and (5.8), together with the instrument accuracies summarized in Table 3.3, can be used to determine the uncertainties in the calculated $Q_{cl,m}$, $Q_{wh,m}$ and $COP_{oa,m}$, while that in W_m can simply be taken as the corresponding instrument uncertainty.

$$\frac{\delta Q_{cl,m}}{Q_{cl,m}} = \sqrt{\left(\frac{\delta m_a}{m_a}\right)^2 + \frac{\delta h_{er,a,m}^2 + \delta h_{es,a,m}^2}{\left(h_{er,a,m} - h_{es,a,m}\right)^2}} \tag{5.13}$$

$$\frac{\delta Q_{wh,m}}{Q_{wh,m}} = \sqrt{\frac{\delta T_{w,e}^2 + \delta T_{w,b}^2}{\left(T_{w,e} - T_{w,b}\right)^2}} \tag{5.14}$$

$$\frac{\delta COP_{oa,m}}{COP_{oa,m}} = \sqrt{\left(\frac{\delta Q_{cl,m}}{Q_{cl,m} + Q_{wh,m}}\right)^2 + \left(\frac{\delta Q_{wh,m}}{Q_{cl,m} + Q_{wh,m}}\right)^2 + \left(\frac{\delta W_m}{W_m}\right)^2} \qquad (5.15)$$

For the CC mode, the uncertainty in $Q_{cl,m}$ can also be calculated by Equation (5.13), while that in COP_m can be determined from Equation (5.15) when $Q_{wh,m}=0$.

Because of the unsteady system behavior as shown above, the maximum possible uncertainties were determined. Results are summarized in Table 5.7. They were found comparable with those in previous studies (Lee et al., 2008; Adriansyah, 2001) and therefore are judged to be acceptable.

Table 5.7   Uncertainties in the calculated system performance

| OT (^{o}C) | Relative uncertainty (%) | | | | | | |
| | CH mode | | | | CC mode | | |
	$Q_{cl,m}$	$Q_{wh,m}$	W_m	$COP_{oa,m}$	$Q_{cl,m}$	W_m	COP_m
25	6.9	25.7	2.3	8.2	6.3	2.0	6.6
30	7.4	16.0	2.2	7.4	6.8	1.9	7.1
35	8.2	9.0	2.1	6.3	7.6	1.9	7.8

5.6   Summary

For evaluating the energy performance and operation characteristics of SEHRAC, a prototype using capillary tube as the expansion device, and with intermittent operation characteristics, was designed, assembled and tested under different outdoor temperatures and space cooling load conditions. In the experiments, different operating parameters on the water, refrigerant and air sides of the prototype were

measured and recorded. The experimental results showed that the water heating objective could be achieved within a range of carefully-determined experimental conditions to confirm the practical use of SEHRAC as the bedroom air-conditioner to reduce the water heating energy use. Further, the fluctuations in operating pressures and temperatures on the refrigerant side of the prototype could be well-explained and were found reasonable to confirm feasible use of capillary tube as the expansion device. The experimental results also showed that the coefficient of performance of the CH mode was constantly higher than that of the CC mode, despite there was a maximum of 10% reduction in the space cooling output. On this basis, a prediction model was developed for evaluating the sole use of SEHRAC for water heating in the entire air-conditioned season. The potential water heating energy saving on wider application of SEHRAC was estimated to be 9.1% of the overall energy consumption of the residential sector in Hong Kong.

CHAPTER 6

SYSTEM OPTIMIZATION OF SEHRAC: PERFORMANCE COMPARISON OF CAPILLARY TUBE AGAINST THERMOSTATIC EXPANSION VALVE

As demonstrated in Chapter 5, SEHRAC is unique for the significant refrigerant pressure fluctuations during its operation. Therefore, the selection of a suitable type of expansion device that can function properly despite the fluctuations is very important, especially considering that the operation of an expansion device is sensitive to the refrigerant pressures. In small capacity refrigeration systems, capillary tube (CT) and thermostatic expansion valve (TEV) are most used. For CT, its feasible use in SEHRAC was confirmed in Chapter 5, but its performance as compared to TEV was not assessed. Thus whether CT or TEV is preferred for use in SEHRAC is still unknown. To fill the research gap, an experimental study to enable a side-by-side comparison of the two expansion devices with the aim of optimizing the system configuration of SEHRAC is presented in this chapter.

6.1   Introduction

In a SEHRAC, same as other refrigeration systems, expansion device is one of the most important components. It functions to regulate the refrigerant flow to the evaporator and to maintain a pressure difference between the high and low pressure sides. Failure to function will be detrimental including refrigerant flooding to damage the compressor, refrigerant starving to lower the evaporator effectiveness, and hunting to cause large fluctuations in evaporator superheat (Dossat, 1997). As operation of SEHRAC can lead to significant refrigerant pressure fluctuations, the selection of a suitable type of expansion device that can function properly despite the fluctuations is very important.

Within the capacity range of SEHRAC, capillary tube (CT) and thermostatic expansion valve (TEV) are most used. CT is a length of small diameter tube and is therefore considered as a fixed type expansion device. As opposed to CT, TEV can actively regulate the refrigerant flow by varying its opening extent according to feedback from a sensing bulb. Thus a question is raised whether CT or TEV is preferred for use in SEHRAC.

Previous relevant works on comparing the use of CT and TEV mainly focused on heat pump water heaters (HPWHs) and conventional room air-conditioners (CRACs). It was revealed that whether CT or TEV is better depends largely on the associated operation characteristics of a refrigeration system. Therefore, previous studied results are not applicable to SEHRAC because its operation characteristics differ largely from HPHW and CRAC. In a HPHW, the water delivered to the condenser is usually tap water with very little variation in temperature throughout the year. Similar condition also applies to CRAC in the cooling months. While for SEHRAC,

due to the heat recovery occurred in the water tank, the tank water temperature is highly fluctuating, varying between 25 $^{\circ}$C and 55 $^{\circ}$C.

In this chapter, to identify whether CT or TEV is preferred for use in SEHRAC, a prototype equipped with the two expansion devices was setup for experimental investigations. In the prototype, the CT and TEV could be alternatively activated by the gate valves provided, thus enabling the direct comparison of the two systems (CT and TEV systems) under the same experimental conditions. In the experiments, the operating parameters on the refrigerant, air and water sides of the systems were monitored. Based on the experimental results, the performances of the two systems were determined and compared.

6.2   Experimental Study

6.2.1   Test Facility

The experiments were conducted in a test facility located at the Hong Kong Polytechnic University. The test facility comprised two completely insulated and separated environmental chambers resembling indoor and outdoor conditions. Detailed descriptions of the test facility can be found in Section 3.2.1.

In the experiments, the desired conditions in the chambers were achieved by the use of PID controllers to provide real-time adjustments of the LGUs outputs and were maintained unchanged throughout each test.

6.2.2 Prototype Design

To accomplish the objectives of this study, a prototype was designed and setup for laboratory experiments. Its schematic is shown in Figure 6.1. Detailed descriptions of the prototype can be found in Section 3.2.2.
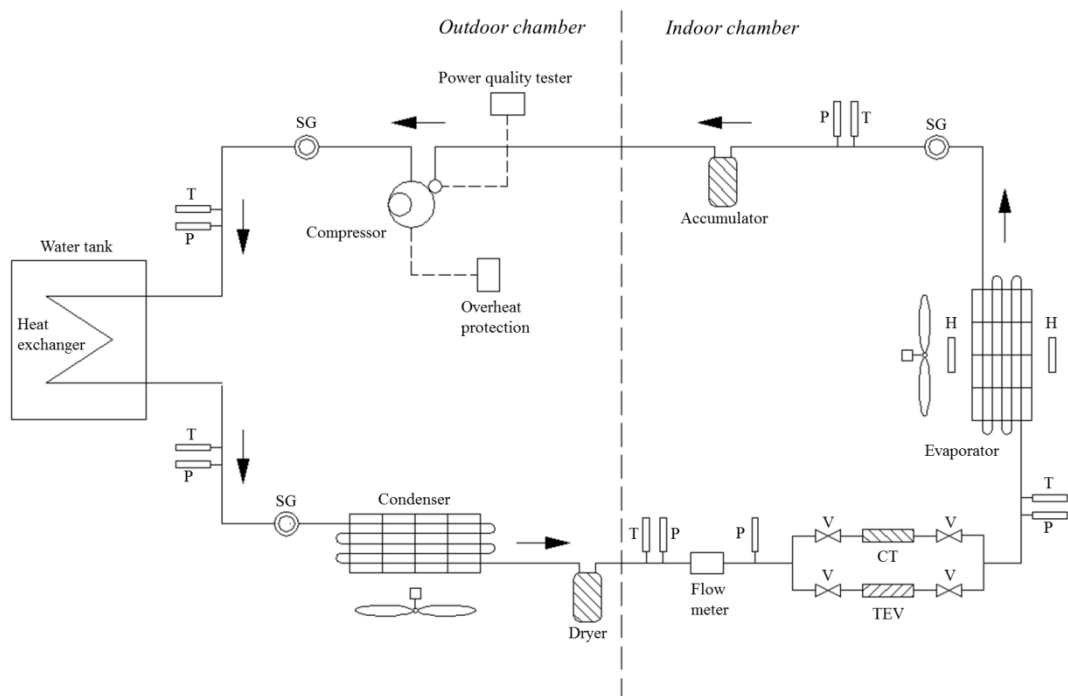
Figure 6.1   Schematic of the prototype for expansion device comparisons
(T: Thermocouple; P: Pressure transmitter; H: Hygrometer; V: Gate valve)

The prototype mainly comprised a split-type air-cooled air-conditioner, a refrigerant-to-water heat exchanger and a cylindrical water tank. The indoor unit was basically a DX evaporator with copper tubes and aluminum fins. The outdoor unit consisted of an air-cooled condenser and a rotary type compressor. The CT and TEV were parallel-connected on a manifold feeding the evaporator. They could be alternatively activated by the gate valves provided. This design enabled carrying out comparative tests on their influences on the system performance.

Detailed specifications of the expansion devices used in this study are summarized in Table 6.1. The original CT supplied with the air-conditioner was used in this study. The tested TEV was a commercially available Danfoss TX2 internally equalized expansion valve with an orifice number of 01. Its sensing bulb was mounted on the horizontal suction line near the evaporator outlet. Non-hydroscopic insulation material was used to insulate the connecting pipings and the expansion devices.

Table 6.1   Specifications of the expansion devices

Capillary tube	Inner diameter=1.4 mm
(CT)	Outer diameter=2.5 mm
	Length=720 mm
Thermostatic expansion valve	Model: Danfoss TX2
(TEV)	Orifice number: 01

6.2.3 Measurements

In the experiments, different operating parameters on the water, refrigerant and air sides of the prototype were measured and recorded. The measuring instruments used are summarized in Section 3.2.3.

6.2.4 Experimental Conditions

In this study, two identical sets of experiments with the prototype operated with CT and TEV were performed. For each set of experiments, the indoor temperature was maintained at 18.5 $^{\circ}$C, while the outdoor temperature was varied from 25 $^{\circ}$C to 35 $^{\circ}$C

with an interval of 5 $^{\circ}$C to become three different experimental conditions (same as Chapter 5). The lower than comfort indoor temperature (=18.5 $^{\circ}$C) was chosen to enable continuous operation of the compressor and thus the proper operation of the expansion devices under low evaporating temperatures can be evaluated. The total volume of water to be heated in the water tank was 130 L (same as Chapter 5).

6.2.5   Experimental Procedures

Before the commencement of the actual experiments, a preliminary test was carried out to check the proper functioning of the TEV and to determine an optimal superheat setting. This is important because the setting can significantly affect the performance of a TEV system. A high evaporator superheat can lead to underutilization of the evaporator surface to degrade the system performance. While if the superheat is set too low, the TEV may lose control on the refrigerant flow and cause "hunting" (refrigerant flow shows sustained oscillations). In this preliminary test, the superheat setting of the TEV was gradually increased to a position when the sustained oscillations started to disappear.

After the preliminary test, two identical sets of experiments with the prototype operated with CT and TEV were performed. For each test, the outdoor chamber was first conditioned to the pre-set condition by the use of the BIACS and the LGUs. The tank water was heated to an initial temperature of 25 $^{\circ}$C. Upon achieving the desired conditions, the prototype, the LGUs in the indoor chamber and all the measuring instruments were powered on to maintain the indoor chamber at 18.5 $^{\circ}$C and 65%

RH. Under this condition, the instantaneous cooling output of the prototype was actively adjusted to exactly offset indoor cooling load generated by the LGUs. The test was continued until the average tank water temperature reached 50 $^{\circ}$C.

6.3 Results and Discussion

This section discusses the performance of the prototype operated with TEV as compared to CT under various outdoor temperatures. The performance is evaluated based on the operation characteristics on the refrigerant side, the space cooling capacity, the water heating capacity, and the system energy efficiency. Due to the large amount of experimental data collected, performance comparisons of the two systems presented below are for an outdoor temperature of 30 $^{\circ}$C. The results obtained for other experimental conditions will also be analyzed and given where necessary.

6.3.1 Refrigerant Side

Proper operation on the refrigerant side can be revealed by checking if, under pressure fluctuations, the expansion device can still feed a proper amount of refrigerant to the evaporator, can keep a suitable degree of evaporator superheat, and can minimize the amount of vapor refrigerant formed in the expansion process to maximize the system capacity.
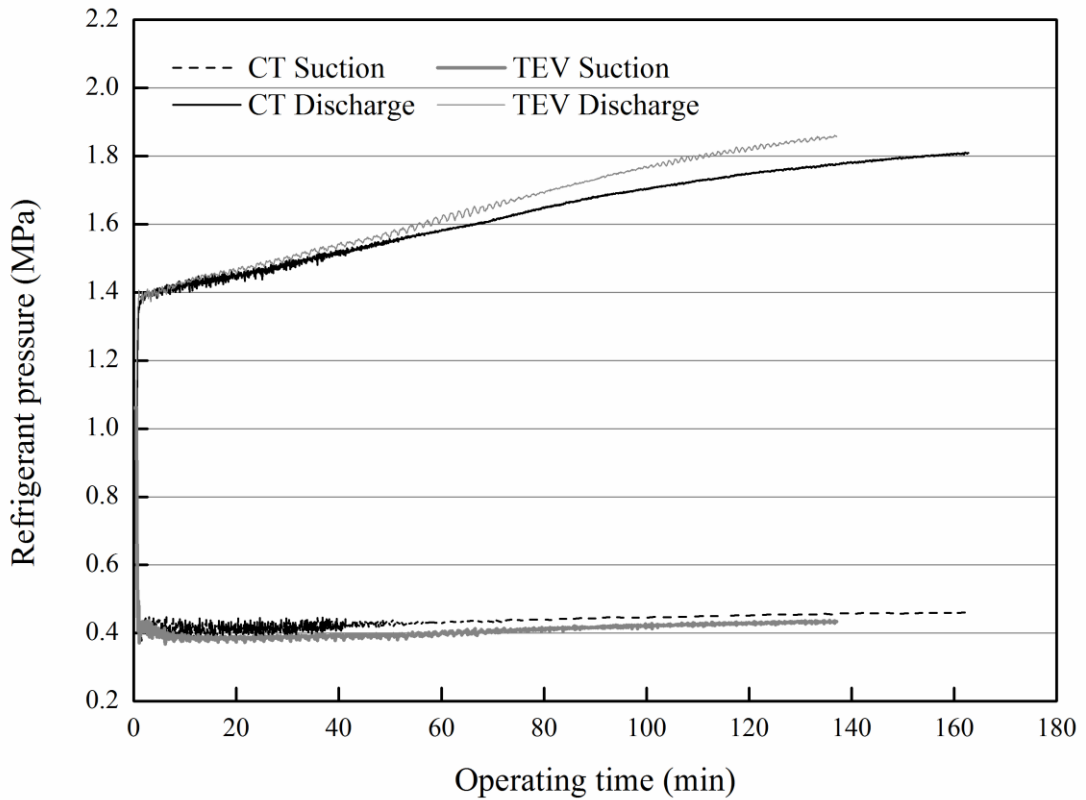
Figure 6.2   Compressor suction and discharge pressures comparison

To illustrate the refrigerant pressure fluctuations during the heat recovery process, Figure 6.2 compares the variations in compressor suction and discharge pressures for the two systems. It can be seen that the discharge pressures for both systems display a continuous increase with operating time. This is due to the fact that as the tank water temperature increases, the heat rejection performance of the prototype drops to increase the condensing pressure and thus discharge pressure. Between the two systems, the TEV system has a slightly higher discharge pressure (0.7% on average) due to the gradual reduction in opening extent of the TEV. While for the suction pressure, as explained in a previous study (Bong et al., 1988), it is less influenced by the heat recovery, thus a very small change is observed for both systems.

98
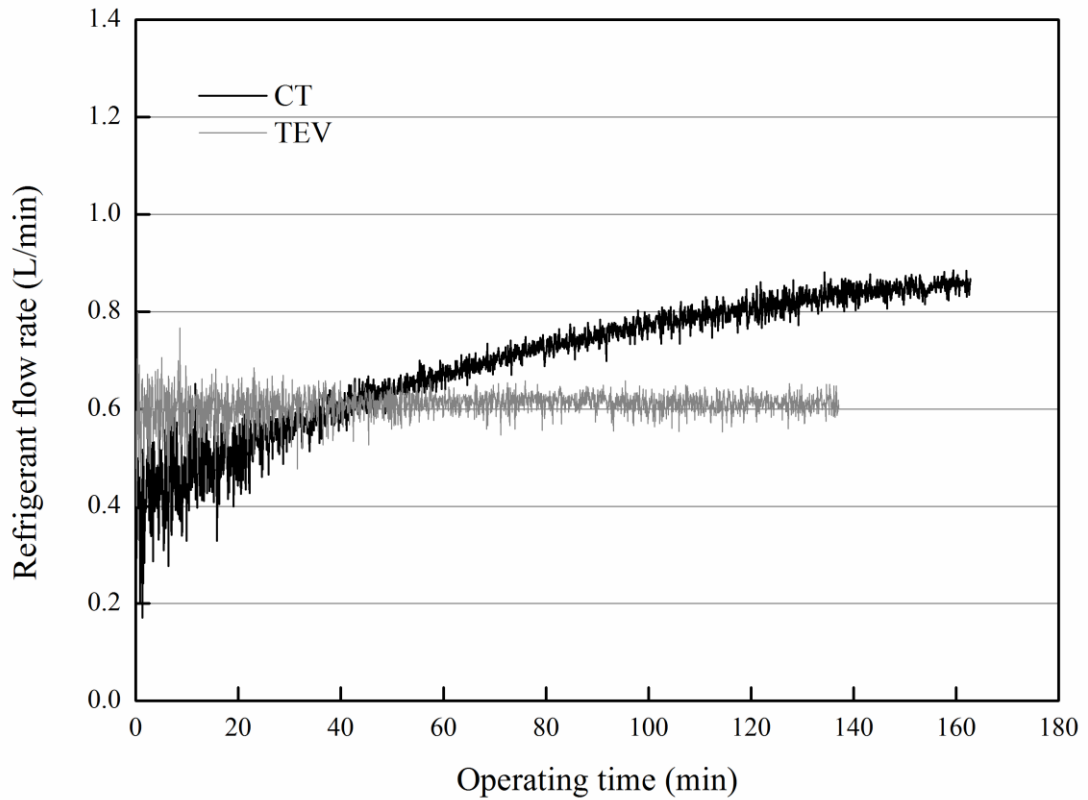
Figure 6.3   Refrigerant flow rates comparison

Figure 6.3 shows the changes in refrigerant flow rate with operating time, illustrating that the flow rate for the CT system increases with the discharge pressure. This is reasonable because the flow resistance across a CT is fixed so that the refrigerant flow rate at any one time depends on the pressure difference across it (Dossat, 1997). On the contrary, the refrigerant flow rate for the TEV system is fairly stable despite the discharge pressure increase. This is due to the active control provided by the TEV. At a particular valve opening position, the pressure increase also tends to increase the refrigerant flow, but that subsequently lowers the degree of superheat at the evaporator outlet. To restore the pre-set level of superheat, the TEV will reduce its opening extent and throttle the refrigerant flow. The flow rate thus does not vary much during the heat recovery process.
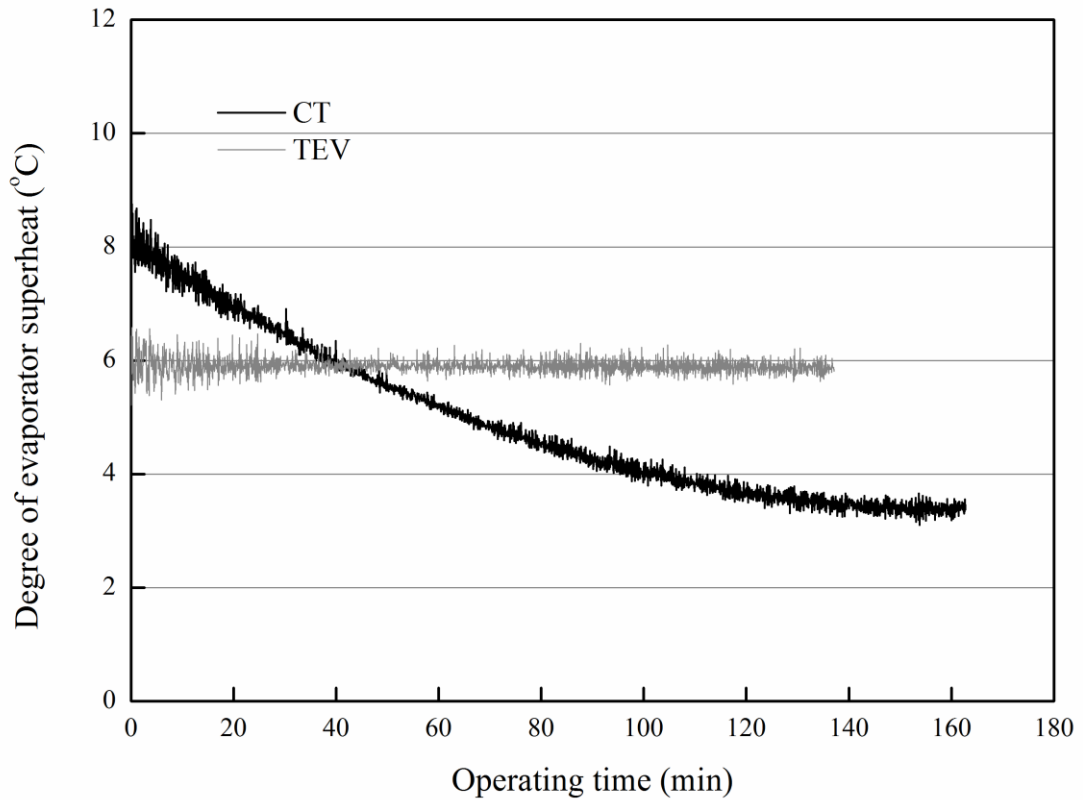
Figure 6.4   Degrees of superheat comparison

Figure 6.4 compares the degrees of evaporator superheat for the two systems, which are taken as the temperature difference between the saturated refrigerant and the refrigerant at the evaporator outlet. For the TEV system, the degree of superheat can be maintained constant as the discharge pressure increases due to the active control provided by the TEV, but the same cannot be done by the CT. For the CT system, the degree of superheat is high initially and decreases significantly with operating time. The high initial superheat value can lower the evaporator effectiveness and thus system performance and efficiency. While the decrease, resulted from the rise in refrigerant flow (Figure 6.3), will increase the risk of compressor flooding.

It should be noted that the results in Figure 6.4 were obtained under a lower than comfort indoor temperature of 18.5 $^{\circ}$C, which is considered the worst scenario where

the evaporating temperature was low, but the refrigerant flow rate was high to increase the risk of compressor flooding (Moreno-Rodriguez et al., 2013). The positive degrees of evaporator superheat obtained (8.1 $^{\circ}$C to 3.4 $^{\circ}$C for the CT system; 5.9 $^{\circ}$C for the TEV system) therefore confirm the feasible use of CT and TEV in SEHRAC under higher indoor temperature conditions.

The presence of vapor refrigerant at the evaporator inlet can reduce the refrigeration effect and thus is considered a loss to the system capacity (Dossat, 1997). This vapor is called flash gas and is formed in the expansion process due to a drop in saturated temperature with reduced refrigerant pressure. The amount of flash gas at the evaporator inlet is represented by its fraction in two-phase flow (vapor content, $x_{ei,r}$). $x_{ei,r}$ can be estimated by the following equation:

$$x_{ei,r} = \frac{h_{ei,r} - h_{sl}}{\sigma} \tag{6.1}$$

where $h_{ei,r}$ is the enthalpy of refrigerant at the evaporator inlet (kJ/kg); h_{sl} is the enthalpy of saturated liquid refrigerant (kJ/kg); σ is the latent heat of vaporization of refrigerant (kJ/kg).

The enthalpies in Equation (6.1) can be evaluated by a set of curve-fitted equations (Cleland, 1986). By assuming an isenthalpic expansion process, $h_{ei,r}$ is equal to the refrigerant enthalpy before the expansion device, which can subsequently be determined based on the corresponding pressure and temperature.
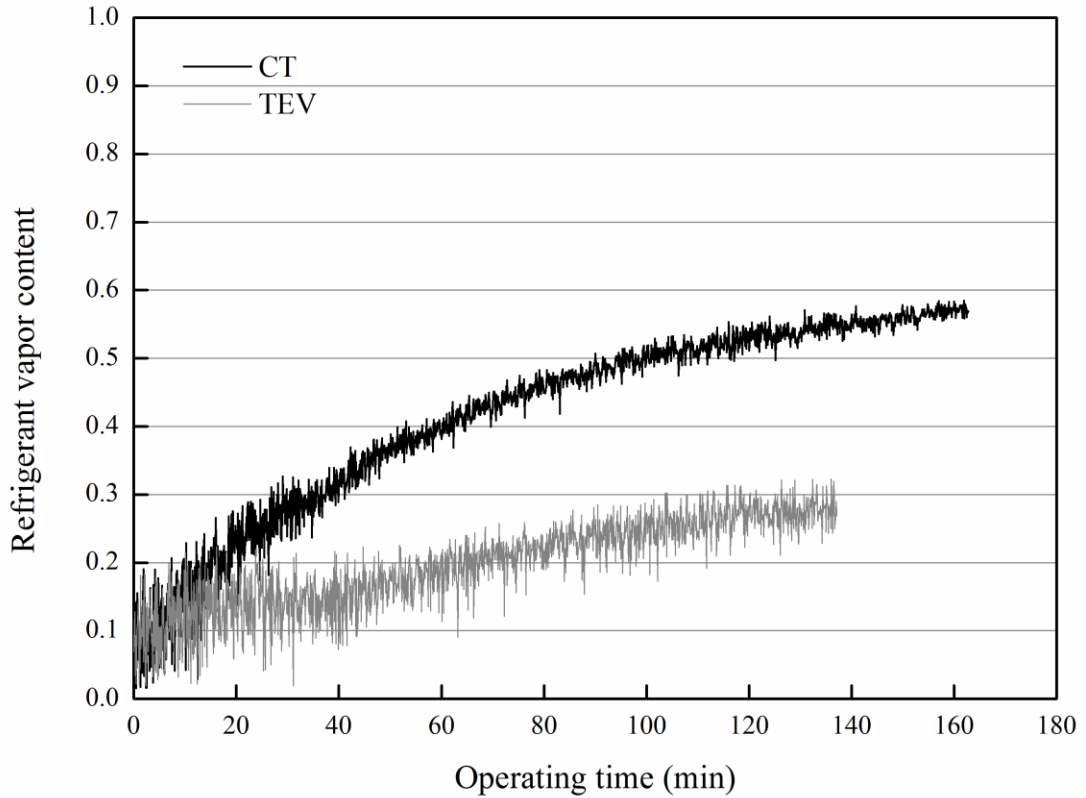
Figure 6.5   Refrigerant vapor contents comparison

Figure 6.5 compares $x_{ei,r}$ for the two systems, illustrating $x_{ei,r}$ increases with operating time for both systems. This can be explained by the fact that as the water temperature increases, the amount of heat rejection drops to lower the sub-cooling effect. As a result, more flash gas has to be generated to cool down the remaining liquid refrigerant to the required evaporating temperature. Between the two systems, $x_{ei,r}$ for the TEV system is constantly smaller, especially after the initial stage. This is attributed to the higher heat rejection amount for the TEV system to enhance the sub-cooling effect, as compared to the CT system (Dossat, 1997).

In the above, the pressure fluctuations, refrigerant flow rates, degrees of evaporator superheat and refrigerant vapor contents at the evaporator inlet for the CT and TEV systems are explained and compared.

102

6.3.2   Space Cooling Capacity

In this study, the space cooling capacity (Q_{cl}) of the prototype is determined based on the enthalpy drop of air across the evaporator (Equation (6.2)), while the air enthalpy is quantified by Equations (5.4) to (5.6) (Chapter 5).

$$Q_{cl} = m_a \left(h_{er,a} - h_{es,a} \right)$$
(6.2)

where m_a is the evaporator supply air flow rate (kg/s); $h_{er,a}$ and $h_{es,a}$ are the evaporator return and supply air enthalpies (kJ/kg), respectively.

Figure 6.6 compares the space cooling capacities for the CT and TEV systems at an operating time interval of 10-minute. It is noted that despite the TEV can operate to maintain a stable refrigerant flow and evaporator superheat in response to the refrigerant pressure fluctuations, the cooling capacity experiences a drop because of the increase in $x_{ei,r}$, resulting in less amount of liquid refrigerant available for effective cooling. This indicates the inadequacy of TEV when used in SEHRAC but is reasonable because TEV is typically a linear controller operating simply in response to a change in evaporator superheat (Broersen and Van der Jagt, 1980).

It is also reasonable to see that the cooling capacity for the TEV system is on average 19.0% larger than the CT system. This is due to the better control of evaporator superheat (as explained in Section 6.3.1) and the interactive influence of refrigerant flow rate and $x_{ei,r}$ on the cooling capacity. In the initial stage, the larger cooling capacity for the TEV system can be explained by the higher refrigerant flow

and the slightly lower $x_{ei,r}$. After that, despite the refrigerant flow rate for the CT system increases rapidly to exceed the TEV system, the rise in $x_{ei,r}$ outweighs to give a smaller cooling capacity.
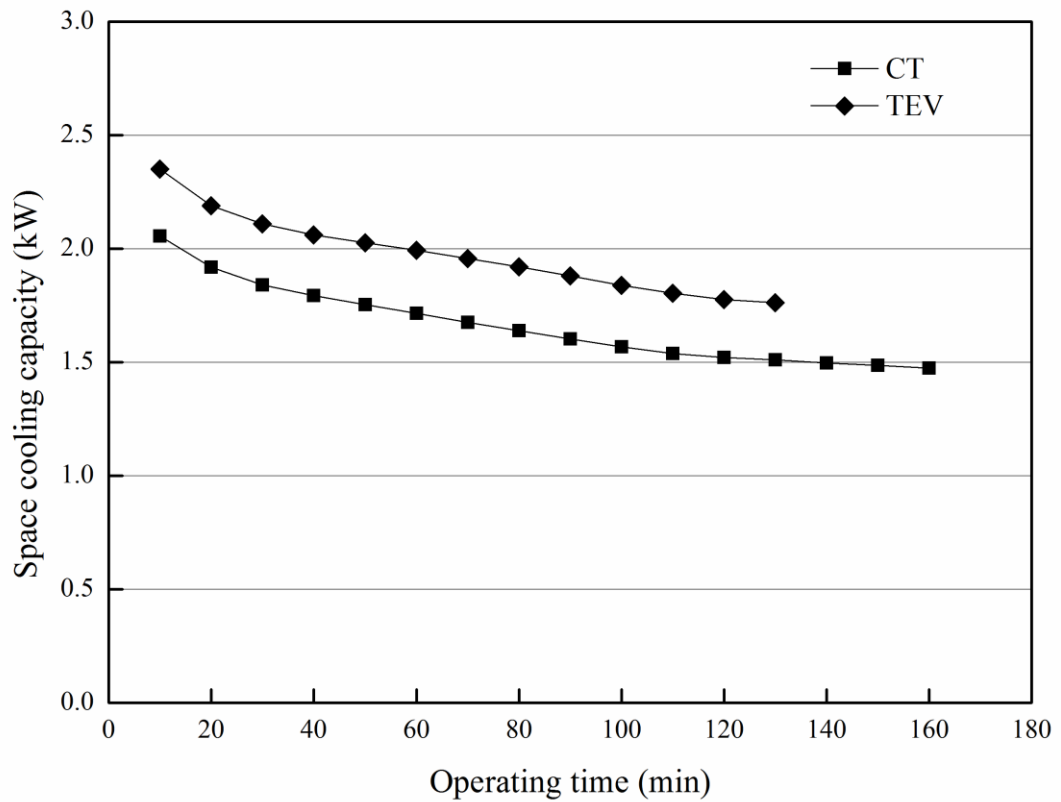
Figure 6.6   Space cooling capacities comparison

6.3.3   Water Heating Capacity

In this study, the water heating capacity (Q_{wh}) of the prototype is deduced from the increase rate of average tank water temperature (T_w):

$$Q_{wh} = c_{p,w} \rho_w V_w \frac{dT_w}{d\tau} \qquad (6.3)$$

where $c_{p,w}$ is the specific heat capacity of water (kJ/kg K); ρ_w is the water density (kg/m^3); V_w is the total volume of water in the water tank (m^3); T_w is the average tank water temperature (^{o}C); τ is the operating time (s).

Figure 6.7 compares the water heating capacities for the CT and TEV systems at an operating time interval of 10-minute. It can be seen that the heating capacities for both systems decrease continuously with operating time. This can be explained by the increase in tank water temperature to decrease the temperature difference between the refrigerant and the water. The heat transfer performance of the heat exchanger is thus adversely affected. As a result, the amount of vapor refrigerant condensed in the heat exchanger is reduced to lower the amount of heat rejection in the water tank. For the same reason, it is noted that the heating capacities for both systems drop at a much lower rate in the first 40-minute due to the higher temperature difference initially.

Furthermore, it is reasonable to note that the heating capacity for the TEV system is on average 18.7% larger than the CT system because of the higher amount of recoverable heat resulted from larger space cooling capacity. It can also be explained by the higher compressor discharge pressure for the TEV system (Figure 6.2) and thus higher refrigerant temperature at the water tank inlet to enhance the heat transfer performance of the heat exchanger (Moreno-Rodriguez et al., 2013).

From the above analysis, it can be concluded that the use of TEV can result in a larger space cooling capacity and water heating capacity due to its active control characteristics.
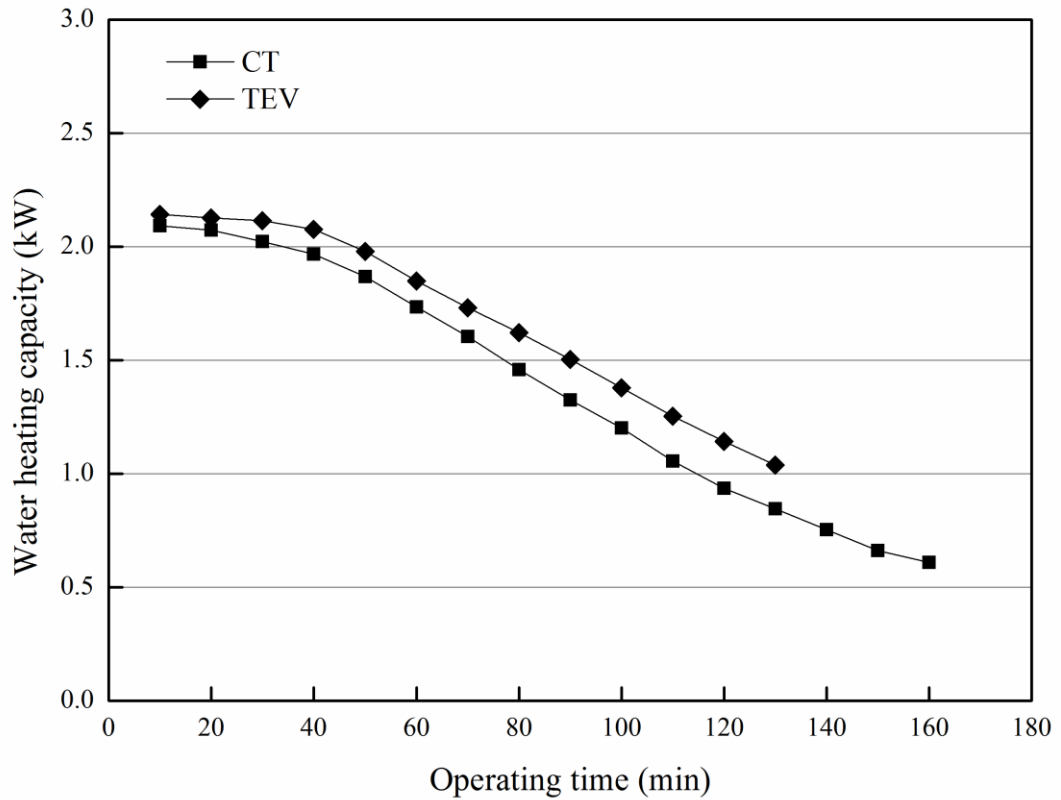
Figure 6.7   Water heating capacities comparison

6.3.4   Energy Performance

Figure 6.8 compares the power consumptions for the CT and TEV systems. Due to the rise in compressor discharge pressure as shown in Figure 6.2, the power consumptions for both systems experience a continuous increase with operating time. It is also noted that owing to the higher discharge pressure for the TEV system (Figure 6.2), it has slightly larger power consumption than the CT system.

In this study, the system energy efficiency is quantified by the use of overall coefficient of performance (COP_{oa}), which takes into account the space cooling and

water heating capacities, as well as power consumption (W) of the prototype. COP_{oa} can be mathematically presented as:

$$COP_{oa} = \frac{Q_{cl} + Q_{wh}}{W} \qquad (6.4)$$

Figure 6.8 compares COP_{oa} for the two systems, illustrating that the system efficiency decreases gradually with operating time. According to the previous discussions, this can be ascribed to the corresponding decrease in cooling and heating capacities, as well as the increase in power consumption. Moreover, it is unveiled from Figure 6.8 that despite the larger power consumption for the TEV system, the associated COP_{oa} is still on average 18.6% higher than the CT system.
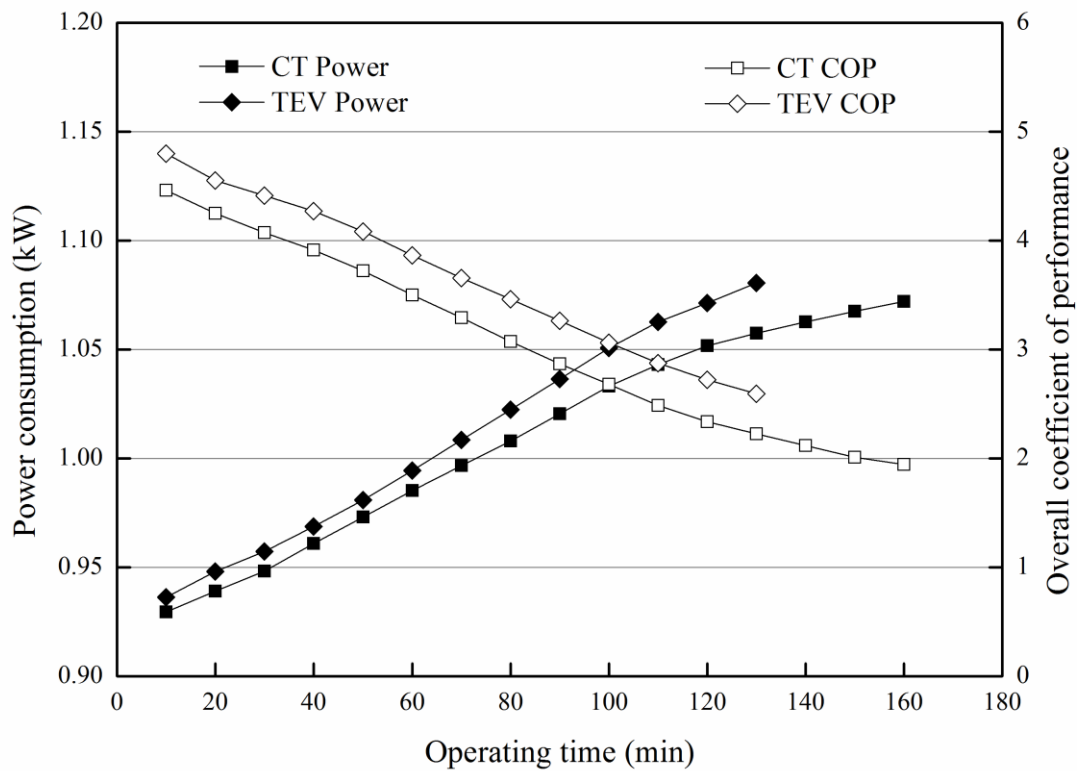
Figure 6.8   Power consumptions and COP_{oa} comparison

To review if the above findings are also valid for other experimental conditions, the time-weighted average cooling and heating capacities, power consumptions and COP_{oa} for both systems are determined and compared for different outdoor temperatures in Figure 6.9. It is noted that a rise in outdoor temperature increases the water heating capacity and simultaneously decreases the space cooling capacity to result in a cancellation effect in system output (sum of cooling and heating capacities). Therefore, the system output shows only a slight decrease with an increase in outdoor temperature from 25 ^{o}C to 35 ^{o}C, which, combined with an increase in power consumption, leads to a drop in COP_{oa} for both systems. It is also noted that similar to the results obtained for an outdoor temperature of 30 ^{o}C, COP_{oa} for the TEV system is 12.5% to 20.9% higher than the CT system, primarily owing to the larger system output.
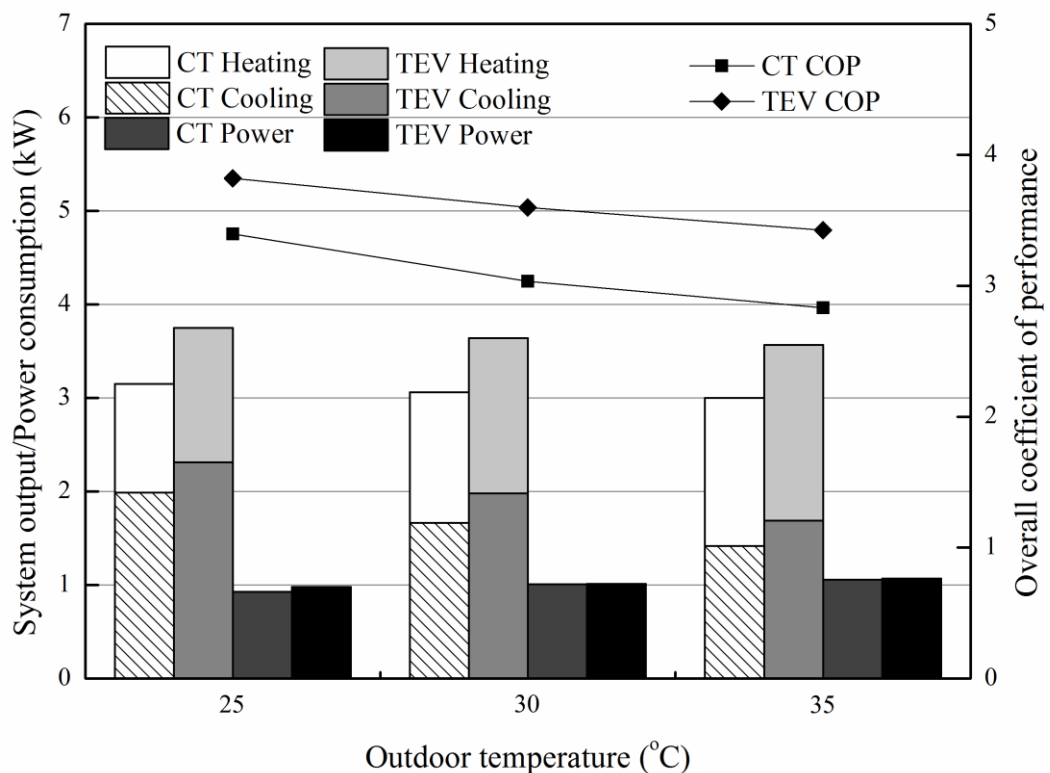
Figure 6.9   Energy performance comparisons for various outdoor temperatures

6.4 Uncertainty Analysis

The uncertainties in the calculated system performance can be determined based on the instrument accuracies summarized in Table 3.3.

By using Kline and McClintock's method (Doebelin, 1983; Holman, 1989), Equations (6.5) to (6.7), derived on the basis of Equations (6.2) to (6.4), can be obtained to determine the uncertainties in the calculated space cooling capacity, water heating capacity and overall coefficient of performance, while that in the power consumption can simply be taken as the corresponding instrument uncertainty.

$$\frac{\delta Q_{cl}}{Q_{cl}} = \sqrt{\left(\frac{\delta m_a}{m_a}\right)^2 + \frac{\delta h_{er,a}^2 + \delta h_{es,a}^2}{\left(h_{er,a} - h_{es,a}\right)^2}} \tag{6.5}$$

$$\frac{\delta Q_{wh}}{Q_{wh}} = \sqrt{\frac{\delta T_w^2 \left(\tau + \Delta\tau\right) + \delta T_w^2 \left(\tau - \Delta\tau\right)}{\left[T_w\left(\tau + \Delta\tau\right) - T_w\left(\tau - \Delta\tau\right)\right]^2}} \tag{6.6}$$

$$\frac{\delta COP_{oa}}{COP_{oa}} = \sqrt{\left(\frac{\delta Q_{cl}}{Q_{cl} + Q_{wh}}\right)^2 + \left(\frac{\delta Q_{wh}}{Q_{cl} + Q_{wh}}\right)^2 + \left(\frac{\delta W}{W}\right)^2} \tag{6.7}$$

Because of the unsteady system behavior as shown above, the maximum possible uncertainties are calculated and summarized in Table 6.2. The results are ranging from 2.1% to 8.8% and are judged to be acceptable as they are less than the ISO's recommendation of 10% (ISO, 2010).

Table 6.2　　　Uncertainties in the calculated system performance

Performance parameter	Relative uncertainty (%)	
	CT system	TEV system
Space cooling capacity	6.8	5.7
Water heating capacity	8.8	5.2
Power consumption	2.2	2.1
Overall coefficient of performance	5.8	4.6

6.5　Summary

The use of CT and TEV in SEHRAC as the expansion device were side-by-side compared by experimental investigations. To facilitate the investigations, a prototype, which could be switched between the CT and TEV systems, was designed and setup in a test facility for two identical sets of experiments. For each set of experiments, a series of tests under different outdoor temperatures were conducted. It was found that the TEV system could better regulate the refrigerant flow, maintain a stable evaporator superheat, and minimize the rise in refrigerant vapor content at the evaporator inlet. The space cooling and water heating capacities for the TEV system were on average 16.3% to 19.4% and 18.5% to 23.4% larger than the CT system, respectively. Its overall coefficient of performance was also found 12.5% to 20.9% higher for the range of outdoor temperatures. However, for both systems, due to a drop in heat transfer performance of the heat exchanger with operating time, a corresponding drop in cooling and heating capacities was observed. Uncertainty analysis was conducted. It was found that the measured and calculated results in this study were within an acceptable range of uncertainty.

CHAPTER 7

PERFORMANCE IMPROVEMENT OF SEHRAC: USING PHASE CHANGE MATERIAL FOR HEAT STORAGE CAPACITY ENHANCEMENT

As demonstrated in Chapter 6, accumulation of heat in the water tank of SEHRAC can result in an increase in tank water temperature, which will unavoidably affect the space cooling and water heating performances of SEHRAC. Measures to enhance the heat storage capacity of the water tank will thus be beneficial to the overall performance of SEHRAC. For achieving this objective, the use of phase change material (PCM) in the water tank of SEHRAC is proposed. An experimental study is presented in this chapter to confirm and quantify the resultant performance improvement.

7.1   Introduction

It was revealed from the above chapters that the increase in tank water temperature resulted from heat recovery unavoidably affects the space cooling and water heating performances of SEHRAC. Therefore, measures to enhance the heat storage capacity of the water tank will be beneficial to the overall performance of SEHRAC.

For achieving this objective, the use of phase change material (PCM) in the water tank of SEHRAC is proposed in this study. PCM is capable of storing and releasing large amounts of energy when charging and discharging. During charging, the material changes from solid to liquid and vice versa for discharging. As reported, PCMs can typically store 5 to 14 times more energy per unit volume than water (Sharma et al., 2009). The phase change characteristics also allow heat storage or release at an almost constant temperature.

For SEHRAC, the benefit of using PCM with a high energy storage density is twofold. First, its overall performance can be improved with the heat storage capacity of the water tank enhanced by PCM charging. And when it is not operating, PCM discharging can partially offset the heat loss from the water tank to better maintain the hot water at desired temperature.

In this chapter, to confirm and quantify the resultant performance improvement by the use of PCM, a prototype SEHRAC was designed and setup in a test facility for laboratory experiments. Two identical sets of experiments with and without the use of PCM (abbreviated as wPCM and woPCM scenarios) under a range of outdoor temperatures were conducted. In the experiments, the operating parameters on the refrigerant, air and water sides of the system were closely monitored. Based on the experimental results, the heat storage capacity of the water tank, the refrigerant side operation characteristics, as well as the space cooling, water heating and overall energy performances were examined and compared for the two scenarios.

7.2   Experimental Study

7.2.1   Test Facility

The experiments were conducted in a test facility located at the Hong Kong Polytechnic University. The test facility comprised two completely insulated and separated environmental chambers resembling indoor and outdoor conditions. Detailed descriptions of the test facility can be found in Section 3.2.1.

In the experiments, the desired conditions in the chambers were achieved by the use of PID controllers to provide real-time adjustments of the LGUs outputs and were maintained unchanged throughout each test.

7.2.2   Prototype Design

To accomplish the objectives of this study, a prototype was designed and setup for laboratory experiments. The schematic of the prototype is shown in Figure 7.1. It mainly comprised a split-type air-cooled air-conditioner and a heat recovery water tank. Inside the water tank, there were a helical heat exchanger and a cylindrical PCM container. Detailed descriptions of the prototype can be found in Section 3.2.2.

The PCM container was placed inside the helical heat exchanger and was located centrally in the water tank (Figure 7.1). It was made of aluminum with longitudinal fins added to the external surface to enlarge the total heat transfer area for

minimizing the thermal resistance between the container and the water. A cross-sectional view (with detailed dimensions) and a photograph of the PCM container are shown in Figures 7.2 and 7.3, respectively. The dimensions were determined by reference to a study by Castell et al. (2008), which was also on domestic hot water heating but on a solar-powered system.
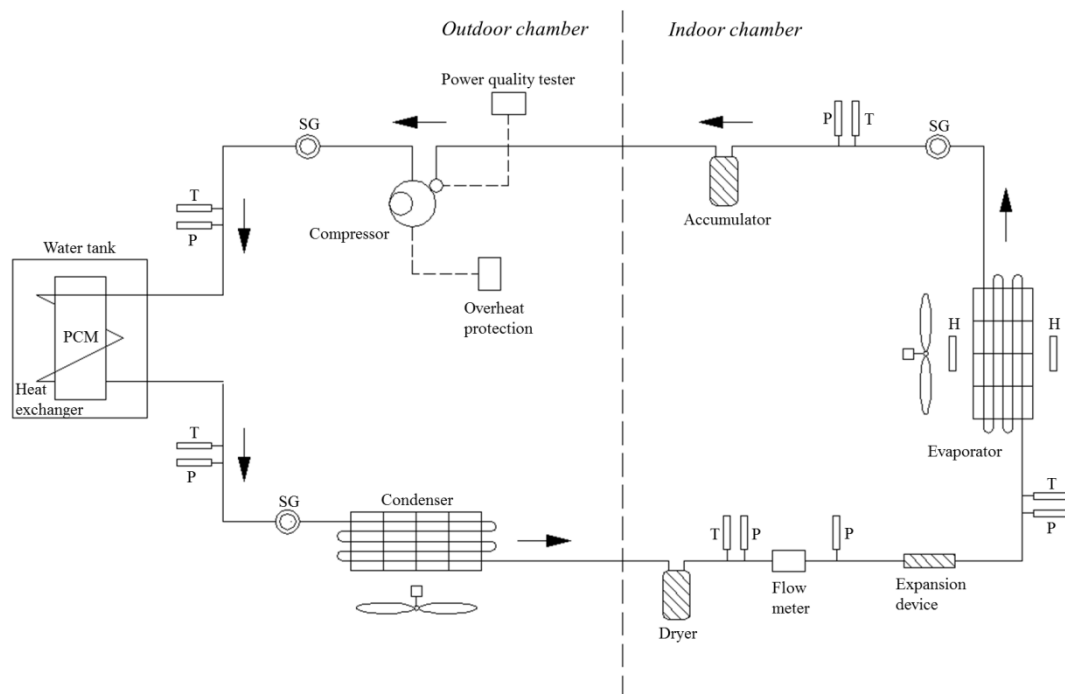
Figure 7.1   Schematic of the prototype for evaluating the use of PCM
(T: Thermocouple; P: Pressure transmitter; H: Hygrometer; PCM: PCM container)

The temperature of hot water for direct residential use often ranges between 35 ^{o}C and 50 ^{o}C (Chen and Lee, 2010). There are a number of PCMs with phase change temperatures within this range; namely salt hydrates, fatty acids and paraffin waxes (Cabeza et al., 2011). Among them, paraffin waxes are considered the most suitable option for domestic hot water applications owing to their non-toxicity, wide availability, low cost and non-corrosive property (Zalba et al., 2003).

In this study, Paraffin wax RT44HC supplied by Rubitherm Technologies GmbH was chosen as the latent heat storage material. Given the poor heat conduction performance of the paraffin, expanded graphite (EG) with a high thermal conductivity was mixed into it to form an EG/paraffin composite PCM. To enable uniform distribution of EG in the composite, an ultra-sonic stirrer was used during the addition of EG to the melted paraffin. The properties of the paraffin and the EG used are summarized in Table 7.1.
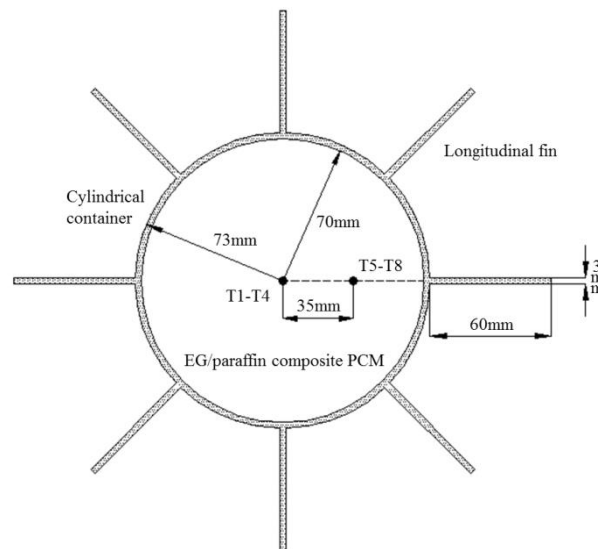
Figure 7.2   Cross-sectional view of the PCM container

(T1-T4 and T5-T8: Temperature measurements numbered from top to bottom)
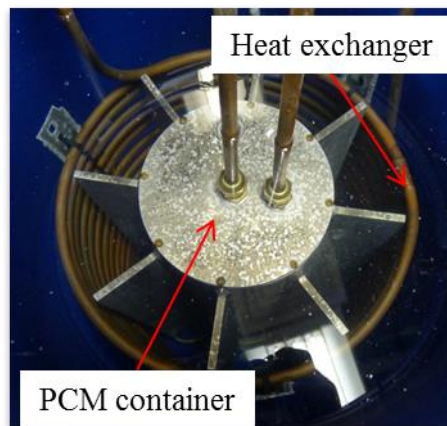
Figure 7.3   Photograph of the PCM container

EG is highly porous and has a good compatibility with organic materials. In an EG/paraffin composite PCM, EG serves as a solid matrix to enable the impregnation of paraffin into its pores by capillary and surface tension forces (Xia et al., 2010). A conductive network is then formed by EG to enhance the overall thermal conductivity. For achieving a balance between thermal conductivity and energy storage density, too high or too low an EG content is not desirable. Previous literatures recommended 7% to 15% by volume and 10% was most commonly adopted (Cabeza et al., 2006; Castell et al., 2008; Öttinger and Bacher, 2010). Therefore, the composite PCM (hereinafter referred to as the PCM) with an EG content of 10% by volume was used in this study. Its thermal conductivity measured by using transient hot-wire method was 1.2 W/m K, while the total mass that could be encapsulated in the PCM container was about 12.6 kg.

Table 7.1　　Properties of the paraffin and the EG

Paraffin	
Melting temperature range	39.1 $^{\circ}$C to 42.5 $^{\circ}$C
Solidification temperature range	43.6 $^{\circ}$C to 42.3 $^{\circ}$C
Latent heat of fusion	256.9 kJ/kg
Specific heat capacity	2 kJ/kg K (solid and liquid)
Thermal conductivity	0.2 W/m K (solid and liquid)
EG	
Average particle size	180 μm
Bulk density	10 kg/m^3
Carbon content	≥95%
Moisture content	≤5%
Thermal conductivity	23 W/m K

7.2.3   Measurements

In the experiments, the operating parameters on the refrigerant, air and water sides of the system were closely monitored (detailed in Section 3.2.3). Besides those, Pt100 RTDs were used for measuring the PCM temperatures along two longitudinal axes of the container. Along each axis, temperature measurements were taken at four equally spaced positions (T1-T4 and T5-T8 in Figure 7.2).

7.2.4   Experimental Conditions

The experiments carried out in this study were classified as heat charging and discharging tests. Heat charging referred to water heating in the water tank, while heat discharging referred to heat loss from the water tank to the atmosphere. For each test, two identical sets of experiments with and without the use of PCM (wPCM and woPCM scenarios) were conducted.

For the heat charging test, the indoor temperature was maintained at 22 $^{\circ}$C, while the outdoor temperature was varied from 25 $^{\circ}$C to 35 $^{\circ}$C with an interval of 5 $^{\circ}$C to become three different experimental conditions (same as Chapters 5 and 6). The outdoor temperature range was determined by reference to Hong Kong's climate data during the air-conditioned season (BEAM Society, 2010).

For the heat discharging test, the indoor chamber was left idle, while the outdoor chamber (where the water tank was located) was maintained at 23 $^{\circ}$C. The

temperature was chosen because it corresponds to Hong Kong's annual average outdoor temperature in the typical meteorological year (Chan et al., 2006).

7.2.5   Experimental Procedures

7.2.5.1 Heat Charging Experiments

The outdoor chamber was first conditioned to the pre-set condition. The tank water and the PCM (in the case of the wPCM scenario) were heated to an initial temperature of 25 ^{o}C, which is Hong Kong's annual average tap water temperature (Chen and Lee, 2010). Upon achieving the desired conditions, the prototype, the LGUs in the indoor chamber and all the measuring instruments were powered on to maintain the indoor chamber at 22 ^{o}C and 55% RH. Under this condition, the indoor cooling load (generated by the LGUs) was actively adjusted to exactly offset the instantaneous cooling output of the prototype.

For the wPCM scenario, the experiment was stopped on complete melting of the paraffin in the PCM. The complete melting was confirmed by checking if the PCM temperatures measured at positions T1 to T4 (Figure 7.2) had exceeded the melting temperature range and reached a thermal equilibrium with the surrounding water. The four measurement positions were chosen because they were furthest from the heat transfer boundary. The time spent for the entire experiment was recorded. An identical experiment, with the same time spent, was then carried out for the woPCM scenario to enable their direct comparisons. The above-described experiments, both

for the wPCM and woPCM scenarios, were repeated for the three outdoor temperature conditions.

7.2.5.2 Heat Discharging Experiments

The tank water and the PCM (in the case of the wPCM scenario) were heated to an initial temperature of 50 ^{o}C (maximum hot water temperature for direct residential use (Chen and Lee, 2010)). The water was then left to cool down naturally to the minimum use temperature (=35 ^{o}C) in an ambient of 23 ^{o}C. The time elapsed for the entire experiment was recorded. The procedures were repeated for the woPCM scenario to enable their direct comparisons.

7.3   Results and Discussion

This section discusses the performance of the prototype operated in the wPCM scenario as compared to that in the woPCM scenario. For heat charging, the performance is evaluated based on the heat storage capacity of the water tank, the refrigerant side performance, the space cooling and water heating capacities, as well as the overall energy performance. For heat discharging, the performance is evaluated based on the heat retention time of the tank water. Due to the large amount of experimental data collected, performance evaluations for heat charging are presented for an outdoor temperature of 30 ^{o}C. The results obtained for other experimental conditions will also be analyzed and given where necessary.

7.3.1 Heat Storage Capacity of the Water Tank

During heat charging, whether the use of PCM can enhance the heat storage capacity of the water tank and can eventually lower the tank water temperature are important to the performance improvement of the prototype.
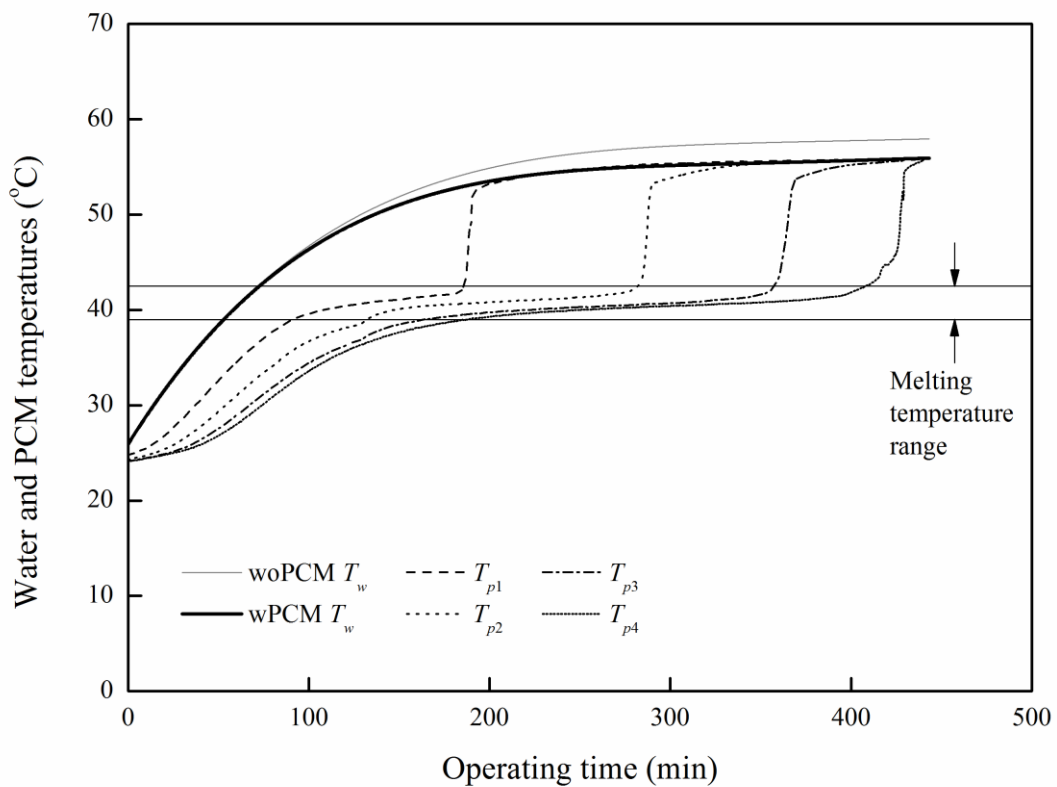
Figure 7.4   Water and PCM temperatures during heat charging

Figure 7.4 compares the time varying average tank water temperatures (T_w) for the wPCM and woPCM scenarios. In the figure, T_w is taken as the arithmetic mean of the water temperatures measured at 12 different positions in the water tank. It can be seen that upon the prototype is switched on, owing to the condensation of the hot vapor refrigerant from the compressor discharge, T_w for both scenarios increase gradually to exceed 50 $^{\circ}$C. But the rate of the temperature increase drops with

operating time to indicate a reduced amount of heat rejection in the water tank. It is further noted that T_w for the wPCM scenario is constantly lower during heat charging, with a maximum temperature difference of 2 ^{o}C. This is attributed to the use of PCM in the water tank. As a result, part of the energy stored in the water is absorbed by the PCM to lower the rate of increase in T_w. Moreover, as compared to the T_w profiles shown in Figure 5.3 that were obtained under intermittent operation of the prototype, the rate of increase in T_w as compared to that in Figure 7.4, is much higher.

To demonstrate a proper heat charging, Figure 7.4 shows also the time varying PCM temperatures for the wPCM scenario measured at the four positions along the centered axis of the PCM container (T_{p1} to T_{p4} for T1 to T4 in Figure 7.2). By analyzing the paraffin with differential scanning calorimetry (DSC) technique, its melting temperature range (39.1 ^{o}C to 42.5 ^{o}C) can be identified and is shown as two horizontal lines in Figure 7.4.

Based on the identified melting temperature range, the changes in the PCM temperatures can be explained. It can be seen that the profiles for T_{p1} to T_{p4} are divided into three phases. They are solid sensible heating, phase change and liquid sensible heating phases. In the solid sensible heating phase, the energy absorbed by the PCM is in the form of sensible heat, which raises its temperature linearly from 26 ^{o}C to 39.1 ^{o}C. But the temperature increase, as compared to that in the water, is at a relatively low rate. Upon reaching the temperature of 39.1 ^{o}C, the paraffin in the PCM starts to change phase and turn from solid to liquid, whereby the PCM temperature remains nearly constant. As the temperature increases to exceed 42.5 ^{o}C,

the paraffin in the pores of EG is melted. Energy is then absorbed in the form of sensible heat. As the heat transfer in liquid paraffin can be enhanced by convection (Agyenim and Hewitt, 2010), the PCM temperature therefore jumps immediately to reach a thermal equilibrium with the water.

Besides phase change, the PCM also exhibits a vertical temperature difference. A review of the profiles for T_{p1} to T_{p4} shows that the PCM in the upper part of the container spends much less time to reach a common temperature with the water. This can be explained by the top inlet design of the heat exchanger as described previously. With this configuration, the hot vapor refrigerant discharged from the compressor flows from top to bottom of the water tank, resulting in higher water temperature in the upper part and thus higher heat transfer potential between the water and the PCM.

As for the heat storage capacity of the water tank (H_s), it can be estimated by using Equation (7.1) for the woPCM scenario. While for the wPCM scenario, H_s can be quantified by using Equation (7.2) when the sensible heat stored in the EG is ignored.

$$H_s = c_{p,w} M_w \Delta T_w \tag{7.1}$$

$$H_s = c_{p,w} M_w \Delta T_w + c_{p,pa} M_{pa} \Delta T_{pa} + \lambda M_{pa} \tag{7.2}$$

where $c_{p,w}$ and $c_{p,pa}$ are the specific heat capacities of water and paraffin (kJ/kg K), respectively; M_w and M_{pa} are the total masses of water and paraffin (kg), respectively; ΔT_w and ΔT_{pa} are the temperature increments of water (= 31.9 $^{\circ}$C for woPCM; 29.9

^{o}C for wPCM) and paraffin (= 29.9 ^{o}C) for the entire experiment (^{o}C), respectively; λ is the latent heat of fusion of paraffin (kJ/kg).

In Equation (7.2), the three product terms on the right-hand side represent, respectively, the sensible heat stored in the water, the sensible heat stored in the PCM and the latent heat stored in the PCM. According to Equation (7.2), H_s for the wPCM scenario is estimated to be 20.1 MJ, which is 15.7% higher than that for the woPCM scenario (= 17.4 MJ). It can therefore be seen that, despite the lower T_w, the wPCM scenario still has a higher H_s due to the higher energy storage density of the PCM.

Based on the above, it is evident that the PCM can function as an internal heat sink to lower the rate of water temperature increase during heat charging and to enhance the heat storage capacity of the water tank.

7.3.2 Refrigerant Side Performance

The refrigerant side performance of the prototype can be revealed from the compressor suction and discharge pressures, the refrigerant flow rate and the refrigerant vapor content at the evaporator inlet.

To illustrate the refrigerant pressure fluctuations during heat charging, Figure 7.5 compares the time varying compressor suction ($P_{cs,r}$) and discharge ($P_{cd,r}$) pressures for the two scenarios. It can be seen that $P_{cd,r}$ for both scenarios display a continuous

increase with operating time. This is because as T_w increases, the heat rejection performance of the prototype drops to increase the condensing pressure and thus $P_{cd,r}$. Between the two scenarios, the wPCM scenario has a slightly lower $P_{cd,r}$ due to the lower T_w as revealed in Figure 7.4. While for $P_{cs,r}$, it is less influenced by the heat recovery, thus a very small change is observed for both scenarios.
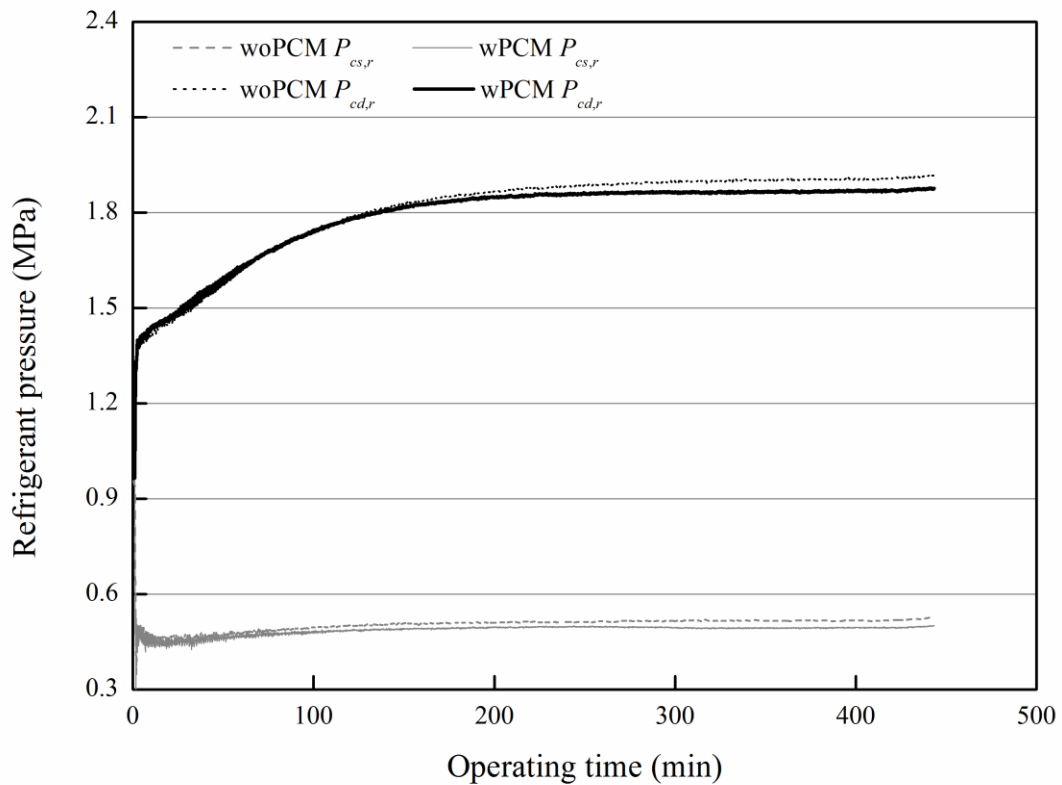
Figure 7.5   Comparisons of compressor suction and discharge pressures

Figure 7.6 compares the time varying refrigerant flow rates (m_r) for the two scenarios, illustrating that m_r for both scenarios are fairly stable despite the pressure fluctuations. This is due to the active control characteristics provided by the TEV. The refrigerant flow in a TEV system depends on the pressure difference across the TEV as well as its opening extent (Dossat, 1997). At a particular opening position, the rise in $P_{cd,r}$ tends to increase m_r, but that subsequently lowers the degree of

superheat at the evaporator outlet. To restore the pre-set degree of superheat, the TEV will reduce its opening extent to throttle the refrigerant flow. Therefore, m_r does not vary much during heat charging. For the same reason, it is noted that m_r for the two scenarios are almost identical despite the difference in $P_{cd,r}$ (Figure 7.5).
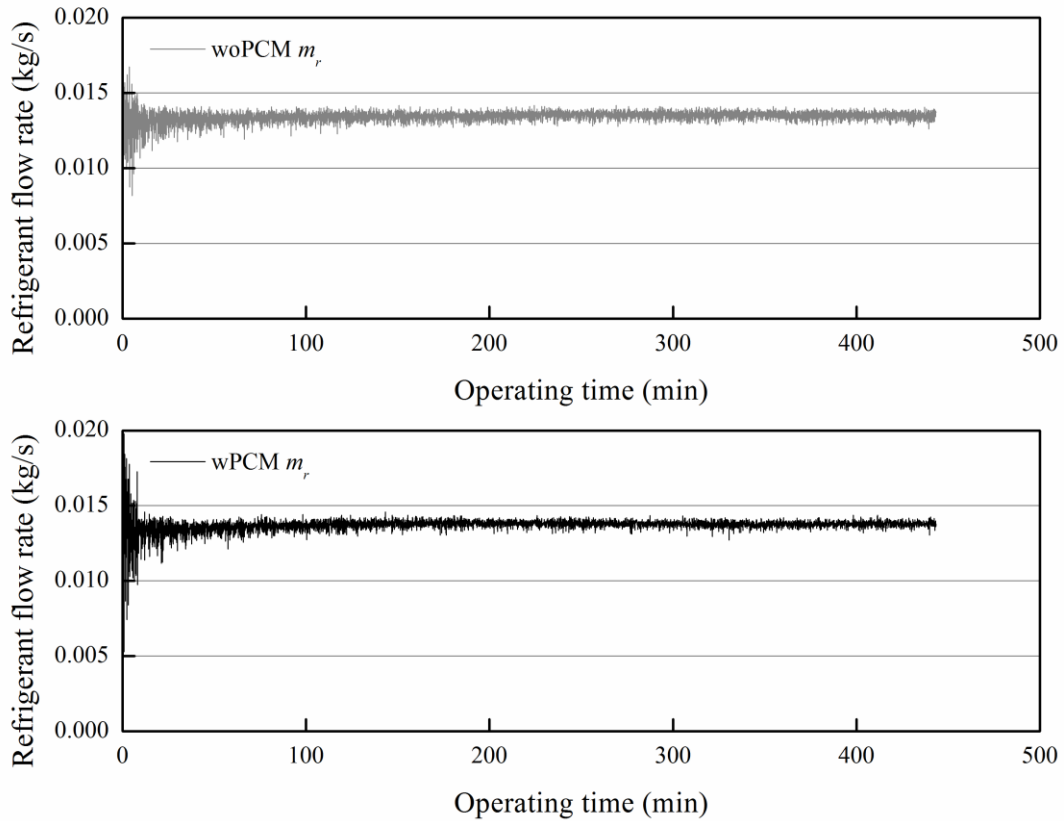
Figure 7.6 Refrigerant flow rate comparisons

The amount of vapor refrigerant at the evaporator inlet is a key indicator of system performance because the presence of vapor can reduce the amount of liquid refrigerant available for effective cooling (Dossat, 1997). The vapor is called flash gas and is formed in the expansion process due to a drop in saturated temperature with reduced refrigerant pressure. The amount of flash gas at the evaporator inlet is represented by its fraction in two-phase flow (vapor content, $x_{ei,r}$). $x_{ei,r}$ is affected by

the heat rejection performance. A better heat rejection performance will result in a lower $x_{ei,r}$ (ASHRAE, 2009). $x_{ei,r}$ can be estimated by using Equation (6.1).

Figure 7.7 compares the time varying $x_{ei,r}$ for the two scenarios, illustrating that they both increase with operating time. This is because as T_w increases, the amount of heat rejection of the prototype drops. Therefore, more flash gas has to be generated to cool down the remaining liquid refrigerant to the required evaporating temperature. Between the two scenarios, it can be seen that $x_{ei,r}$ for the wPCM scenario is constantly lower, especially after the early stage. This can be explained by the lower T_w (Figure 7.4) and thus a better heat rejection performance of the prototype for the wPCM scenario.
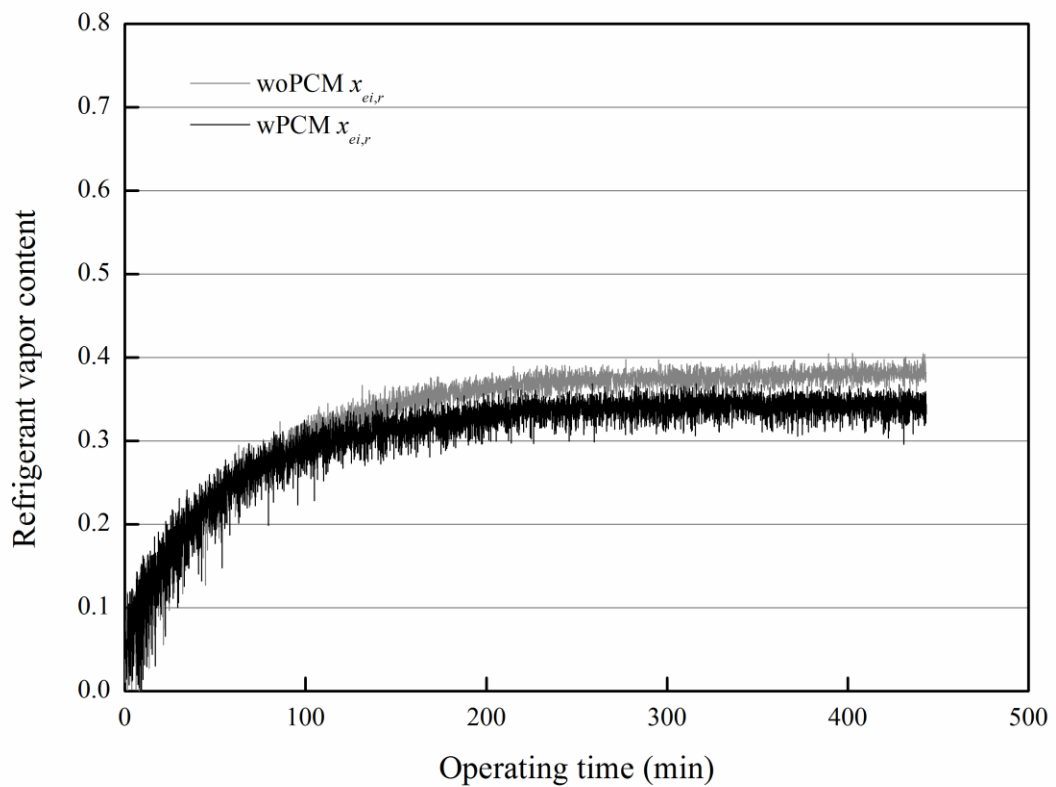
Figure 7.7   Refrigerant vapor content comparisons

In the above, the refrigerant pressure fluctuations, flow rates and vapor contents for the two scenarios are explained and compared to confirm a better refrigerant side performance for the wPCM scenario.

7.3.3 Space Cooling and Water Heating Capacities

The differences in refrigerant side operation characteristics explained above will result in different space cooling and water heating capacities between the two scenarios as discussed below.

In this study, the space cooling capacity (Q_{cl}) of the prototype is determined based on the enthalpy drop of air across the evaporator (Equation (7.3)), while the air enthalpy is quantified by using Equations (5.4) to (5.6).

$$Q_{cl} = m_a \left(h_{er,a} - h_{es,a} \right) \tag{7.3}$$

Similarly, the water heating capacity (Q_{wh}) of the prototype is deduced from the enthalpy drop of refrigerant in the heat exchanger:

$$Q_{wh} = m_r \left(h_{hi,r} - h_{ho,r} \right) \tag{7.4}$$

where $h_{hi,r}$ and $h_{ho,r}$ are the refrigerant enthalpies at the heat exchanger inlet and outlet (kJ/kg), respectively.

Figure 7.8 compares the time varying Q_{cl} for the two scenarios at 20-minute intervals. It can be seen that owing to the slightly lower T_w (Figure 7.4) and $x_{ei,r}$ (Figure 7.7) for the wPCM scenario, the associated Q_{cl} is larger than that for the woPCM scenario by 5.4% on average.

Regarding the cooling capacity profiles, it is noted that despite the rather stable m_r for both scenarios (Figure 7.6), Q_{cl} drops substantially in the early stage and becomes stable afterwards. The drop is attributed to the increase in $x_{ei,r}$ (Figure 7.7), resulting in less amount of liquid refrigerant available for vaporization. While $x_{ei,r}$ continues to increase and tends to be stable, Q_{cl} drops correspondingly and approaches a steady state.
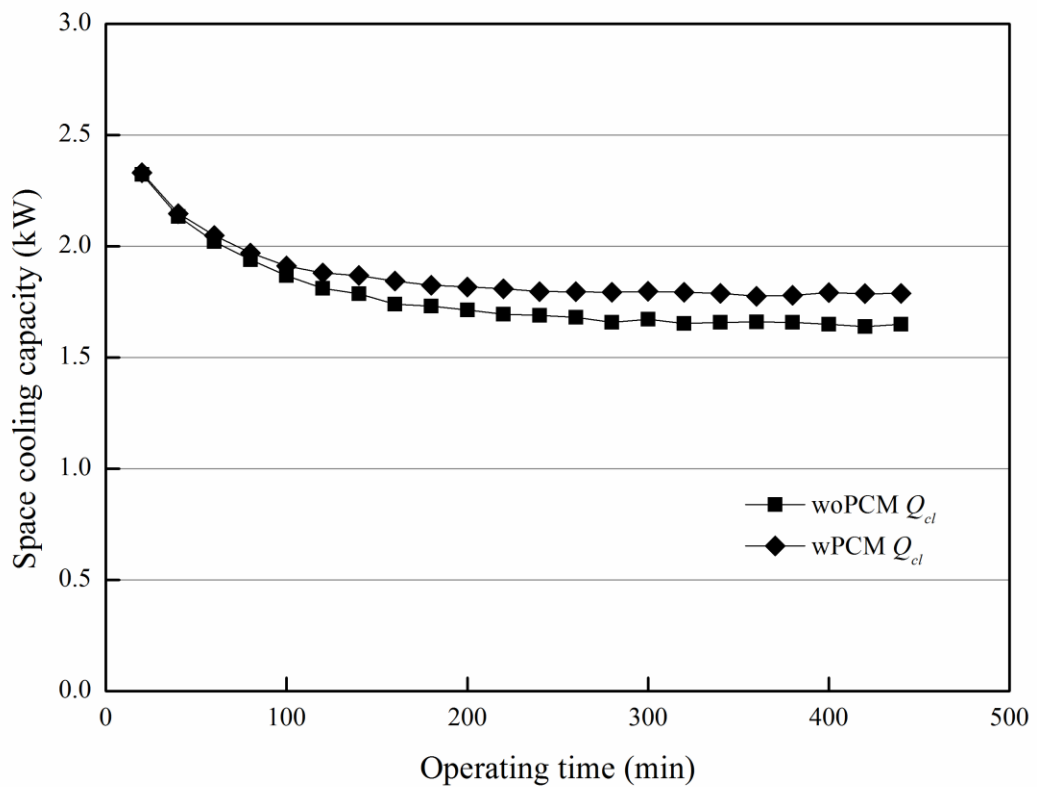
Figure 7.8   Space cooling capacity comparisons

Figure 7.9 compares the time varying Q_{wh} for the two scenarios at 20-minute intervals. It is reasonable to see that Q_{wh} for the wPCM scenario is constantly larger. The average difference is 16.1%. This is attributed to the use of PCM, as identified previously, to lower the rate of increase in T_w during heat charging, which can enhance the heat transfer performance of the heat exchanger.
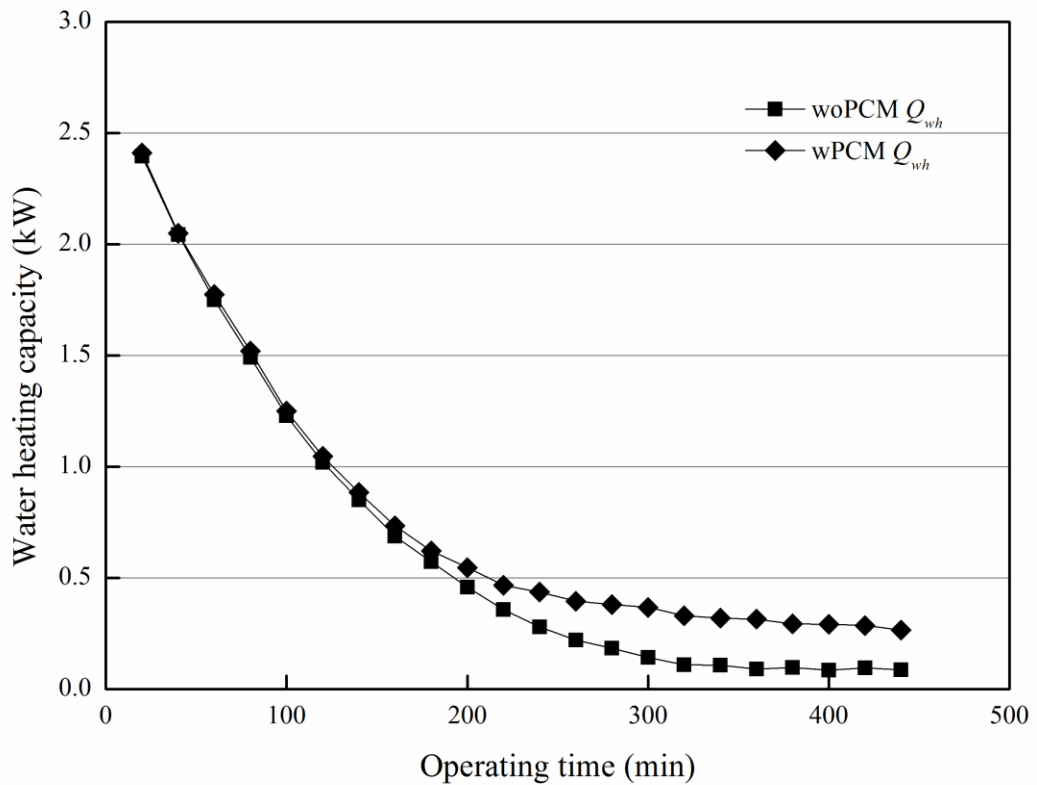
Figure 7.9　　Water heating capacity comparisons

Regarding the heating capacity profiles, it is noted that Q_{wh} drops significantly with operating time for both scenarios. This can be explained by the increase in T_w to decrease the temperature difference between the refrigerant and the water. The heat transfer performance of the heat exchanger is thus adversely affected (Bejan, 1993), leading to reduced amount of vapor refrigerant condensed in the heat exchanger. For

the same reason, it can be seen that Q_{wh} for both scenarios are rather stable in the late

stage due to the corresponding slower increase in T_w (Figure 7.4).

It is evident from the above that both the space cooling and water heating capacities

of the prototype can benefit from the enhanced heat storage capacity of the water

tank.

7.3.4   Overall Energy Performance

In this study, the overall energy performance is quantified by the use of overall

coefficient of performance (COP_{oa}), which takes into account the space cooling and

water heating capacities, as well as power consumption (W) of the prototype. COP_{oa}

is mathematically presented as:

$$COP_{oa} = \frac{Q_{cl} + Q_{wh}}{W} \qquad (7.5)$$

Figure 7.10 compares the time varying COP_{oa} for the two scenarios. It is noted that

COP_{oa} drops gradually with operating time. According to the previous discussions,

this is attributed to the corresponding decrease in Q_{cl} and Q_{wh}. Moreover, it is

unveiled from Figure 7.10 that COP_{oa} for the wPCM scenario is on average 8.9%

higher than that for the woPCM scenario.
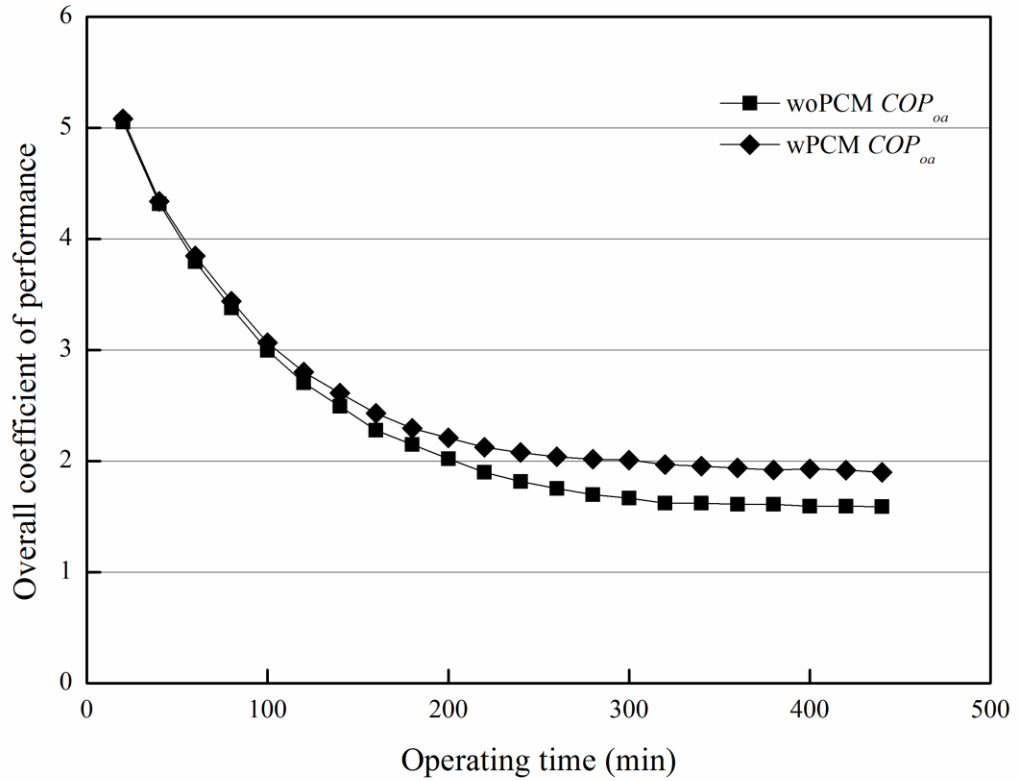
Figure 7.10   Overall energy performance comparisons

To review if the above findings are also valid for other experimental conditions, the time-weighted averages (Y) of Q_{cl}, Q_{wh}, W and COP_{oa} for both scenarios are determined for different outdoor temperature conditions by using the following equation:

$$Y = \frac{\int_0^{\alpha} X(\tau)\, d\tau}{\alpha} \qquad (7.6)$$

where X is the parameter being averaged; τ is the operating time; α is the time spent for the entire experiment.

Results are shown in Figure 7.11. It is noted that a rise in outdoor temperature decreases Q_{cl} and simultaneously increases Q_{wh} to result in a cancellation effect in system output (sum of Q_{cl} and Q_{wh}). Therefore, the system output displays only a slight decrease with an increase in outdoor temperature from 25 ^{o}C to 35 ^{o}C. The decrease, combined with a marginal increase in W, results in a drop in COP_{oa} with outdoor temperature for both scenarios. It is further noted in Figure 7.11 that COP_{oa} for the wPCM scenario is constantly higher, with a difference ranging from 6.9% to 9.8% for different experimental conditions, primarily owing to the larger system output.
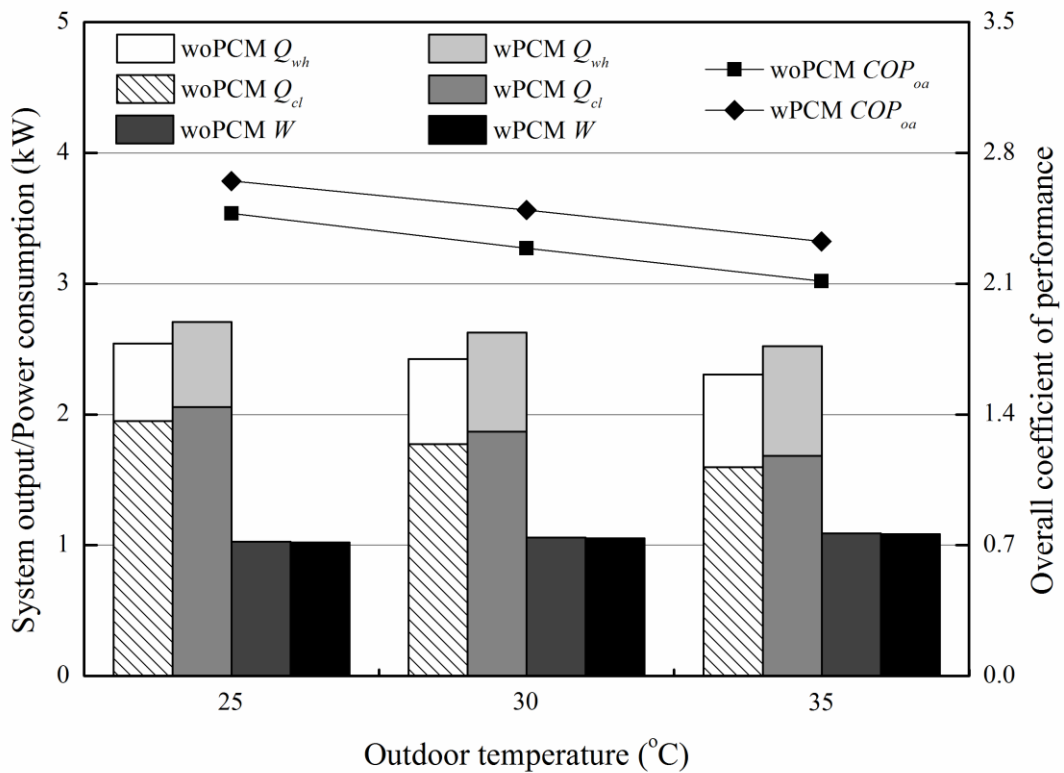
Figure 7.11   Energy performance comparisons for various outdoor temperatures

7.3.5   Heat Retention Time

The heat retention time, defined as the time elapsed for the tank water to drop below the desired temperature (= 35 $^{\circ}$C), can be revealed from the heat discharging test described previously in Section 7.2.5.2.

Figure 7.12 shows the time varying average water (T_w) and PCM (T_p) temperatures for the two scenarios. In the figure, T_p is taken as the arithmetic mean of the temperatures measured at positions T1 to T8 in the PCM container (Figure 7.2). It can be seen that the profiles for T_w are similar in the early stage. But they start to deviate from each other when T_p drops below 43.6 $^{\circ}$C. This is because the PCM has reached the solidification temperature range (43.6 $^{\circ}$C to 42.3 $^{\circ}$C) when the paraffin in it starts to turn from liquid to solid. The latent heat released therefore heats up the water to result in a lower rate of drop in T_w.
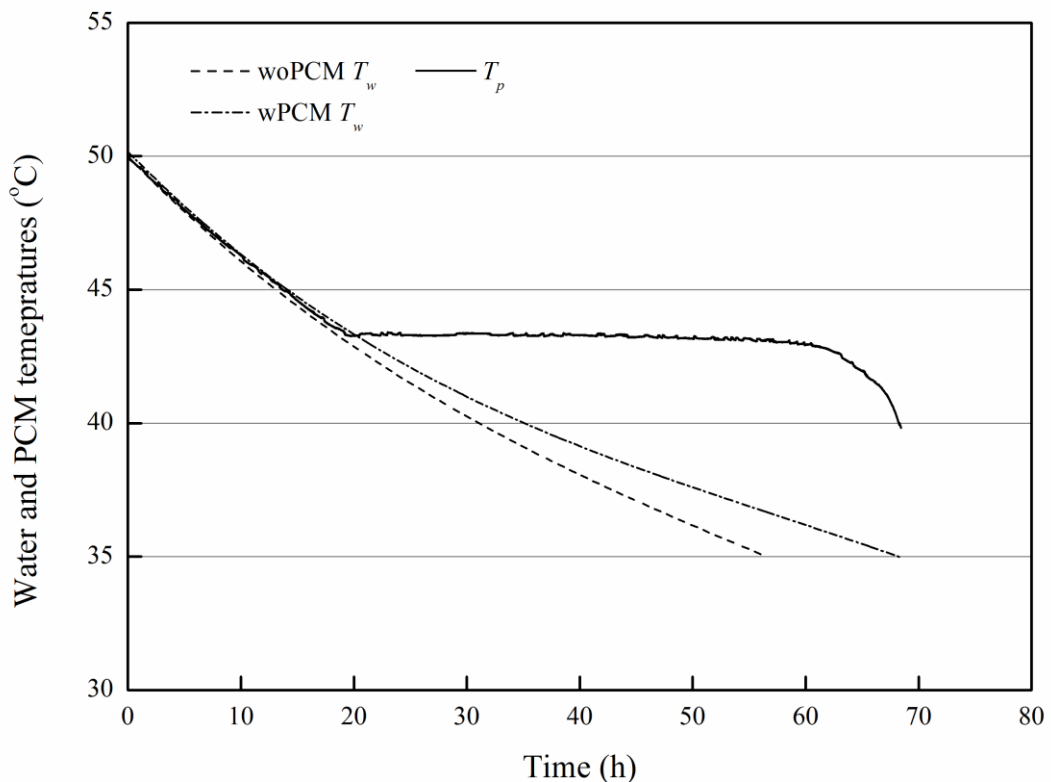
Figure 7.12   Water and PCM temperatures during heat discharging

It was found that the time elapsed for the water to cool down from 50 $^{\circ}$C to 35 $^{\circ}$C is 68.4 hours for the wPCM scenario, and is 56.5 hours for the woPCM scenario. The results indicate that the use of PCM as an internal heat source to partially offset the water tank heat loss can extend the heat retention time by 21.1%.

7.4 Uncertainty Analysis

The uncertainties in the calculated system performance can be determined based on the instrument accuracies summarized in Table 3.3.

Table 7.2　　　Uncertainties in the calculated system performance

Performance parameter	Relative uncertainty (%)	
	woPCM scenario	wPCM scenario
Space cooling capacity	6.7%	6.2%
Water heating capacity	7.9%	7.6%
Power consumption	1.8%	1.8%
Overall coefficient of performance	6.7%	5.8%

By using Kline and McClintock's method (Doebelin, 1983; Holman, 1989), Equations (7.7) to (7.9), derived on the basis of Equations (7.3) to (7.5), can be obtained to determine the uncertainties in the calculated space cooling capacity, water heating capacity and overall coefficient of performance, while that in the power consumption can simply be taken as the corresponding instrument uncertainty.

$$\frac{\delta Q_{cl}}{Q_{cl}} = \sqrt{\left(\frac{\delta m_a}{m_a}\right)^2 + \frac{\delta h_{er,a}^2 + \delta h_{es,a}^2}{\left(h_{er,a} - h_{es,a}\right)^2}} \qquad (7.7)$$

$$\frac{\delta Q_{wh}}{Q_{wh}} = \sqrt{\left(\frac{\delta m_r}{m_r}\right)^2 + \frac{\delta h_{hi,r}^2 + \delta h_{ho,r}^2}{\left(h_{hi,r} - h_{ho,r}\right)^2}} \qquad (7.8)$$

$$\frac{\delta COP_{oa}}{COP_{oa}} = \sqrt{\left(\frac{\delta Q_{cl}}{Q_{cl}+Q_{wh}}\right)^2 + \left(\frac{\delta Q_{wh}}{Q_{cl}+Q_{wh}}\right)^2 + \left(\frac{\delta W}{W}\right)^2} \qquad (7.9)$$

Because of the unsteady system behavior as shown above, the maximum possible uncertainties are calculated and summarized in Table 7.2. The results are ranging from 1.8% to 7.9% and are judged to be acceptable as they are less than the ISO's recommendation of 10% (ISO, 2010).

7.5   Summary

Whether the use of PCM in the water tank of SEHRAC could improve the system performance was investigated in this study. To facilitate the investigations, a prototype SEHRAC integrated with an expanded graphite/paraffin composite PCM was designed and setup in a test facility for laboratory experiments. Both heat charging and discharging tests were carried out. For the heat charging test, two identical sets of experiments with and without the use of PCM (wPCM and woPCM scenarios) under a range of outdoor temperatures were conducted. It was confirmed that the PCM could function as an internal heat sink to lower the rate of water temperature increase and to enhance the heat storage capacity of the water tank. As a result, the space cooling and water heating capacities for the wPCM scenario, as compared to the woPCM scenario, were 5.4% and 16.1% larger, respectively. The overall coefficient of performance was also 6.9% to 9.8% higher. While for the heat

discharging test, it was revealed that the use of PCM could extend the heat retention time of the tank water by 21.1%. The results of this study confirmed that the performance of SEHRAC could be improved by the use of PCM.

CHAPTER 8

CONCLUSIONS AND RECOMMENDATIONS FOR

FUTURE RESEARCH

Air-conditioning and domestic water heating are two dominant energy end-uses in residential buildings in subtropical climates. Hong Kong is not an exception. Space cooling and water heating are responsible for 23% and 19%, respectively, of the overall energy consumption of the residential sector. These figures clearly show that a technology that can simultaneously reduce energy use for space cooling and water heating is highly valuable.

In view of this, a storage-enhanced heat recovery room air-conditioner (SEHRAC) was proposed in this study. SEHRAC is a conventional air-conditioner provided with an additional tank-immersed refrigerant-to-water heat exchanger between the compressor and the air-cooled condenser for recovery of condenser heat for water heating. This installation can serve the purpose of combined space cooling and water heating, and is particularly suitable for applications in subtropical regions, where most households are equipped with air-conditioners to combat the hot and humid summer.

To facilitate the wide application of SEHRAC, this study provided an insight into its effectiveness, energy performance, operation characteristics, system optimization, and performance improvement when used for combined space cooling and water

heating. The conclusions drawn from this study and the recommendations for future research are detailed below.

8.1   Conclusions

8.1.1   Effectiveness Analysis

An effectiveness analysis on the use of SEHRAC to satisfy the daily space cooling and water heating demands of households in a typical residential estate in Hong Kong was carried out. The space cooling loads and air-conditioner energy use of selected residential units were carefully determined by building energy simulations taking into account the inter-shadowing effect among building blocks, the realistic building characteristics, as well as the daily patterns of occupant activity, internal load and air-conditioner utilization. On this basis, the recoverable heat of each studied residential unit was determined and then compared against the water heating demand. Further, for optimal design of the water tank of SEHRAC, its design requirements were also determined and discussed. The key findings are detailed as follows:

1)   The use of a tank-less SEHRAC (i.e. HRAC) to provide simultaneous space cooling and water heating is not feasible in Hong Kong households, due to the fact that the amount of recoverable heat is always lower than the simultaneous water heating demand.

2)   If a water tank is incorporated in HRAC for thermal energy storage, the daily cumulative recoverable heat far exceeds the daily household water heating demand, confirming the effective use of SEHRAC in Hong Kong.

3)   SEHRAC is especially effective in summer when the space cooling load is high but the water heating demand is low. A huge surplus of heat supply (>300%) can be seen in July.

4)   For the densest populated unit in the studied residential estate, the heat transfer effectiveness of the heat exchanger in SEHRAC should be higher than 0.85, if completely free water heating is to be achieved in the entire air-conditioned season.

8.1.2   Energy Performance and Operation Characteristics

For evaluating the energy performance and operation characteristics of SEHRAC, a prototype was designed and setup in a test facility for an experimental study. Two identical sets of experiments with and without water heating under a range of outdoor temperatures and space cooling load conditions were conducted. In the experiments, different operating parameters on the water, refrigerant and air sides of the prototype were measured and recorded. Based on the experimental results, the space cooling, water heating and overall energy performances of the prototype, as well as its dynamic operation characteristics were evaluated. On this basis, the

potential water heating energy saving on wider application of SEHRAC in Hong Kong was also assessed. The key findings are detailed as follows:

1) The water heating objective can be achieved within a range of carefully-determined experimental conditions to confirm the practical use of SEHRAC as the bedroom air-conditioner to reduce the water heating energy use.

2) The intermittent operation characteristics of SEHRAC can lead to significant fluctuations in operating pressures and temperatures on the refrigerant side. SEHRAC using capillary tube can operate satisfactorily despite the fluctuations.

3) As compared to conventional room air-conditioner, SEHRAC has a constantly higher overall coefficient of performance (COP) during its operation, despite there is a maximum of 10% reduction in the space cooling output when the tank water temperature reaches 50 $^{\circ}$C.

4) The potential water heating energy saving on wider application of SEHRAC in Hong Kong corresponds to 9.1% of the overall energy consumption of the residential sector.

8.1.3 System Optimization

Aiming to optimize the system configuration of SEHRAC, the use of capillary tube (CT) and thermostatic expansion valve (TEV) as the expansion device were side-by-side compared by experimental investigations. To facilitate the investigations, a prototype, which could be switched between the CT and TEV systems, was designed and setup for two identical sets of experiments. For each set of experiments, a series of tests under different outdoor temperatures were conducted. The key findings are detailed as follows:

1)   TEV can better regulate the refrigerant flow, maintain a stable evaporator superheat, and minimize the rise in refrigerant vapor content at the evaporator inlet during the operation of SEHRAC.

2)   The space cooling and water heating capacities for the TEV system are on average 16.3% to 19.4% and 18.5% to 23.4% larger than the CT system. The overall COP for the TEV system is also 12.5% to 20.9% higher for a range of outdoor temperatures.

3)   For both systems, due to a drop in heat transfer performance of the heat exchanger with operating time, the associated space cooling and water heating capacities drop correspondingly, and thus performance improvement is needed.

8.1.4   Performance Improvement

Aiming to improve the overall performance of SEHRAC, the use of phase change material (PCM) in the water tank was proposed. Two identical sets of experiments with and without the use of PCM (abbreviated as wPCM and woPCM scenarios) under a range of outdoor temperatures were conducted to confirm and quantify the resultant performance improvement. Based on the experimental results, the heat storage capacity of the water tank, the refrigerant side operation characteristics, as well as the space cooling, water heating and overall energy performances were examined and compared for the two scenarios. The key findings are detailed as follows:

1)   The PCM can function as an internal heat sink to lower the rate of water temperature increase during heat charging and to enhance the heat storage capacity of the water tank.

2)   The space cooling and water heating capacities for the wPCM scenario, as compared to the woPCM scenario, are 5.4% and 16.1% larger, respectively. The overall COP for the wPCM scenario is also 6.9% to 9.8% higher for a range of outdoor temperatures.

3)   The PCM can function as an internal heat source to partially offset the water tank heat loss during heat discharging. The use of PCM can therefore extend the heat retention time of the tank water by 21.1%.

However, there are limitations with the above findings:

1) R22 was used as the working fluid for SEHRAC, the simulation and experimental results obtained in this study may not be applicable to heat recovery air-conditioners using refrigerants with physical or thermal properties deviating largely from R22.

2) The conclusions drawn may be not applicable to other countries or regions having significantly different climatic and living conditions from that of Hong Kong.

3) The PCM investigated for performance improvement of SEHRAC is limited to a paraffin/expanded graphite composite material, while the use of other PCMs may have different space cooling and water heating performance improvements.

4) Considering that space is always a concern in Hong Kong, the wide application of SEHRAC may be limited by the additional space required for locating the water tank.

8.2   Recommendations for Future Research

The present work can be further extended by incorporating the following:

1) A detailed mathematical model, which is capable of evaluating the dynamic performance of SEHRAC under time-varying conditions, can be developed.

The availability of the model can overcome the inherent shortcoming associated with experimental investigations, which can only provide discrete performance evaluations. The model can also be coded into a computer program to enable performance optimization of SEHRAC.

2)   As compared to CT, TEV is a more suitable option for use in SEHRAC as revealed from this study. However, it is noted that the space cooling capacity of the TEV-based SEHRAC still drops with operating time. This may be due to the fact that TEV is a linear controller in response to the evaporator superheat, but the refrigerant side operating parameters vary non-linearly during the operation of SEHRAC. Therefore, an electric expansion device (EEV) with multiple feedbacks and advanced control mechanism may be the best option for use in SEHRAC. The experimental results presented in this study may be useful in developing this control mechanism.

3)   In this study, the PCM used for performance improvement of SEHRAC is limited to a paraffin/expanded graphite composite material. Other PCMs with different phase change temperatures and latent heats may also be investigated for use in this circumstance. The resultant performance improvement may be further enhanced if an optimal PCM is used.

APPENDIX A

Table A.1   Daily patterns of occupant activity, internal load and air-conditioner
utilization (Bedroom)

Item		Bedroom			
		Occupancy	Lighting	SPA[a]	AC[b]
Daily patterns:					
Hour					
From	To				
0	1	1	0.3	0.8	On
1	5	1	0	0	On
5	6	1	0	0	On
6	7	1	0.5	0	On
7	8	0.25	0.2	0	Off
8	9	0	0.3	0	Off
9	10	0	0	0	Off
10	11	0	0	0	Off
11	12	0	0	0	Off
12	13	0	0	0	Off
13	14	0.25	1	0	On
14	15	0.25	1	0.33	On
15	16	0.25	1	0.33	On
16	17	0.25	1	0.33	On
17	18	0.25	0	0.33	On
18	19	0.25	1	0.33	On
19	20	0.25	1	0.8	On
20	21	0.5	1	0.8	On
21	22	0.5	1	0.8	On
22	23	0.5	1	1	On
23	24	1	0.6	1	On
Installed power (W):					
Unit type					
1P			302	176	
1B			104	44	
2B			104	44	

[a] SPA=Small power appliance

[b] AC=Air-conditioner

Table A.2   Daily patterns of occupant activity, internal load and air-conditioner
utilization (Living/dining room)

Item		Living/dining room			
		Occupancy	Lighting	SPA[a]	AC[b]
Daily patterns:					
Hour					
From	To				
0	1	0	0	0.19	Off
1	5	0	0	0.19	Off
5	6	0	0	0.19	Off
6	7	0	0.3	0.37	Off
7	8	0.25	0.5	0.54	Off
8	9	0.5	0	0.54	Off
9	10	0.5	0	0.54	Off
10	11	0.5	0	0.54	Off
11	12	0.5	0	0.54	Off
12	13	0.45	0	0.54	Off
13	14	0.5	0.5	0.63	On
14	15	0.5	0	0.43	On
15	16	0.5	0	0.43	On
16	17	0.5	0	0.43	On
17	18	0.5	0	0.43	On
18	19	0.5	0.5	0.43	On
19	20	0.75	1	1	On
20	21	1	1	1	On
21	22	1	1	1	On
22	23	1	1	1	Off
23	24	0	0.5	1	Off
Installed power (W):					
Unit type					
1P			-	-	
1B			250	132	
2B			250	132	

[a] SPA=Small power appliance

[b] AC=Air-conditioner

REFERENCES

Abhat A, 1983. Low temperature latent heat thermal energy storage: Heat storage materials. Solar Energy, 30: 313-332.

Adriansyah W, 2001. Combined air-conditioning and tap water heating plant, using CO_2 as refrigerant for Indonesian climate condition (PhD Thesis). Norway: Norwegian University of Science and Technology.

Agrawal N, Bhattacharyya S, 2008. Optimized transcritical CO_2 heat pumps: Performance comparison of capillary tubes against expansion valves. International Journal of Refrigeration, 31: 388-395.

Aguilar C, White DJ, David LR, 2005. Domestic water heating and water heater energy consumption in Canada. Canada: Canadian Building Energy End-Use Data and Analysis Centre.

Agyenim F, Eames P, Smyth M, 2009. A comparison of heat transfer enhancement in a medium temperature thermal energy storage heat exchanger using fins. Solar Energy, 83: 1509-1520.

Agyenim F, Hewitt N, 2010. The development of a finned phase change material (PCM) storage system to take advantage of off-peak electricity tariff for improvement in cost of heat pump operation. Energy and Buildings, 42: 1552-1560.

Agyenim F, Hewitt N, Eames P, Smyth M, 2010. A review of materials, heat transfer and phase change problem formulation for latent heat thermal energy storage systems (LHTESS). Renewable and Sustainable Energy Reviews, 14: 615-628.

Alexander DK, 1996. HTB2 – A model for the thermal environment of buildings in operation (release 2.0a). UK: University of Wales College of Cardiff.

Alexander DK, Ku Hassan KA, Jones PJ, 1997. Simulation of solar gains through external shading devices. in: Proceedings of Building Simulation 97 – Fifth International IBPSA Conference, Prague, Czech Republic, 355-362.

Anderson TN, Morrison GL, 2007. Effect of load pattern on solar-boosted heat pump water heater performance. Solar Energy, 81: 1386-1395.

ASHRAE, 1983. ASHRAE Standard 16: Method of testing for rating room air conditioners and packaged terminal air conditioners. USA: American Society of Heating, Refrigerating and Air-Conditioning Engineers.

ASHRAE, 2009. ASHRAE Handbook – Fundamentals. USA: American Society of Heating, Refrigerating and Air-Conditioning Engineers.

ASHRAE, 2010. ASHRAE Standard 116: Methods of testing for rating seasonal efficiency of unitary air conditioners and heat pumps. USA: American Society of Heating, Refrigerating and Air-Conditioning Engineers.

ASHRAE, 2011. ASHRAE Standard 140: Standard method of test for the evaluation of building energy analysis computer programs. USA: American Society of Heating, Refrigerating and Air-Conditioning Engineers.

Autodesk, 2004. AutoCAD 2003: User's guide. USA: Autodesk Inc.

Baby R, Balaji C, 2012. Experimental investigations on phase change material based finned heat sinks for electronic equipment cooling. International Journal of Heat and Mass Transfer, 55: 1642-1649.

BEAM Society, 2010. BEAM Plus for existing buildings. Hong Kong: Green Building Council.

Bejan A, 1993. Heat transfer. USA: John Wiley & Sons.

Bong TY, Hawlader MNA, Mahmood W, 1988. Influence of expansion device on the performance of an air-conditioner with a desuperheater. ASHRAE Transactions, 94: 661-672.

Broersen PMT, Van der Jagt MFG, 1980. Hunting of evaporators controlled by a thermostatic expansion valve. Journal of Dynamic Systems, Measurement, and Control, 102: 130-135.

BSI, 1975. British Standard 5141: Specification for air heating and cooling coils. UK: British Standards Institution.

Cabeza LF, Castell A, Barreneche C, de Gracia A, Fernández AI, 2011. Materials used as PCM in thermal energy storage in buildings: A review. Renewable and Sustainable Energy Reviews, 15: 1675-1695.

Cabeza LF, Ibanez M, Sole C, Roca J, Nogués M, 2006. Experimentation with a water tank including a PCM module. Solar Energy Materials and Solar Cells, 90: 1273-1282.

Canbazoğlu S, Şahinaslan A, Ekmekyapar A, Aksoy YG, Akarsu F, 2005. Enhancement of solar thermal energy storage performance using sodium thiosulfate pentahydrate of a conventional solar water-heating system. Energy and Buildings, 37: 235-242.

Castell A, Solé C, Medrano M, Roca J, Cabeza LF, García D, 2008. Natural convection heat transfer coefficients in phase change material (PCM) modules with external vertical fins. Applied Thermal Engineering, 28: 1676-1686.

Census and Statistics Department, 2015. Trends in population and domestic households in Hong Kong. Hong Kong: Hong Kong SAR Government.

Centre of Environmental Technology, 1999. HK-BEAM: An environmental assessment for new residential buildings (version 3/99). Hong Kong: Centre of Environmental Technology.

Chan ALS, Chow TT, Fong SKF, Lin JZ, 2006. Generation of a typical meteorological year for Hong Kong. Energy Conversion and Management, 47: 87-96.

Chaturvedi SK, Chen DT, Kheireddine A, 1998. Thermal performance of a variable capacity direct expansion solar-assisted heat pump. Energy Conversion and Management, 39: 181-191.

Chen H, Lee WL, 2010. Combined space cooling and water heating system for Hong Kong residences. Energy and Buildings, 42: 243-250.

Chen H, Lee WL, Yik FWH, 2008. Applying water cooled air conditioners in residential buildings in Hong Kong. Energy Conversion and Management, 49: 1416-1423.

Choi JC, Kim SD, 1992. Heat-transfer characteristics of a latent heat storage system using $MgCl_2$ $6H_2O$. Energy, 17: 1153-1164.

Choi JM, Kim YC, 2002. The effects of improper refrigerant charge on the performance of a heat pump with an electronic expansion valve and capillary tube. Energy, 27: 391-404.

Cleland AC, 1986. Computer subroutines for rapid evaluation of refrigerant thermodynamic properties. International Journal of Refrigeration, 9: 346-351.

Copeland, 1982. Compression ratio as it affects compressor reliability (AE17-1268). USA: Emerson Climate Technologies.

De Gracia A, Oró E, Farid MM, Cabeza LF, 2011. Thermal analysis of including phase change material in a domestic hot water cylinder. Applied Thermal Engineering, 31: 3938-3945.

Demirbas MF, 2006. Thermal energy storage and phase change materials: An overview. Energy Sources, Part B: Economics, Planning, and Policy, 1: 85-95.

Dincer I, Kanoglu M, 2011. Refrigeration systems and applications. USA: John Wiley & Sons.

Dincer I, Rosen M, 2002. Thermal energy storage: Systems and applications. USA: John Wiley & Sons.

Doebelin EO, 1983. Measurement systems application and design. USA: McGraw-Hill.

Dossat RJ, 1997. Principles of refrigeration. USA: Prentice-Hall.

Electrical and Mechanical Services Department, 2007. Performance-based building energy code. Hong Kong: Hong Kong SAR Government.

Electrical and Mechanical Services Department, 2015a. Hong Kong energy end-use data. Hong Kong: Hong Kong SAR Government.

Electrical and Mechanical Services Department, 2015b. Mandatory energy efficiency labelling scheme. Hong Kong: Hong Kong SAR Government.

Farzad M, O'Neal DL, 1993. Influence of the expansion device on air conditioner system performance characteristics under a range of charging conditions. ASHRAE Transactions, 99: 3-13.

Feng C, Kai W, Shouguo W, Ziwen X, Pengcheng S, 2009. Investigation of the heat pump water heater using economizer vapor injection system and mixture of R22/R600a. International Journal of Refrigeration, 32: 509-514.

Fernandez N, Hwang Y, Radermacher R, 2010. Comparison of CO_2 heat pump water heater performance with baseline cycle and two high COP cycles. International Journal of Refrigeration, 33: 635-644.

Guo JJ, Wu JY, Wang RZ, Li S, 2011. Experimental research and operation optimization of an air-source heat pump water heater. Applied Energy, 88: 4128-4138.

Hepbasli A, Kalinci Y, 2009. A review of heat pump water heating systems. Renewable and Sustainable Energy Reviews, 13: 1211-1229.

Hoeschele MA, Springer DA, 2008. Field and laboratory testing of gas tankless water heater performance. ASHRAE Transactions, 114: 453.

Holman JP, 1989. Experimental methods for engineers. USA: McGraw-Hill.

Hong Kong SAR Government, 2015. Hong Kong: The facts. Hong Kong: Hong Kong SAR Government.

Housing Authority, 2015. Housing in figures. Hong Kong: Hong Kong SAR Government.

Huang BJ, Lee CP, 2004. Long-term performance of solar-assisted heat pump water heater. Renewable Energy, 29: 633-639.

Hundy GH, Trott AR, Welch TC, 2008. Refrigeration and air-conditioning. UK: Butterworth-Heinemann.

Inaba H, Matsuo K, Horibe A, 2003. Numerical simulation for fin effect of a rectangular latent heat storage vessel packed with molten salt under heat release process. Heat and Mass Transfer, 39: 231-237.

ISO, 2010. ISO Standard 5151: Non-ducted air conditioners and heat pumps – testing and rating for performance. Switzerland: International Organization for Standardization.

Kalhori B, Ramadhyani S, 1985. Studies on heat transfer from a vertical cylinder, with or without fins, embedded in a solid phase change medium. Journal of Heat Transfer, 107: 44-51.

Kara O, Ulgen K, Hepbasli A, 2008. Exergetic assessment of direct-expansion solar-assisted heat pump systems: Review and modeling. Renewable and Sustainable Energy Reviews, 12: 1383-1401.

Karagoz S, Yilmaz M, Comakli O, Ozyurt O, 2004. R134a and various mixtures of R22/R134a as an alternative to R22 in vapour compression heat pumps. Energy Conversion and Management, 45: 181-196.

Kenisarin M, Mahkamov K, 2007. Solar energy storage using phase change materials. Renewable and Sustainable Energy Reviews, 11: 1913-1965.

Kim BH, O'Neal DL, 2005. Effect of refrigerant flow control on the heating performance of a variable-speed heat pump operating at low outdoor temperature. Journal of Solar Energy Engineering, 127: 277-286.

Kim M, Kim MS, Chung JD, 2004. Transient thermal behavior of a water heater system driven by a heat pump. International Journal of Refrigeration, 27: 415-421.

Kousksou T, Bruel P, Cherreau G, Leoussoff V, El Rhafiki T, 2011. PCM storage for solar DHW: From an unfulfilled promise to a real benefit. Solar Energy, 85: 2033-2040.

Kuznik F, Virgone J, Roux JJ, 2008. Energetic efficiency of room wall containing PCM wallboard: A full-scale experimental investigation. Energy and Buildings, 40: 148-156.

Laipradit P, Tiansuwan J, Kiatsiriroat T, Aye L, 2008. Theoretical performance analysis of heat pump water heaters using carbon dioxide as refrigerant. International Journal of Energy Research, 32: 356-366.

Lam JC, 1993. A survey of electricity consumption and user behavior in some government staff quarters. Building Research and Information, 21: 109-116.

Lane GA, 1983. Solar heat storage: Latent heat materials. USA: CRC Press.

Lee WL, Chen H, Yik FWH, 2008. Modeling the performance characteristics of water-cooled air-conditioners. Energy and Buildings, 40: 1456-1465.

Li YW, Wang RZ, Wu JY, Xu YX, 2007. Experimental performance analysis on a direct-expansion solar-assisted heat pump water heater. Applied Thermal Engineering, 27: 2858-2868.

Liebenberg L, Meyer JP, 1998. Potential of the zeotropic mixture R-22/R-142b in high-temperature heat pump water heaters with capacity modulation. ASHRAE Transactions, 104: 418.

Liu M, Saman W, Bruno F, 2012. Development of a novel refrigeration system for refrigerated trucks incorporating phase change material. Applied Energy, 92: 336-342.

Lomas KJ, Eppel H, Martin CJ, Bloomfield DP, 1997. Empirical validation of building energy simulation programs. Energy and Buildings, 26: 253-275.

Maidment GG, Missenden JF, James RW, Tozer RM, 1999. Analysis of the expansion valves used for controlling refrigerant feed into delicatessen cabinets in supermarkets. Journal of Food Engineering, 40: 47-58.

Marsh AJ, 2010. Autodesk-Ecotect (version 5.6). USA: Autodesk Inc.

Mazman M, Cabeza LF, Mehling H, Nogués M, Evliya H, Paksoy HO, 2009. Utilization of phase change materials in solar domestic hot water systems. Renewable Energy, 34: 1639-1643.

Mehling H, Cabeza LF, Hippeli S, Hiebler S, 2003. PCM-module to improve hot water heat stores with stratification. Renewable Energy, 28: 699-711.

Mesalhy O, Lafdi K, Elgafy A, 2006. Carbon foam matrices saturated with PCM for thermal protection purposes. Carbon, 44: 2080-2088.

Mohanraj M, Jayaraj S, Muraleedharan C, 2009. Performance prediction of a direct expansion solar assisted heat pump using artificial neural networks. Applied Energy, 86: 1442-1449.

Moreno-Rodriguez A, Garcia-Hernando N, González-Gil A, Izquierdo M, 2013. Experimental validation of a theoretical model for a direct-expansion solar-assisted heat pump applied to heating. Energy, 60: 242-253.

Morrison GL, 1994. Simulation of packaged solar heat-pump water heaters. Solar Energy, 53: 249-257.

Neksa P, Rekstad H, Zakeri GR, Schiefloe PA, 1998. CO_2-heat pump water heater: Characteristics, system design and experimental results. International Journal of Refrigeration, 21: 172-179.

Öttinger O, Bacher J, 2010. Material mixtures for heat storage systems and production method. US Patent 7704405 B2.

Pandiyarajan V, Pandian MC, Malan E, Velraj R, 2011. Experimental investigation on heat recovery from diesel engine exhaust using finned shell and tube heat exchanger and thermal storage system. Applied Energy, 88: 77-87.

Paramount, 2013. How heat pumps work. USA: Paramount Pool Products.

Powertime, 2015. A cheaper and eco-friendly alternative for your hot water. South Africa: Powertime Co.

Saikawa M, Hashimoto K, 2011. Evaluation on efficiency of CO_2 heat pump cycle for hot water supply. Transactions of the Japan Society of Refrigerating and Air Conditioning Engineers, 18: 217-223.

Sakai I, Takagi M, Terakawa K, Ohue J, 1976. Solar space heating and cooling with bi-heat source heat pump and hot water supply system. Solar Energy, 18: 525-532.

Sharma A, Tyagi VV, Chen CR, Buddhi D, 2009. Review on thermal energy storage with phase change materials and applications. Renewable and Sustainable Energy Reviews, 13: 318-345.

Sporlan, 2011. Thermostatic expansion valves: Theory of operation, application, and selection. USA: Parker Hannifin Corporation.

Stoecker WF, Smith LD, Emde BN, 1981. Influence of the expansion device on the seasonal energy requirements of a residential air conditioner. ASHRAE Transactions, 87: 349-360.

Stritih U, 2004. An experimental study of enhanced heat transfer in rectangular PCM thermal storage. International Journal of Heat and Mass Transfer, 47: 2841-2847.

Vince CM, Ronald E, 2001. Experimental study of an R407C heat pump water heater. ASHRAE Transactions, 107: 112-119.

Wan KSY, 2003. Energy performance assessment method for residential buildings in Hong Kong (PhD Thesis). Hong Kong: The Hong Kong Polytechnic University.

Wan KSY, Yik FWH, 2004. Building design and energy end-use characteristics of high-rise residential buildings in Hong Kong. Applied Energy, 78: 19-36.

Whitman WC, Johnson WM, Tomczyk JA, 2005. Refrigeration & air conditioning technology. USA: Cengage Learning.

Winkelmann FC, Birdsall BE, Buhl WF, Ellington KL, Erdem AE, Hirsch JJ, Gates S, 1993. DOE-2 supplement: Version 2.1E. USA: Lawrence Berkeley National Laboratory.

World Population Review, 2015. Hong Kong population. USA: World Population Review.

Xia L, Zhang P, Wang RZ, 2010. Preparation and thermal characterization of expanded graphite/paraffin composite phase change material. Carbon, 48: 2538-2548.

Xu G, Zhang X, Deng S, 2006. A simulation study on the operating performance of a solar–air source heat pump water heater. Applied Thermal Engineering, 26: 1257-1265.

Yao Y, Jiang Y, Deng S, Ma Z, 2004. A study on the performance of the airside heat exchanger under frosting in an air source heat pump water heater/chiller unit. International Journal of Heat and Mass Transfer, 47: 3745-3756.

Yik FWH, 2000. BECRES – A program for predicting electricity use for air-conditioning in residential buildings. Hong Kong: The Hong Kong Polytechnic University.

Yuen B, 2010. Squatters no more: Singapore social housing. USA: Global Urban Development.

Zalba B, Marín JM, Cabeza LF, Mehling H, 2003. Review on thermal energy storage with phase change: Materials, heat transfer analysis and applications. Applied Thermal Engineering, 23: 251-283.

Zhang J, Wang RZ, Wu JY, 2007. System optimization and experimental research on air source heat pump water heater. Applied Thermal Engineering, 27: 1029-1035.